UNIVERSITY OF OKLAHOMA

GRADUATE COLLEGE

RAMAN SPECTROSCOPY AND ITS APPLICATIONS TO ICE-SEDIMENT-BRINE MATRICES IN RECURRING SLOPE LINEAE ON MARS

A THESIS

SUBMITTED TO THE GRADUATE FACULTY

in partial fulfillment of the requirements for the

Degree of

MASTER OF SCIENCE

By

DANIEL P. MASON
Norman, Oklahoma
2020

RAMAN SPECTROSCOPY AND ITS APPLICATIONS TO ICE-SEDIMENT-BRINE MATRICES IN RECURRING SLOPE LINEAE ON MARS

A THESIS APPROVED FOR THE

SCHOOL OF GEOSCIENCES

BY THE COMMITTEE CONSISTING OF

Dr. Megan E. Elwood Madden, Chair

Dr. Kato T. Dee

Dr. Shannon A. Dulin

TABLE OF CONTENTS

Abstract	v
Introduction	1
Methodology	9
Results	14
Discussion	39
Implications for Mars	45
Conclusions	54
Appendix	55
Works Cited	100

Abstract:

Raman spectroscopy is an ideal tool to analyze the geochemical make up of various compounds, be they solid, liquid, gas, or a combination of multiple phases. This research seeks to determine how changes in both temperature and sediment level impact the spectral signatures of various Mars-analogue brines saturated with sulfate, perchlorate, and chloride salts, and how these data might apply to recurring slope lineae that may be occurring on Martian slopes. This work will allow a reference dataset to be created, which will be instrumental in helping to identify characteristics of unknown samples of brine, including the solid-liquid phase transition, the cooling rates, the degree of sediment inclusion, and the overall chemical composition of *in situ* brines and aqueous solutions.

This, in turn, will allow for a more thorough understanding of the role of aqueous processes throughout the Solar System, and can help clarify the role these processes might play on bodies thought to contain various quantities of brines, ices, and/or sediment-- including Mars, Europa, Enceladus, Titan, and other icy moons-- providing an additional tool to use in the search for extraterrestrial life. It is likely that these data and observations will grow in importance in the coming years, as more space missions seek to utilize analytical techniques such as Raman spectroscopy to understand planetary geologic processes more fully.

Introduction:

Mars was one of the first planets other than Earth to be discovered by humankind. Mars is the fourth planet from the Sun. It orbits on average 230 million kilometers away, is composed of rocks that are generally basaltic in composition (Ehlmann, 2014), and though the planet has a tilt like that of Earth, its average temperatures are generally much colder due in part to its greater distance from the Sun. Mars also has a surface pressure of about 600 pascals (Bargery, 2011), much less than Earth's 101,000 pascals. Pure liquid water is not stable on the Martian surface today for extended periods of time due to both the colder temperatures and lower pressures that the planet experiences. These conditions generally foster either water ice or the sublimation/evaporation of water into the atmosphere.

Martian geologic history is split up into the Noachian (4.1 Ga to 3.8 Ga), Hesperian (3.8 Ga to 3.0 Ga), and Amazonian (3.0 Ga to present) periods (Carr, 2010). While today, pure liquid water is highly unlikely at the surface due to both the cold temperatures (Chevrier, 2012) and low pressures, surface water was likely present on Mars during the Noachian (Bargery, 2011) about four billion years ago, as evidenced by erosional and other surficial features. Sulfate deposits from the Hesperian (Carr, 2010) also hint at aqueous activity, while ices likely played a role around three billion years ago during the Amazonian (Carr, 2010). It is thought that liquid water likely played a larger role during early Martian history-- eroding surficial features, forming paleo-shorelines (Clifford, 2001), and even potentially flooding portions of the planet (Solomon, 2005). However, it is speculated liquid water played much less of a role as time progressed into the later Hesperian and Amazonian (Solomon, 2005), as much of the liquid water at Mars' surface began to disappear; much of it was either transferred to the atmosphere via evaporation or sublimation (with some subsequently lost to space), integrated into the soil as hydrated

minerals, or frozen into ices that are largely stored either underground or at the poles (Squyres, 1984).

Recurring Slope Lineae:

While the surface of modern Mars is cold and dry, it is still possible that Mars has small-scale flows of transient liquid water on its surface today. These flows are called recurring slope lineae. Recurring slope lineae (RSL) are "narrow dark features that incrementally lengthen down steep low-albedo slopes when temperatures are warm, subsequently fade, and reoccur annually" (Stillman, 2018). They can be found on Martian hillsides that often have a slope greater than 25° (Horne, 2018). Recurring slope lineae are transient in nature, as they are not permeant fixtures of the Martian landscape. They recur cyclically, either over the course of the Martian day as brines freeze and thaw (Stillman, 2016), or over the course of the year as RSL grow and contract (Stillman, 2016). They are often found in the lower and mid-latitudes of Mars, within about 25 degrees of the equator (Dundas, 2013), though some have been found upwards of 30 to 35 degrees from the equator (Dundas, 2013). Many of those observed so far have been found in the southern hemisphere where temperatures would likely be warmest (Dundas, 2013), while fewer, but still some, have been found north of the equator.

Consideration of these factors have led to two main hypotheses for how recurring slope lineae form. These hypotheses advocate that recurring slope lineae have either a non-aqueous formation mechanism, likely from dry sediment flows (Edwards, 2016; Schmidt, 2017), or that recurring slope lineae are formed by water (McEwan, 2015; Chevrier, 2012; Horne, 2018) in some capacity.

For example, recurring slope lineae may be formed by a non-aqueous process, as might be the case if dry sediment flows on Martian hillsides are involved in their formation. These flows could be due to small amount of subsurface gas escaping and triggering these dry flows of largely silt-sized grains (Schmidt, 2017). This could lead to streaks on Martian hillsides.

Conversely, RSL might have an aqueous formation mechanism. They may form from hygroscopic interactions that ultimately lead to deliquescence (McEwan, 2015); effectively, salts on the Martian surface could absorb enough water from the atmosphere that they eventually become saturated and form a liquid brine. Groundwater is also a potential formation mechanism for recurring slope lineae (McEwan, 2015). In terrestrial environments, there are many examples of groundwater intercepting the surface and creating natural features such as springs. It is possible that this same process may be occurring on Mars, wherein groundwater reaches the surface due to fractures in bedrock (Abotalib, 2019), helped by topography, thereby forming recurring slope lineae. RSL may similarly be formed from the presence of a subsurface briny aquifer (Stillman, 2016) or by the presence and melting of Martian ices (Chevrier, 2012).

Recurring slope lineae-- if aqueous in origin-- are likely highly saline, as salt depresses the freezing point of water. This would lead to, instead of the fresh water as seen on Earth, very briny surface water on Mars. Perchlorate, sulfate, and chloride salts have all been found by numerous missions to Mars (Massé, 2015), and may be indicative of the transient presence of liquid water at various locations (Chevrier, 2012). The *Phoenix* lander, for example, has directly detected perchlorate salts-- and may have even detected liquid brine-- in the higher latitudes of Mars (McEwan, 2011; Chevrier, 2009).

Salts would allow water to stay liquid at much lower temperatures than if the water were pure. The presence of these various salts, therefore, has the potential to impact the geochemistry

and surficial geology of Mars through the formation of brines and-- by extension-- other aqueous processes, even if the planet typically experiences cold temperatures.

Heat flow and evaporation models generally support what was already suspected about RSL-- that temperatures at lower latitudes near the Martian equator can become warm enough in certain seasons to melt most ices, whereas temperatures in the higher latitudes and nearer to the poles generally would only be warm enough to melt at most a select few brine-rich near-surface ices, regardless of the season or the depth of the ice (Chevrier, 2012). Rates of evaporation and freezing of surface liquid cannot necessarily be treated as separate issues, either-- as liquid that quickly evaporates would not have time to refreeze into surface ice at that location. In the top few meters of regolith, as both depth and latitude increase, both the variability of temperature for and average temperature within the regolith decrease, meaning fewer and fewer brine-rich near-surface ices can become warm enough to melt.

As depth increases into the tens to hundreds of meters, however-- and assuming an axial tilt of 25 degrees-- the temperature shifts from being largely constant to beginning to increase (Root, 2012). At depths of up to a kilometer, the magnitude of this increase is dependent partially upon latitude. Less temperature change is observed at higher latitudes where the surface is colder, while greater-- but still slight-- changes are observed closer to the equatorial regions. Nonetheless, subsurface liquid brines still have the potential-- due to fractures in the subsurface or the differences in pressure at the surface versus at depth (Abotalib, 2019), for example-- to seep towards the surface and flow down a slope, forming recurring slope lineae. This is dependent, of course, on the composition of, and therefore melting point for, each respective brine. At lower temperatures, only chlorides and perchlorates are generally stable as liquids, whereas sulfate brines and pure water are generally only stable as liquids at higher temperatures.

Salty water also has the potential to impact Martian soil in other ways. Electrical conductivity experiments testing Mars-analogue soil mixed with various salts (including magnesium perchlorate and calcium perchlorate), under various humidity conditions, and at consistent temperatures of around 290 K found that the color of the soils tested changed when they became moist (Heinz, 2016), possibly due to water particles adsorbing to the intermixed salts. As the sample became wetter, the particles in it also became more interconnected, and thereby increased the electrical conductivity. The conductivity and moisture level of Mars-analogue soil can therefore change based, in part, on the salt content of the material and relative humidity of the area-- both of which can influence the overall level of deliquescence experienced by materials. Therefore, aqueous activity can change the color of the sediment with which it interacts, potentially forming recurring slope lineae. These processes, within the spatial context of recurring slope lineae observations, can help scientists and researchers better understand all the potential mechanisms at play regarding the formation of RSL, from electrical conductively to spatial extent.

Mars-analogue temperature, pressure, and atmospheric composition conditions were also used to determine how quickly different chlorate solutions of various concentrations evaporated (Hanley, 2012). Using this data in conjunction with the pre-existing literature, stability diagrams for various solutions of chlorate salts were constructed. It should be noted that changes in concentration due to evaporation changed the activity of the remaining water, thereby also impacting the freezing point of the solution.

Ices are a potential contributing factor to the ice-brine ratios-- and therefore chemistry-- of these recurring slope lineae as well. The average temperature of Mars is quite cold, ranging from 130 K to around 290 K (Bargery, 2011). These temperatures, even with salts depressing the

freezing point of water, are generally low enough to freeze brines. This may have implications not only for the local chemistry at locations missions have already landed at-- as was evidenced by the detection of perchlorate salts found by the *Phoenix* lander-- but may also impact the geochemistry of potential future mission sites, as a site that has experienced recent aqueous alteration of some sort will be geologically distinct from locations that have not.

Recurring slope lineae likely also contain sediment, which may include dust, physically weathered rock, and/or clays. It is possible that this weathered material might help, in conjunction with salts, to further depress the freezing point of these brines (Fairén, 2009), albeit minimally when compared to the role salts would play. Sediments on Mars have almost certainly mixed with brines at some point in Martian history (Chevrier, 2012), thereby-- like salts-- impacting not only the brines' physical state but their geochemistry as well, since both salts and sediment are an integral part of Martian surficial geology (Heinz, 2016). The brines themselves, if at depth, may flow through tens to up to hundreds of meters of bedrock, permafrost, and/or regolith before reaching the surface (Abotalib, 2019). Taken together, these factors could contribute to flows of cold saltwater, in many cases mixed with sediment, on the Martian surface-- even today. Therefore, while brines may contribute to recurring slope lineae, the brines' exact compositions, prevalence, and sources are nonetheless unclear.

Raman spectroscopy:

Raman spectroscopy uses the interaction of laser light with compounds to identify the composition and concentration of materials. When interacting with a photon of laser light, electrons in the molecules of covalently bonded materials typically absorb some of the photon's energy and get promoted to a higher energy state. The electrons then proceed to lose some of or all of that energy and fall down to a lower energy state, emitting photons of a different

wavelength than the excitation laser light. These interactions can be measured by collecting the photons and plotting the number of photons produced with different wavelengths in the form of a Raman spectrum. The peaks within the spectra are characteristic of different elements, materials, and compositions.

When laser light hits an object, it can interact with that object through Rayleigh scattering or Raman scattering. Rayleigh scattering takes place when the resultant light is of the same wavelength as the original laser light. Raman scattering occurs when the resultant light is of a different wavelength than the original light. This shift is due to one of two scenarios (Edwards, 2005; Lohumi, 2017). In one case, the target object absorbs some of the light from the laser, causing the objects' bonds to vibrate. The material then emits photons of light at a lower frequency and longer wavelength than the original light; this is known as Stokes scattering. Alternatively, the material may release photons with additional energy in the form of anti-Stokes scattering; here, the resultant light has a higher frequency and shorter wavelength than the incident light.

The Raman spectrometer collects the light emitted by the material and produces a Raman spectrum, where the wavenumber (1/cm) and intensities of the peaks can be used to identify both the composition and concentration of various compounds. The wavenumber (x-axis) is simply a measure of the change in wavelength between the incident photon and resultant photon. While not relevant to this study, the intensities of these peaks can also be used to determine solute concentration changes within the sample (McGraw et al., 2018). The wavenumber of the peaks themselves are representative of certain compositions. For example, the spectrum for sulfate salts dissolved in water to form brine has several notable peaks at low wavenumbers (Figure 1). One of the most intense peaks is the main sulfate peak at approximately 982 wavenumbers; sodium

sulfate also displays minor peaks around 456 cm^{-1}, 613 cm^{-1}, and 1112 cm^{-1} (Figure 1), while magnesium sulfate does so at approximately 451 cm^{-1}, 617 cm^{-1}, 1113 cm^{-1}. The peak at 1644 wavenumbers, on the other hand, is caused by the bonds of the water molecule bending (Wang, 2004). In certain spectra, including the sulfate spectra, additional water peaks are also present at higher wavenumbers, including at ~3210 cm^{-1} and 3420 cm^{-1} (Duričković, 2011; Yang, 2019), due to the OH bonds of the water molecule stretching.

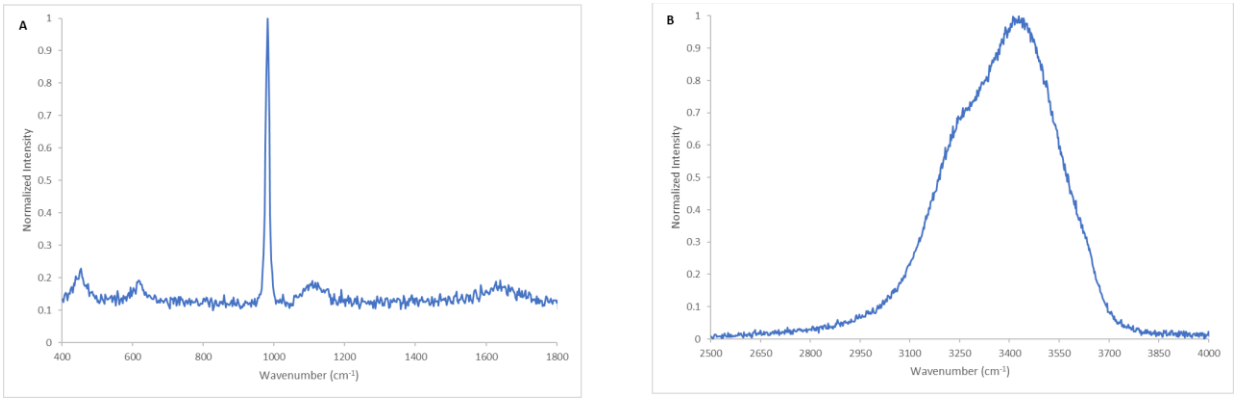

Figure 1: The main peak positions of a sulfate brine at both lower wavenumbers (A) and higher wavenumbers (B).

My research attempts to accurately determine the Raman spectra of various ice-brine and ice-sediment-brine mixtures, and catalogue differences in the spectra based on their composition and temperature. Using this technique, I aim to further our understanding of ice-sediment-brine systems on Mars and the geochemical processes which may impact recurring slope lineae. By studying the spectra of brines at low temperatures and/or with various levels of sediment incorporated, we can more accurately discern the nature of recurring slope lineae if they are encountered on Mars during future space missions. These missions may include the ExoMars mission that will consist of a Raman spectrometer and be launched by the European Space

Agency (Rull, 2017), or the Mars 2020 rover mission, which will be launched by NASA (Wiens, 2017).

I chose to investigate sulfate, perchlorate, and chloride brines because these salts are all prevalent on Mars (Massé, 2015), as are phyllosilicates, including kaolinite and montmorillonite (Ehlmann, 2011). Basalt is also present, and can weather to form clays (Milliken, 2009). Additionally, as Mars' average temperature ranges from 200 K to 295 K, changes in ice-brine and ice-sediment-brine mixtures become readily apparent.

Methodology:

Raman spectra were acquired using a Renishaw InVia High Resolution Raman microscope and spectrometer in conjunction with a Linkam THMS 600/720 temperature-controlled stage. Both a 785 nm (red) and 532 nm (green) laser (45 watts, Renishaw) were used at 1% laser power in streamline mode to gather data, using a 50x objective along with a 1200 l/cm grating. I collected data from twelve different solutions-- ultrapure water, $MgCl_2$, $MgSO_4$, $MgSO_4$-NaCl, $MgSO_4$-$NaClO_4$, Na_2SO_4, Na_2SO_4-NaCl, Na_2SO_4-$NaClO_4$, NaCl, NaCl-$NaClO_4$, and $NaClO_4$ brines. Each endmember brine was saturated with its respective salt at 295 K, while each mixed brine was composed of a 50/50 mix by volume of its respective saturated endmembers. I acquired spectra by focusing the laser on a 0.4 mL sample of brine placed within a quartz crucible within the Linkam heating/cooling stage. The laser was focused just below the surface of the sample when liquid and focused on the surface of the solids which formed at lower temperatures.

Data gathered from these twelve solutions included spectra collected over a range of temperatures, following the same series of steps. I first collected spectra over three different

spectral ranges at 295 K-- first an extended scan between 100-4500 cm^{-1}, then a static spectra-- centered at 700 cm^{-1} for the 785 nm laser and 1450 cm^{-1} for the 532 nm laser-- to collect peaks that occur at low wavenumbers around 100-1000 cm^{-1}, and then another static spectra-- centered between 3250 cm^{-1} and 3450 cm^{-1}, regardless of the laser-- to observe peaks present at higher wavenumbers around 3000-4000 cm^{-1}.

I then lowered the temperature to 200 K at a rate of 100 K/min, and proceeded to collect an extended spectra from 100-4500cm^{-1} before raising the temperature to approximately 5 K below the melting point of the respective solution being tested (see Table 1 for melting points), where extended spectra were then collected at 1 K increments until the temperature was 5 K above the approximate melting point of the solution. During these smaller temperature adjustments around the melting point, the temperature changed at a rate of at least 20 K/min. Melting points were determined beforehand, using a separate sample of solution, by gradually warming the sample until it was approximately 5 K below the melting point reported in the literature. The temperature was then increased in increments of 1 K until a slushy to aqueous consistency was observed in the sample. The temperature at which this slushy or aqueous consistency was first observed was classified as the experimentally derived melting point for that respective solution.

Once this initial series of extended spectra was collected, I lowered the temperature back to 200 K, and collected a static spectrum from 100-1000 cm^{-1} for 100 seconds and repeated the same temperature path used for the extended spectra. This process was repeated once more to collect static spectra from 3000-4000 cm^{-1}. Finally, the temperature was raised to 295 K, where I collected spectra again at both low and high wavenumbers, as well as over the extended range to see if there were any changes that occurred compared to the spectra I collected before repeated

freezing and thawing. In cases where both solid and liquid were present in a sample simultaneously, two spectra were taken-- one of a location on the sample where the solution was solid, and one location on a different part of the sample where the solution was liquid. Individual samples of each solution were used to test each of the two lasers. This process took four to five hours to complete per laser per solution and was repeated with both the red and green lasers for ultrapure water and each of the eleven brines.

I used WiRE 4.1 spectral processing software to process and analyze the spectra. In some cases, cosmic gamma rays were present in the spectra due to random interactions of cosmic rays with the detector. This interaction created abrupt and random spikes in the data. These spikes were mitigated by using the "zap" feature to edit the spectra, whereby the affected parts of the spectra where cosmic rays were present were trimmed so that the cosmic ray peaks were removed from the data. I also used WiRE to subtract the baseline, by fitting the baseline through fixed points on the spectrum and treating it as a fourth order polynomial. I then normalized the intensity range of each spectra to a value between 0 and 1 to maintain consistency between all spectra. Curve fits were also completed in WiRE for spectra of interest to determine peak positions.

I conducted similar experiments to investigate the effects of sediment on the Raman spectra. We selected two clay standards from the University of Oklahoma's research collection which had been obtained from the Clay Minerals Society-- montmorillonite and kaolinite. The montmorillonite used (STx-1) was sourced from Gonzales County, Texas; the kaolinite (KGa-1) from Washington County, Georgia. I also used a subset of the brines analyzed in the freezing experiments. Five of the twelve solutions-- ultrapure water, $CaCl_2$, $MgCl_2$, $MgSO_4$-$NaClO_4$, and Na_2SO_4-NaCl-- that were used in the ice experiments were also used here, as they collectively

provided insight into all seven individual endmember compositions without having to test each individual solution again. Through trial and error, I determined the appropriate sediment-brine ratio that would allow the sample to be saturated without water pooling or drying up too quickly, in order to more easily acquire spectra; 0.2 grams of montmorillonite mixed with 280 µl (0.28 mL) of solution created a sediment-brine mix with the consistency of paste. This same ratio was used for the kaolinite and yielded a consistency more analogous to wet paint.

I measured Raman spectra from the mixed sediment-brine samples using both the red and green lasers at 1% power in streamline mode. Extended spectra (100-4500 cm^{-1}) and low wavenumber spectra (focusing on the 100-1000 cm^{-1} range) were collected using both lasers. Spectra focusing on higher (3000-4000 cm^{-1}) wavenumbers were also taken with the green laser, as well as spectra focusing on the 1644 cm^{-1} water peak-- if present-- for the red laser. Thus, we collected five to six types of spectra per brine between both lasers.

The ice-sediment-brine experiments followed a similar, but not identical, temperature path to the ice-brine experiments. Spectra were first taken at 295 K, before the temperature was dropped to 200 K at a rate of 100 K/min. I then raised the temperature in increments of 10 K at a rate of 100 K/min, except for when the temperature was within 3 K of the melting point of the brine-- in this case, the temperature interval was changed to 1 K, and was raised at a rate of 20 K/min. This process was repeated three times to collect spectra over the extended range, as well as static spectra at low and high wavenumbers. I used a fresh sample of sediment-brine mix for each temperature path to avoid potential complications from evaporation during repeated freeze-thaw cycles. The ice-sediment-brine data were processed to subtract the baseline and normalize the intensity using WiRE software. In this case, the Raman spectra collected from the ice-sediment-brine experiments were processed in a similar way that the ice data were, except that

while the baseline was fitted through fixed points as a fourth order polynomial for the ice spectra, it was fitted using intelligent fitting for all sediment spectra. This allowed the peaks in the sediment spectra to be more easily identified.

Evaporation tests were also conducted by separately mixing 0.28 mL of ultrapure water with 0.2 grams of each of the sourced clays. A sample of 0.28 mL of ultrapure water with no sediment was also created. The samples were mixed in the same way as those used for sediment experiments were and were weighed on a scale once every hour for ten hours. The samples were also weighed after twenty-three and twenty-four hours of evaporation. This allowed for evaporation rates for each clay and ultrapure water to be easily determined.

Results:

Spectra from different brine compositions:

In liquid brines, sulfate and perchlorate salts showcase distinct spectra. Liquid chloride brines, on the other hand, generally do not produce indicative features (Figure 2), with their spectra being most like that of ultrapure water (UPW).

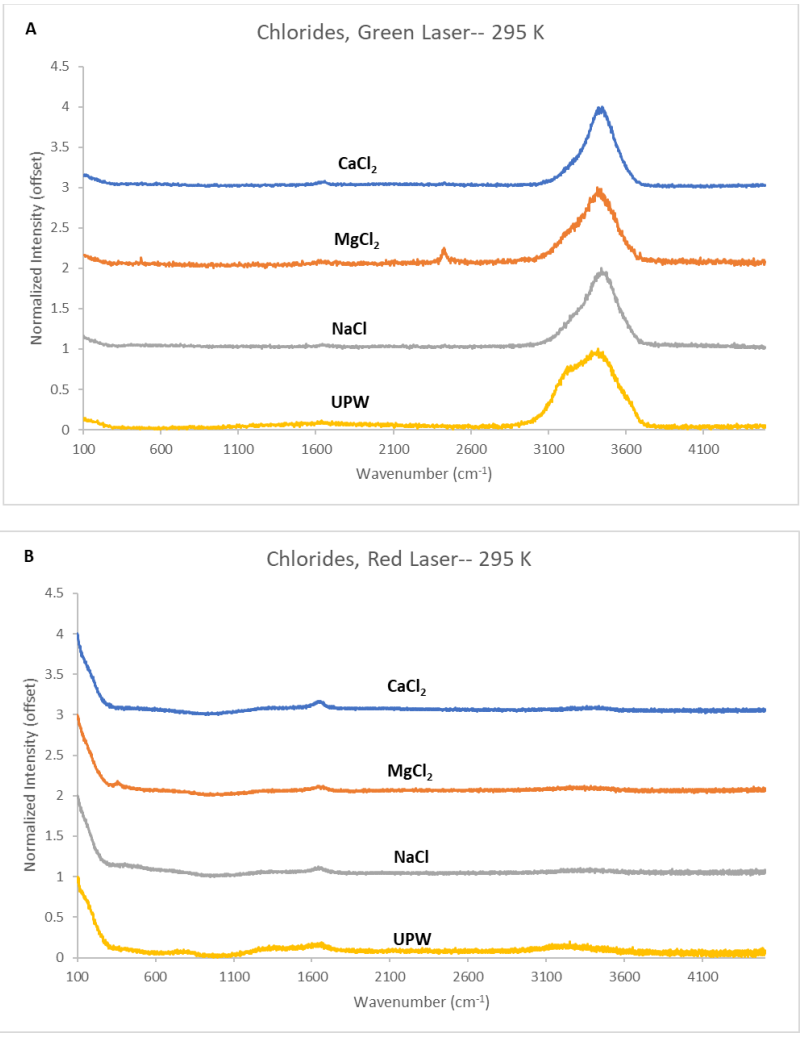

Figure 2: Chloride brines produce similar spectra when compared with each other and compared to ultrapure water, using both the 532 nm green (A) and 785 nm red (B) lasers. No major differences are observable with either laser, though slight differences are observed with

the 532 nm laser between 3050 cm^{-1} and 3450 cm^{-1}. The peak around 2400 cm^{-1} for the magnesium chloride taken with the 532 nm laser is an artefact of fluorescence from artificial lighting-- as determined using a blackout curtain-- and is not indicative of magnesium chloride.

The 532 nm laser yielded slightly different spectral results than its 785 nm counterpart. In all cases, the 532 nm green laser has a much more prominent water peak in the higher wavenumbers than the 785 nm red laser. This peak maximizes around 3430 cm^{-1} for the 532 nm laser and around 3213 cm^{-1} for the 785 nm laser when sampling ultrapure water (Figure 3), with other prominent but slightly less intense ultrapure water peaks at 3205 cm^{-1} and 3436 cm^{-1}, respectively. This ~3200 cm^{-1} peak is generally consistent with a symmetric OH-stretch of the water bonds (Duričković, 2011; Yang, 2019), while the ~3400 cm^{-1} peak is generally consistent with an asymmetric OH-stretch (Duričković, 2011). The 532 nm laser's ~3200 cm^{-1} band maximizes around 3230 cm^{-1} for the chloride brines, while the ~3400 cm^{-1} band maximizes around 3440 cm^{-1} for all samples.

Other peaks are prominent in the spectra produced by both the 532 nm and 785 nm lasers, including the main sulfate and perchlorate peaks, as well as several other minor peaks indicative of these two brines. When aqueous, the main sulfate peak is centered at approximately 982 cm^{-1}, regardless of which laser is being used. The main perchlorate peak is centered around 938 $\pm$2 cm^{-1}.

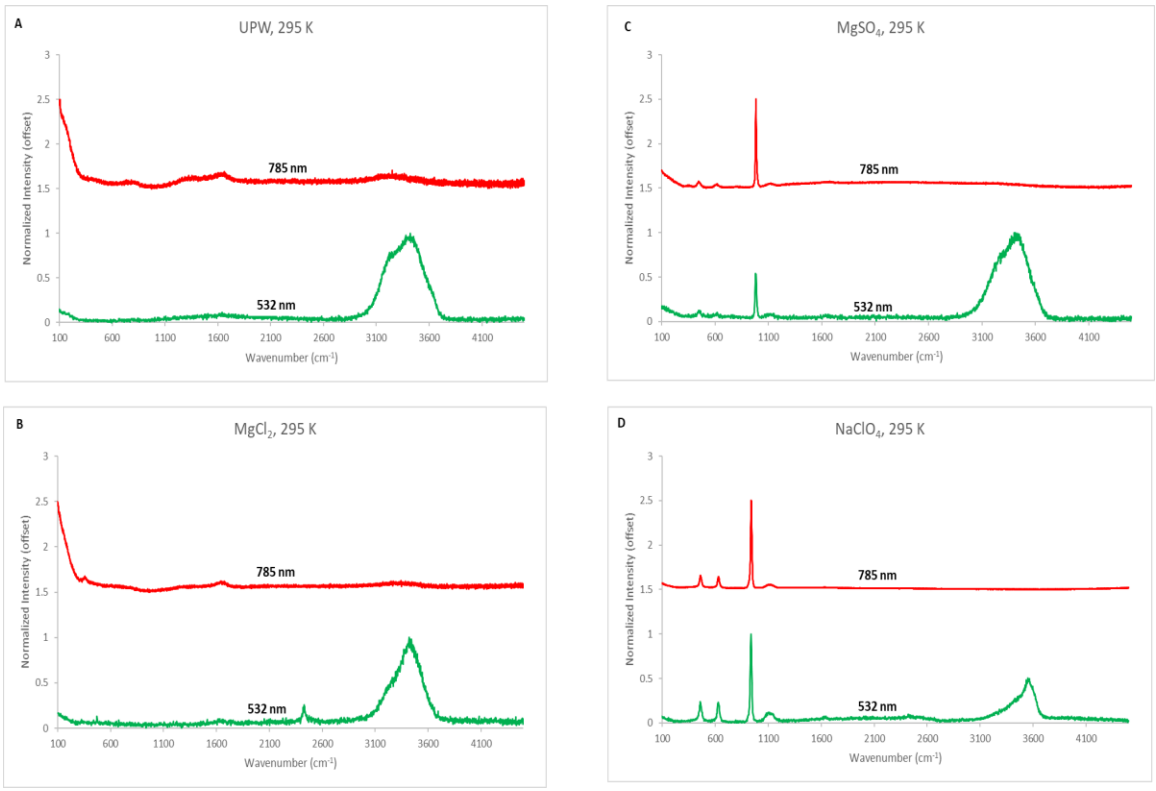

Figure 3: Spectra of A) ultrapure water (UPW), as well as B) chloride ($MgCl_2$), C) sulfate ($MgSO_4$), and D) perchlorate ($NaClO_4$), brines taken at 295 K with a 785 nm red laser and a 532 nm green laser. The peak around 2400 cm^{-1} in the magnesium chloride 532 nm laser spectra is an artefact from artificial fluorescent lighting and is not indicative of magnesium chloride.

Therefore, anion chemistry produces distinct Raman peaks at different wavenumbers. In addition, the location, intensity, and shape of some peaks change with temperature and may be used to differentiate between liquid brines and ices. Both solid and liquid peak positions associated with each solution are outlined in the appendix in Table A1.

Melting Points:

As temperatures increased from 200 K, the samples melted from a solid to a liquid state. In most cases, the experimentally derived melting point was within $\pm$2 K of the literature-derived melting point (Table 1). The two notable exceptions to this rule are a) $CaCl_2$, which has an experimentally derived melting point of 219 K, but a literature-derived value of 223 K, and b) $MgSO_4$-NaCl, whose constituent endmembers have melting points of 270 K and 250 K, respectively, but which when mixed in a 50/50 ratio has a melting point of 236 K.

Table 1: Melting Points of Brines

Brine	Melting T (K): This Study	Eutectic T (K): From Literature
$CaCl_2$	218-219	223 (Möhlmann, 2011)*
NaCl-$NaClO_4$	232-233	-----
$MgSO_4$-$NaClO_4$	234	-----
Na_2SO_4-$NaClO_4$	235-236	-----
$NaClO_4$	235-237	238.9 (Toner, 2014)
$MgSO_4$-NaCl	236-237	-----
$MgCl_2$	239-240	240.2 (Toner, 2014)
Na_2SO_4-NaCl	250-251	251 (Möhlmann, 2011)*
NaCl	251-252	251 (Möhlmann, 2011)*; 251.9 (Toner, 2014)
$MgSO_4$	270-271	269 (Möhlmann, 2011)*; 269.4 (Toner, 2014)*
Na_2SO_4	271-272	271 (Möhlmann, 2011)*; 271.8 (Lewis, 2010)*
Ultrapure water	274	273.2 (Chevrier, 2012)

**hydrated phase explicitly stated in literature*

Ices:

Spectra look markedly different at 200 K when ice forms. This is observed with each of the Mars-analogue brines tested, using both the 532 nm and 785 nm lasers. For example, both $MgCl_2$ and ultrapure water show the appearance of distinct peaks at lower wavenumbers when the temperature is dropped to 200 K (Figure 4). While these peaks are much more apparent with the 785 nm red laser, they are also present with the 532 nm green laser.

A similar change can be seen using the 532 nm green laser when observing the ~3200 cm^{-1} peak for each of the brines in Figure 4. When each brine is liquid, an asymmetric bump appears at the higher wavenumbers of each spectra. When these brines are frozen into ice, these bumps become much more jagged and showcase several sharp peaks (Figure 4). In the case of either the sodium perchlorate or magnesium sulfate-sodium perchlorate mix, for example, these sharp peaks include a very intense peak at ~3600 cm^{-1}, a characteristic peak associated with solid sodium perchlorate brine.

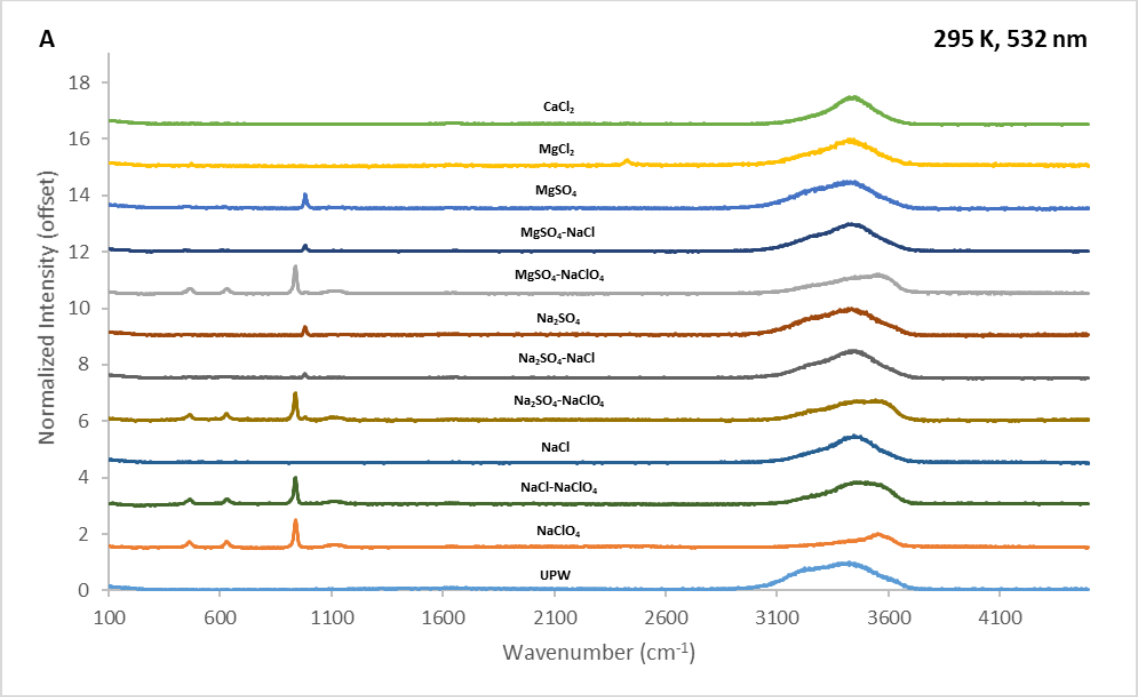
A
295 K, 532 nm
Normalized Intensity (offset)
Wavenumber (cm-1)
CaCl2
MgCl2
MgSO4
MgSO4-NaCl
MgSO4-NaClO4
Na2SO4
Na2SO4-NaCl
Na2SO4-NaClO4
NaCl
NaCl-NaClO4
NaClO4
UPW

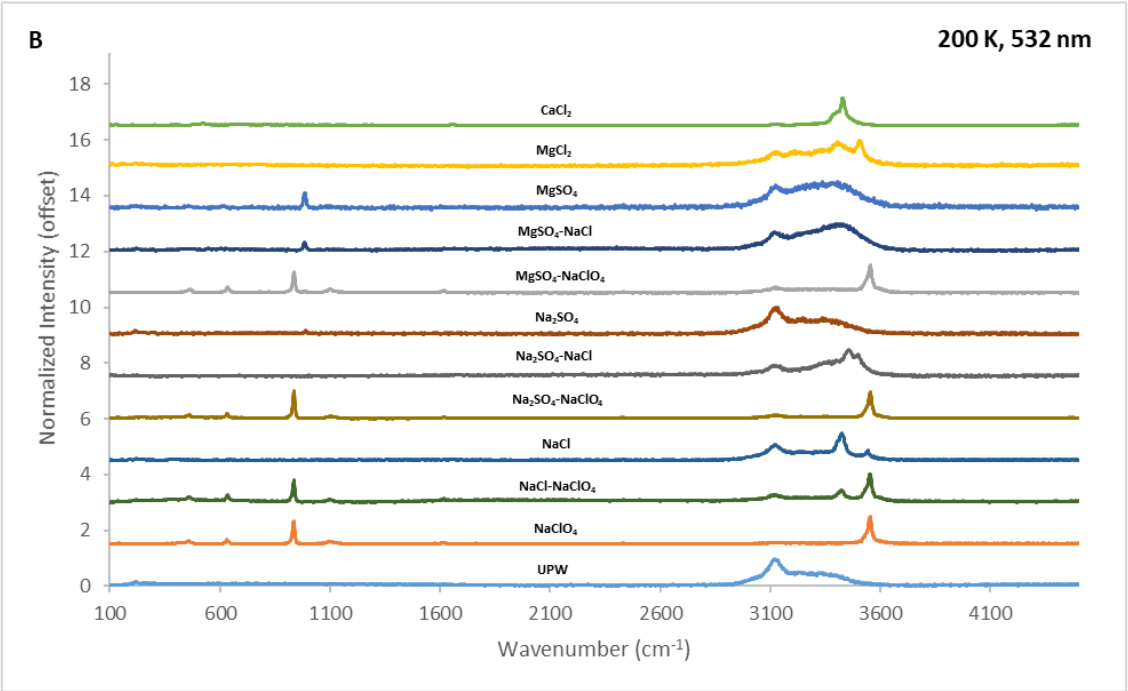
B
200 K, 532 nm
Normalized Intensity (offset)
Wavenumber (cm-1)
CaCl2
MgCl2
MgSO4
MgSO4-NaCl
MgSO4-NaClO4
Na2SO4
Na2SO4-NaCl
Na2SO4-NaClO4
NaCl
NaCl-NaClO4
NaClO4
UPW

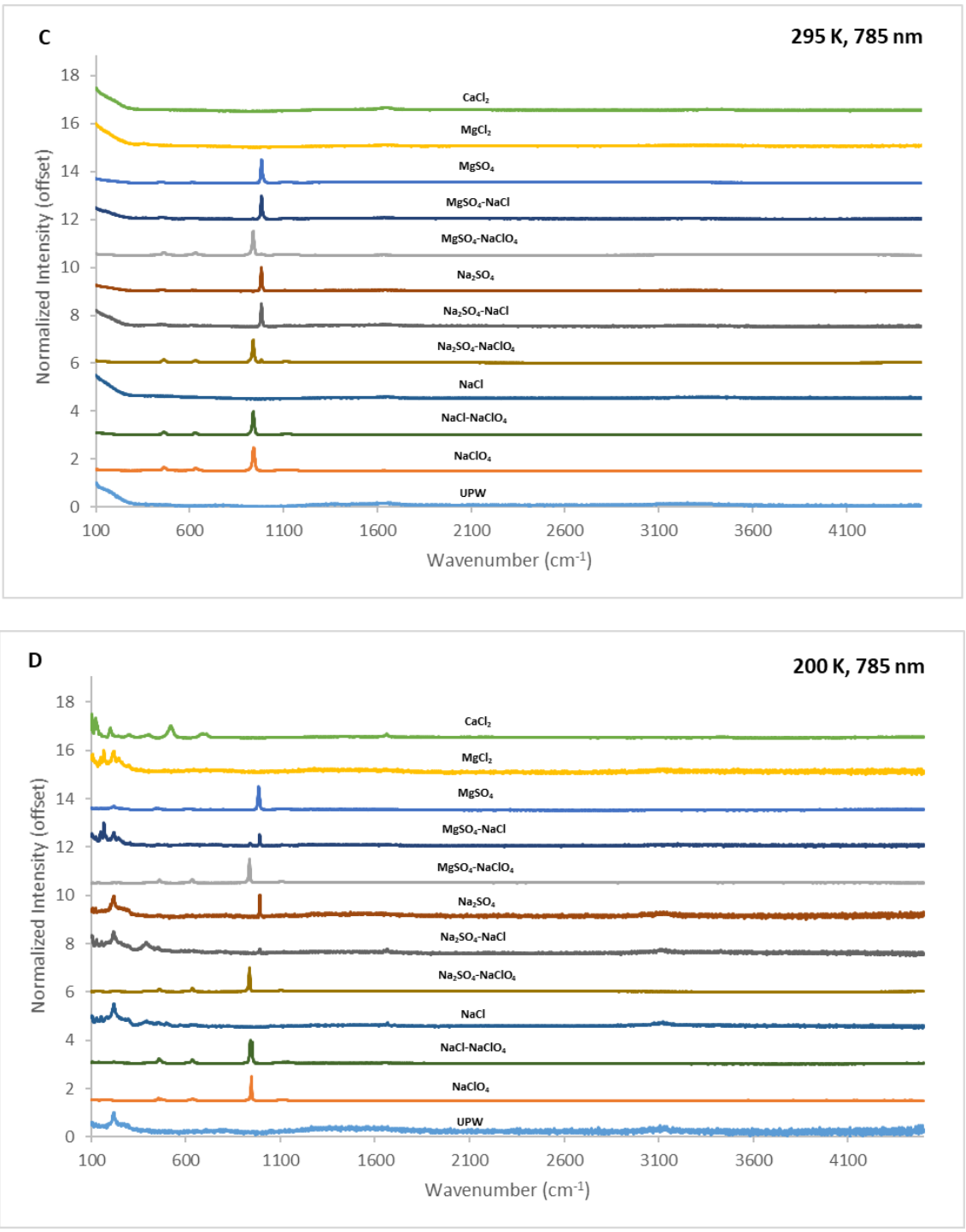

Figure 4: Extended scans of all twelve saturated brines that were tested with both the 532 nm green laser (A and B) and 785 nm red laser (C and D), as well as at both 295 K (A and C) and 200 K (B and D).

Partial Melting:

Each of the twelve brines tested experienced temperatures at which both solid and liquid were present in the sample simultaneously. This occurred at or within a couple degrees of the melting points of each brine. In some cases-- such as with $CaCl_2$ (Figures 5A, 5B, 5D, and 5E) or $NaClO_4$ (Figures 5C and 5F)-- the spectra acquired in the few degrees above the melting point even continued to appear more similar to the ice spectra than to the liquid spectra. This occurred, at various times, with both the 532 nm and 785 nm lasers.

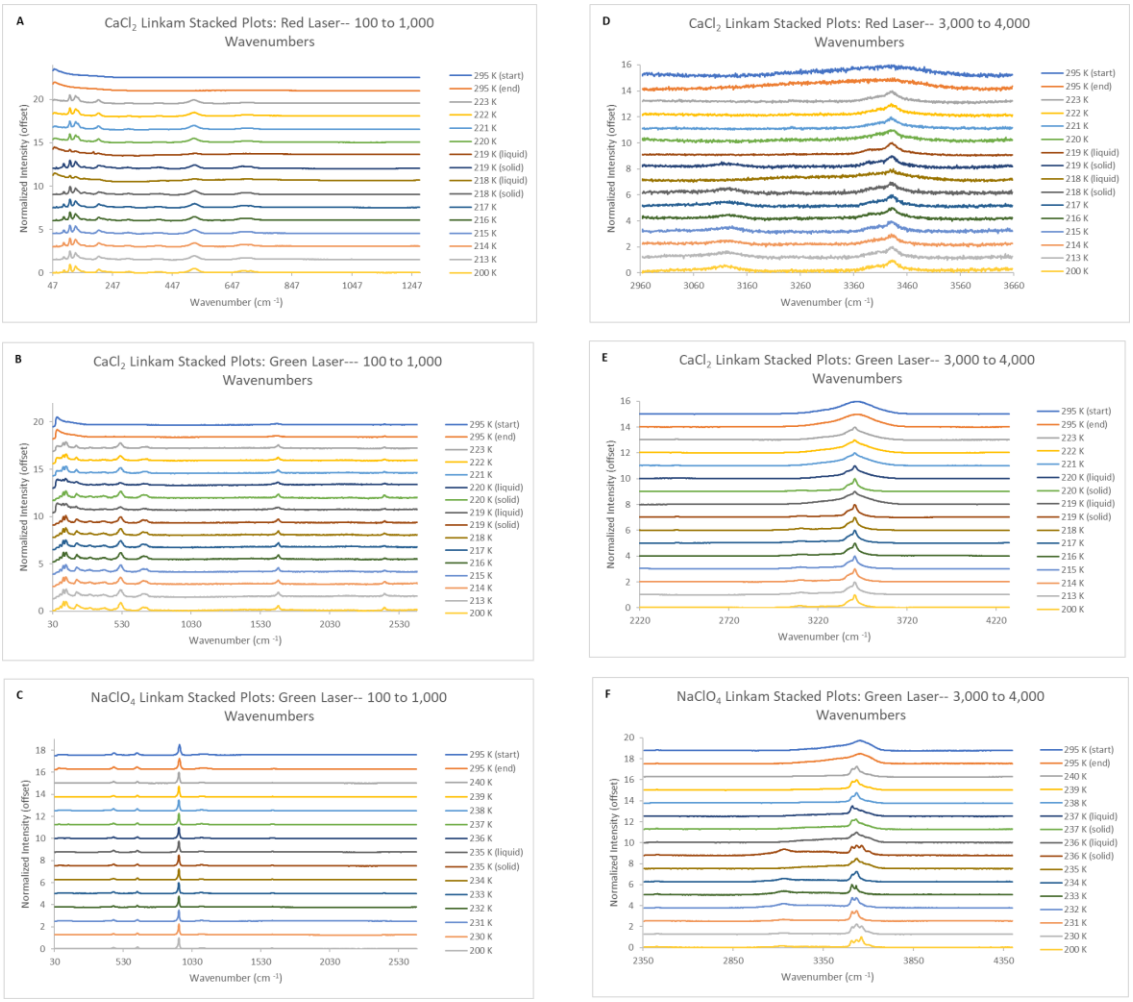

Figure 5: The partial melting of $CaCl_2$ and $NaClO_4$ can be seen near their respective melting points with multiple spectra taken at the same temperature.

Mixed Brines:

In the case of the mixed brines, differences in the shape and position of the peak maximum observed for the ~3400 cm^{-1} OH-band between the two endmembers is readily apparent (Figure 6). For example, at 295 K, the peak maximum is observed at 3438 cm^{-1} in saturated endmember $MgSO_4$ brine and 3453 cm^{-1} in saturated endmember NaCl. However, in the mixed $MgSO_4$-NaCl solution, the peak maximum is observed at an intermediate wavenumber-- 3443 cm^{-1}. At 200 K, the curve for the $MgSO_4$ endmember brine maximizes at 3370 cm^{-1}, while the NaCl endmember peak maximizes at 3424 cm^{-1}. Again, the $MgSO_4$-NaCl mixed brine maximizes at an intermediate value-- 3406 cm^{-1}.

In both cases, the peak of the mixed brine maximizes at a point between its two respective endmembers, regardless of the temperature at which the brine is observed. However, this trend is not apparent when the liquid brines and ices are observed with the 785 nm laser since the 785 nm peaks at higher wavenumbers are much less discernable from the background noise.

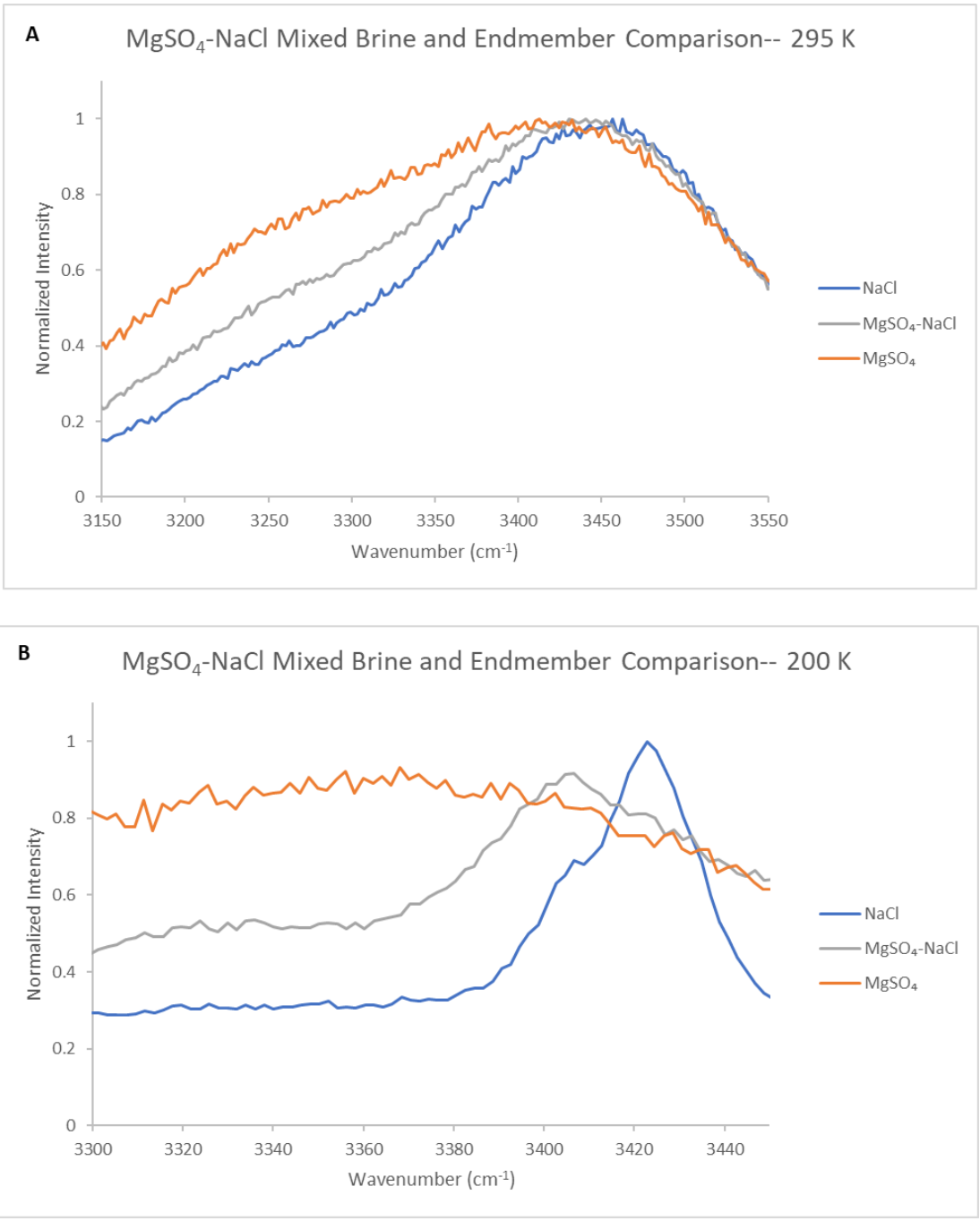

Figure 6: The shift in the OH-stretching band between $MgSO_4$, NaCl, and $MgSO_4$-NaCl solutions at 295 K (A) and at 200 K (B) when using the 532 nm green laser.

However, a different pattern is observed in mixed sulfate-perchlorate brines (Figures 7A and 7B). The minor sulfate peaks appear at approximately 460 cm^{-1}, 611 cm^{-1}, 1095 cm^{-1} and

1133 cm^{-1} (Wang, 2006) when $MgSO_4$ is solid, and at 451 cm^{-1}, 617 cm^{-1}, and 1113 cm^{-1} (Wang, 2006) when $MgSO_4$ is aqueous; the minor perchlorate peaks appear at approximately 461 cm^{-1}, 626 cm^{-1}, and 1095 cm^{-1} (Nebgen, 1965). In the experiments where sulfate and perchlorate brines are mixed, it appears that the ~460 cm^{-1} perchlorate peak maximizes between 460 cm^{-1} and 464 cm^{-1} (regardless of temperature) and that the ~620 cm^{-1} perchlorate peak maximizes between 630 cm^{-1} and 635 cm^{-1} (regardless of temperature). These peak positions are heavily skewed toward being more consistent with what would be expected of perchlorate peaks. The ~1110 cm^{-1} sulfate peak, however, shifts from ~1100 cm^{-1} when solid, to ~1115 cm^{-1} when liquid. This could be consistent with either brine.

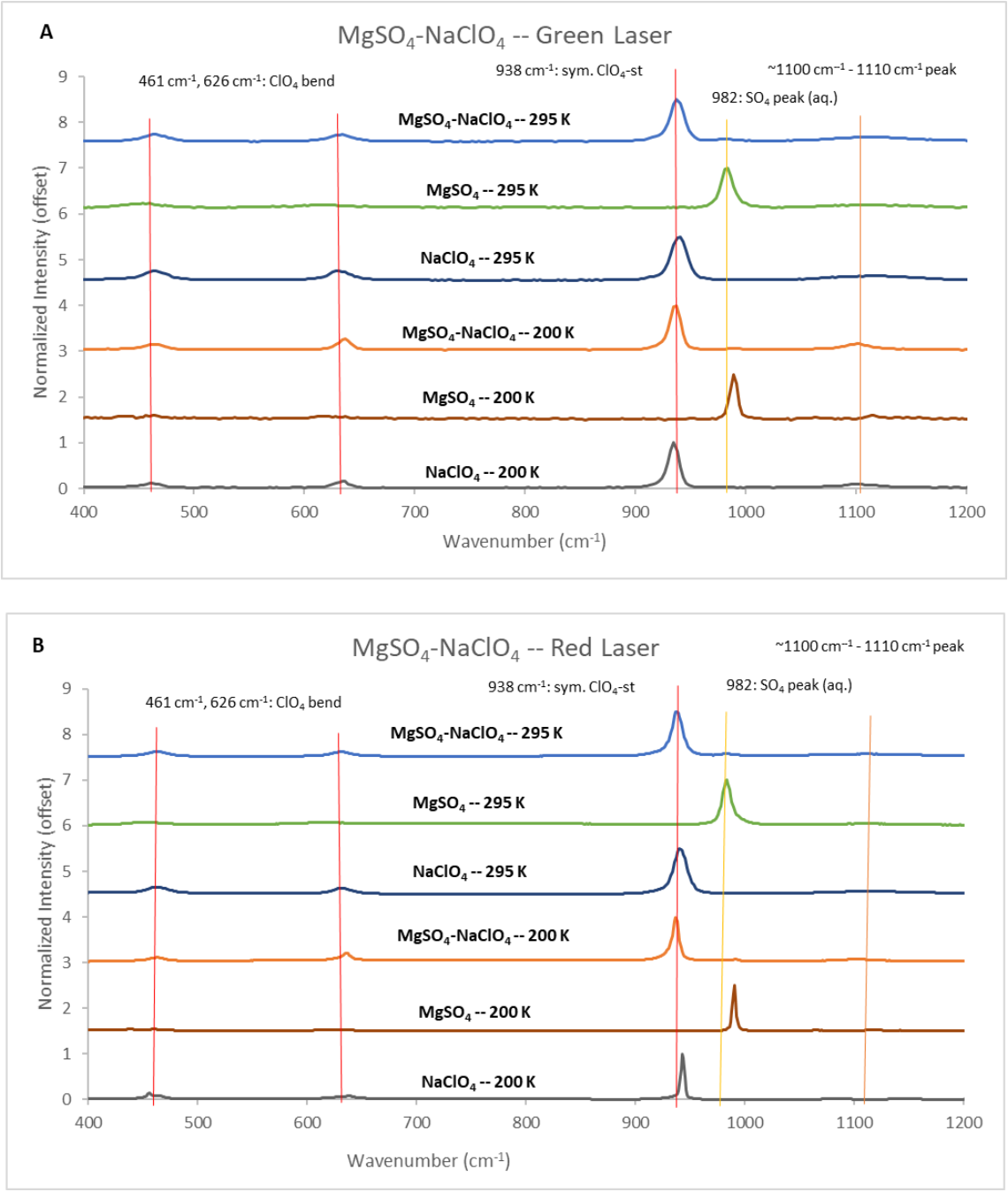

Figure 7: The minor peaks in sulfate-perchlorate mixed brines. While the two lower peaks more closely align with the perchlorate peak positions regardless of temperature, the higher ~1110 cm^{-1} peak could be consistent with either brine.

Figure 8A shows a sulfate-perchlorate mix. The peaks that appear when the endmember brines are liquid maximize at a value between the two endmembers when the brines are mixed. Similar trends are observed when the brines are ice.

Mixed brines other than sulfate-perchlorate mixes also show distinct changes between their solid and liquid forms. This mixed brine behavior is observed in the sulfate-chloride brine mix (Figure 8B). The solid magnesium sulfate spectra collected at 200 K contains an OH-stretch band that maximizes around 3100 cm^{-1} when solid and a second OH-stretch band that maximizes around 3400 cm^{-1}. The solid sodium chloride (200 K) displays this same 3100 cm^{-1} OH-stretch band, but it also contains a sharp peak just past 3400 cm^{-1}, as well as a smaller peak around 3550 cm^{-1}. Peaks similar to both endmembers are observed in the sulfate-chloride mixed brine, which-- in addition to showcasing the 3100 cm^{-1} bump found in both spectra-- appears to gradually increase in intensity (similar to the sulfate spectra) before jutting up with a less sharp peak around 3400 cm^{-1} (similar to the chloride) before finally producing a sharp peak again at 3550 cm^{-1}, again similar to the chloride. The mixed brine is a combination of its two respective endmembers, and components of both endmember compositions are observed to occur simultaneously in the mixed brine's spectra.

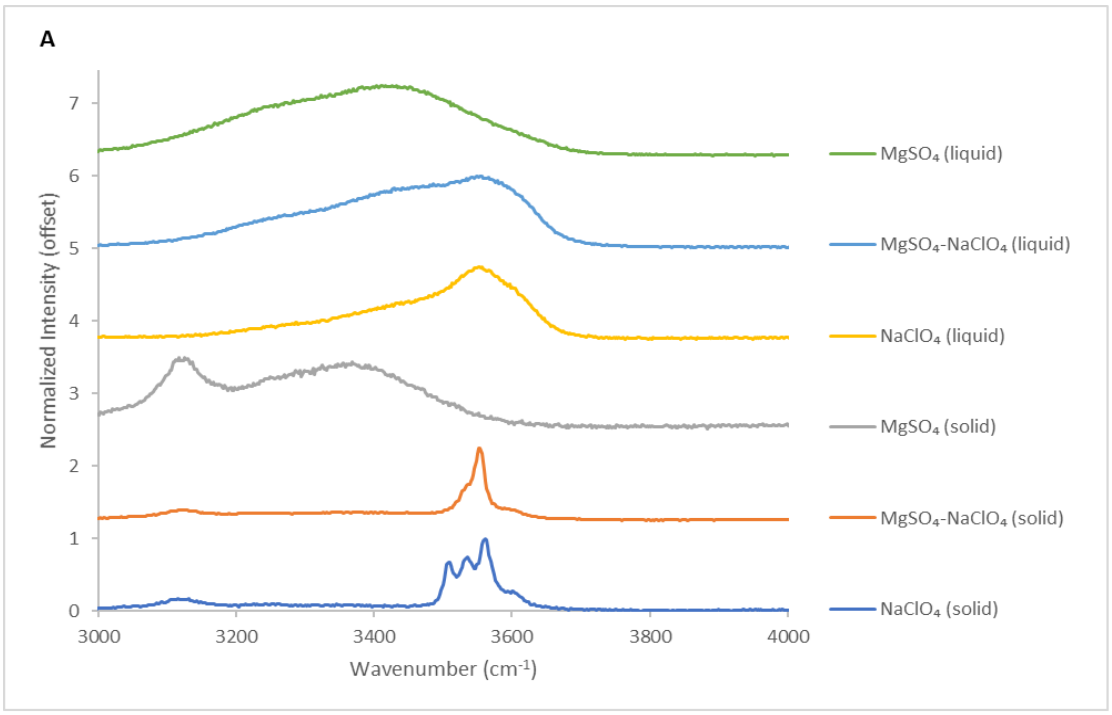

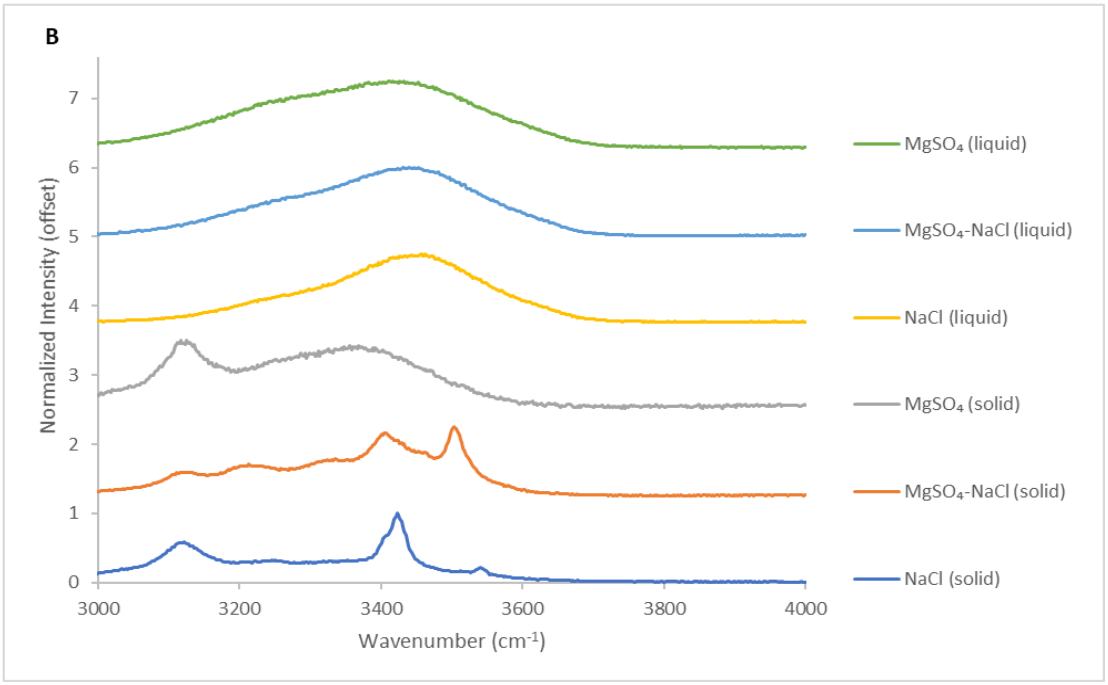

Figure 8: A comparison of both the solid and liquid phases of the $MgSO_4$-$NaClO_4$ (A) mixed brine and the $MgSO_4$-NaCl (B) mixed brine, showcasing how each of the mixed brines' spectra show telltale signatures of both respective endmember compositions using the 532 nm green laser.

Freezing Rates:

Differences in peak position between the solid and liquid sulfate spectra were also observed when the brines were cooled at different rates. In the liquid brines, the sulfate peak is reliably observed at 982 cm^{-1}. When solid, the position of the peak shifts to higher wavenumbers. However, the exact position of the peak varies depending upon the rate of cooling (Figure 9A). Slower cooling rates (10 K and 5 K/min) resulted in greater peak shift during freezing, with the sulfate peak observed around 990 cm^{-1} in the frozen brine. More rapid cooling (100 K and 20 K/min) resulted in a smaller peak shift, with the sulfate peak in the frozen brine observed around 987 cm^{-1}.

Within this bimodal distribution, slight shifts in the exact peak position are also apparent between samples (Figure 9B) cooled at the same rate. $MgSO_4$ cooled at 100 K/min exhibited-- at various times-- peak positions of 985 cm^{-1}, 987 cm^{-1}, and 989 cm^{-1}, depending on the sample being tested. Nevertheless, this is generally consistent with both the bimodal distribution that was observed, as well as being within the margin of error expected from spectroscopic measurements.

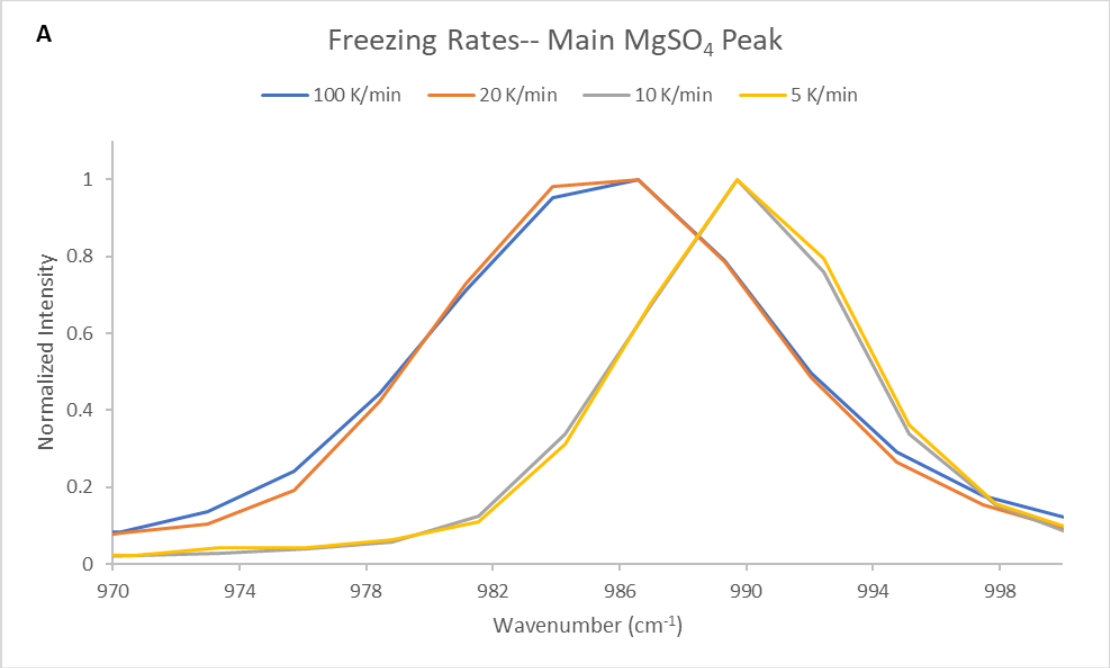

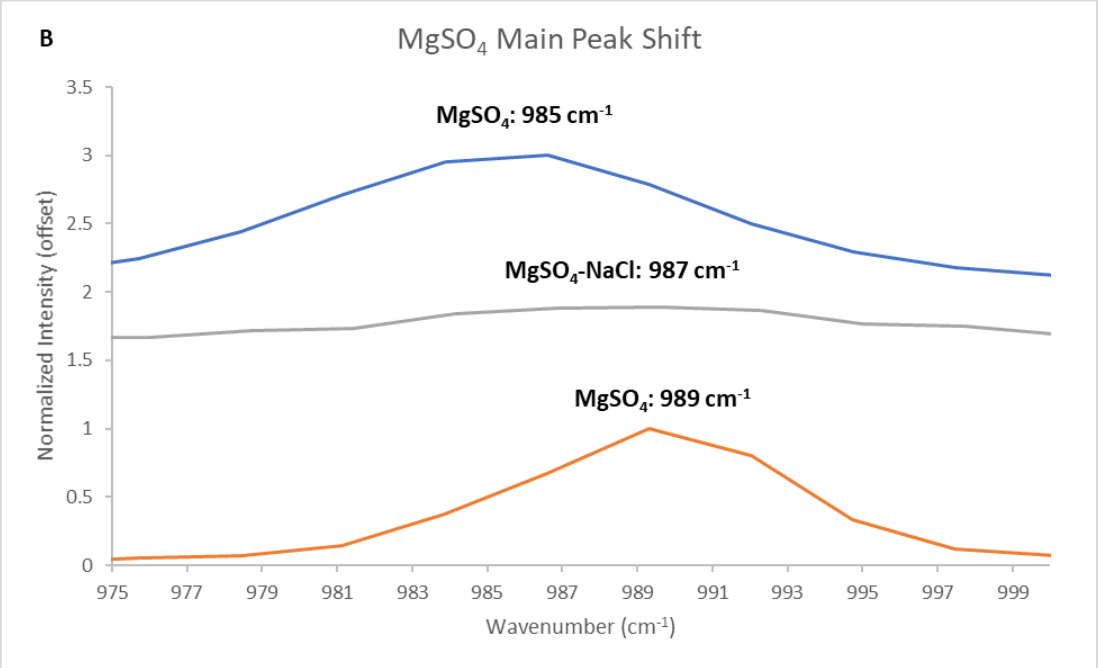

Figure 9: The peak position of the main $MgSO_4$ peak using the 532 nm laser at 200 K can show A) a bimodal distribution when different freezing rates are accounted for, while also showing B) a slight shift in the exact peak position between various samples of $MgSO_4$, after being cooled at a rate of 100 K/min.

Raman Analysis of Brines and Sediment:

The addition of sediment also affected the overall Raman spectral signature of the brines. Our samples used approximately equal amounts of sediment and brine (~2:2 to 2:3 ratio by weight). While the characteristic brine peaks are still noticeable, the spectra produced by the sediment predominates.

Figure 10 shows the overall spectral signature of montmorillonite, with distinct peaks at approximately 201 cm^{-1}, 432 cm^{-1}, and 709 cm^{-1} (Bishop, 2004), as well as at ~1260 cm^{-1}. The peaks indicative of montmorillonite are clearly visible both when the clay is dry and when it is mixed with a brine (Figure 10A). When mixed with sulfate, the sulfate peak from the brine at 982 cm^{-1} is also prominent. When the sediment-brine mixture is frozen, the intensity of the peaks at low wavenumbers increases and the sulfate peak position shifts to ~990 cm^{-1}, similar to the changes observed in the brine-only experiments.

When montmorillonite is mixed with magnesium chloride (Figure 10B) or ultrapure water (Figure 10C), the resultant spectra is clearly that of a wet clay, regardless of temperature or brine composition. When liquid, the clay-brine spectra appear slightly more intense than their respective dry spectra counterparts. The differences when the clay-brine mix is frozen, however, are even more pronounced, with several of the newly formed ice peaks below 450 cm^{-1} now visible for both the magnesium chloride and ultrapure water mixes. These newly formed peaks can be used to help differentiate both liquid clay-brine mixtures and frozen clay-brine mixtures of the same composition from one another, while also differentiating between compositionally different frozen clay-brine mixes. For example, at 200 K $MgCl_2$ showcases numerous peaks, while the ultrapure water showcases significantly fewer peaks at those same wavenumbers.

As was the case with the sulfate brine-montmorillonite mix, however, the montmorillonite spectrum predominates over the liquid or ice-brine spectra when clay and brine are mixed. This, again, leads to spectra that predominantly look like the spectra of their respective clays, but nonetheless showcase additional peaks consistent with their respective brines. The exact level of similarity, however, is dependent upon the brine in question. At a glance, for example, the spectra of sulfate and perchlorate clay-brine mixes are much more readily distinct from the spectra of their dry clay counterparts than the clay-brine spectra of the chlorides are to their dry counterparts, due to the intense anion peaks present in each of the former brines.

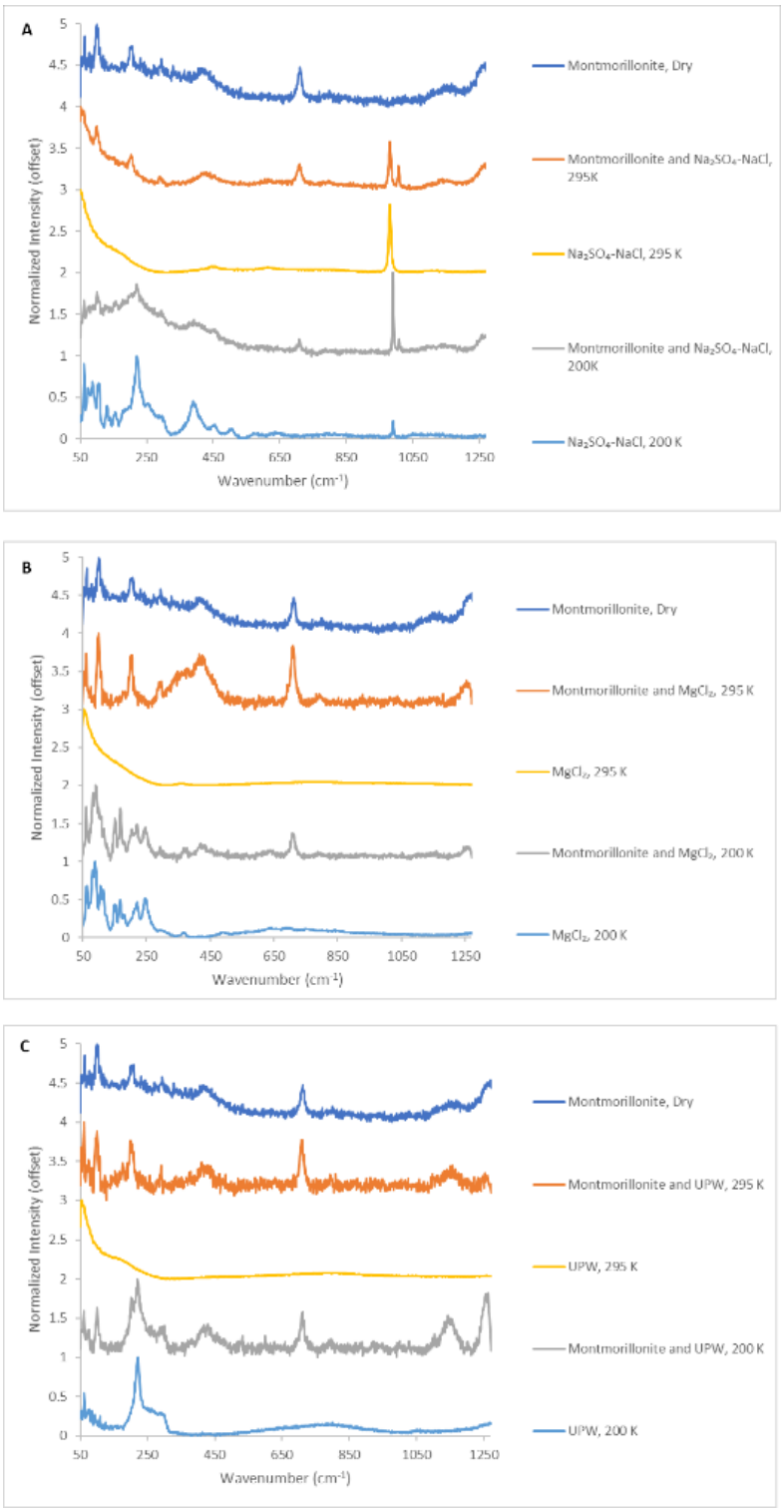

Figure 10: Spectra from the 785 nm red laser of 0.2 grams of montmorillonite mixed with 0.28 mL of Na_2SO_4-NaCl (A), $MgCl_2$ (B), or UPW (C) brine, as well as sediment-free liquid and

solid spectra of each respective brine. The wetted sediment spectra showcase distinct regions where both brine and clay peaks are visible simultaneously, namely in the wavenumbers below 450 cm^{-1}.

When the montmorillonite was mixed with sulfate-bearing brines, a new peak appeared around 1010 cm^{-1} (Figure 11). This peak was observed, using the 785 nm laser, when either the Na_2SO_4 or $MgSO_4$ endmember brine was mixed with montmorillonite, but not in the UPW-montmorillonite experiments (Figure 11A). The peak is also not present in spectra of the brine alone (Figure 11B) and is not readily apparent in any context with the 532 nm laser. This peak is consistent with the spectra of gypsum (780 nm laser excitation source, RRUFF database; Lafuente, 2015).

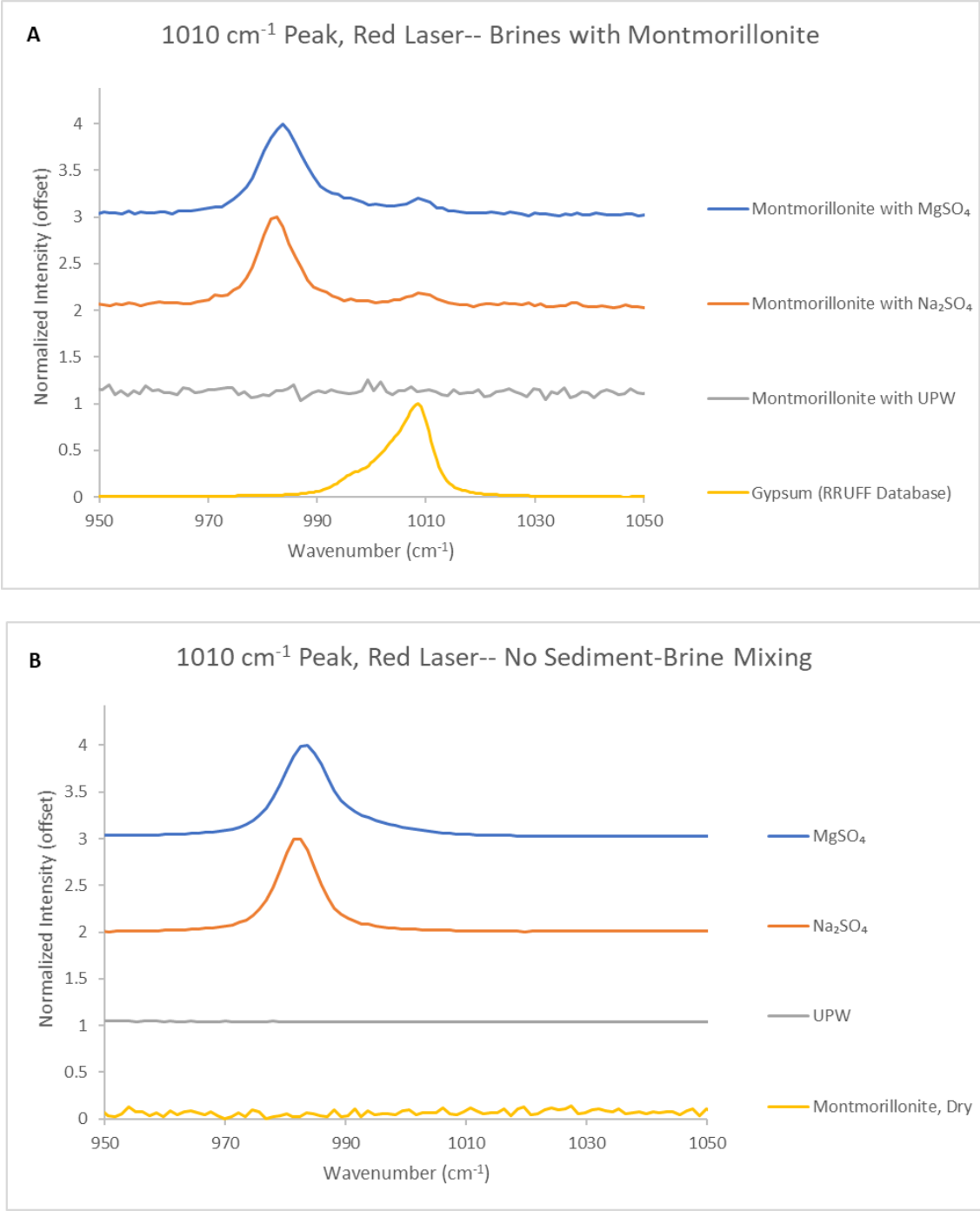

Figure 11: Using a 785 nm laser, the 1010 cm^{-1} peak is present in $MgSO_4$ and Na_2SO_4 when either is mixed with montmorillonite can clearly be seen just to the right of the main sulfate peak at 982 cm^{-1}. The 1010 cm^{-1} peak of gypsum can also be seen. The 1010 cm^{-1} is absent when ultrapure water is used, or when montmorillonite is not included in the brine mixtures.

Evaporation Experiments:

Water evaporated from the sediment-UPW experiments over the course of three to five hours (Figure 12), depending on the clay used. All the water had evaporated from the montmorillonite-UPW experiment within approximately four hours, at an average rate of 0.042 g H_2O/hr. leaving just the dried-out clay remaining (Figure 13). Kaolinite dried out within about three hours (Figure 14), at an average rate of 0.058g H_2O/hr, also leaving behind dry clay. Ultrapure water took around five hours to evaporate, at an average rate of 0.054 g H_2O/hr.

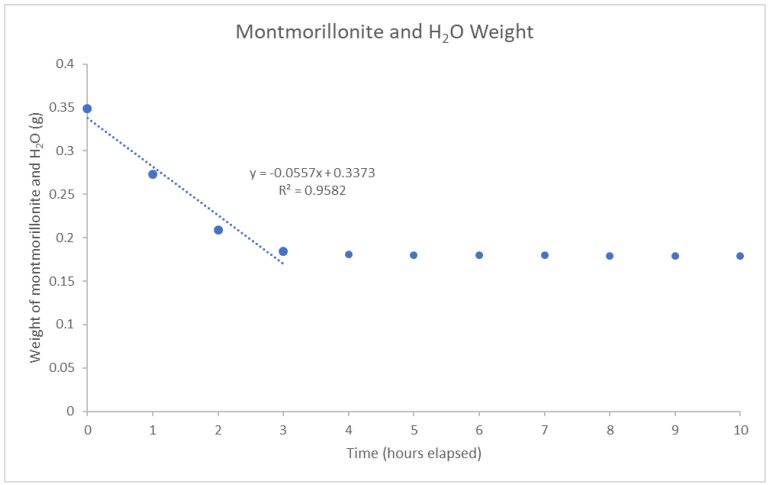

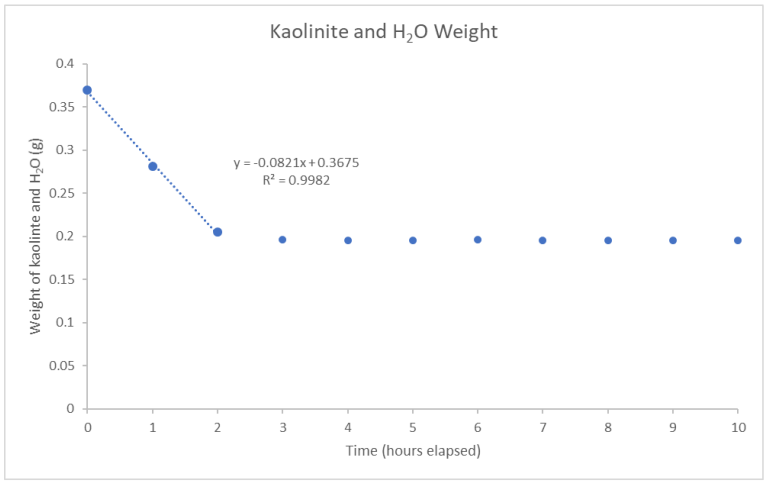

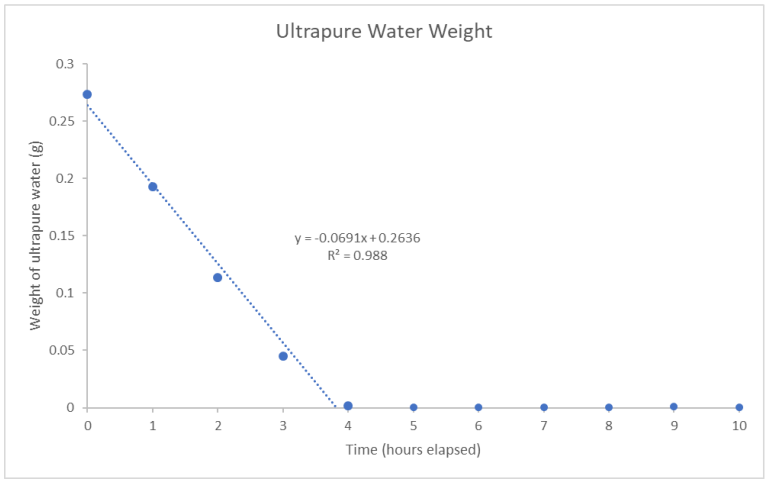

Figure 12: The loss of ultrapure water from a sample of montmorillonite (A), kaolinite (B), and with no sediment included (C); the starting composition was 0.205g $\pm$ 0.005 g of both montmorillonite and kaolinite, mixed with 0.28 mL of ultrapure water.

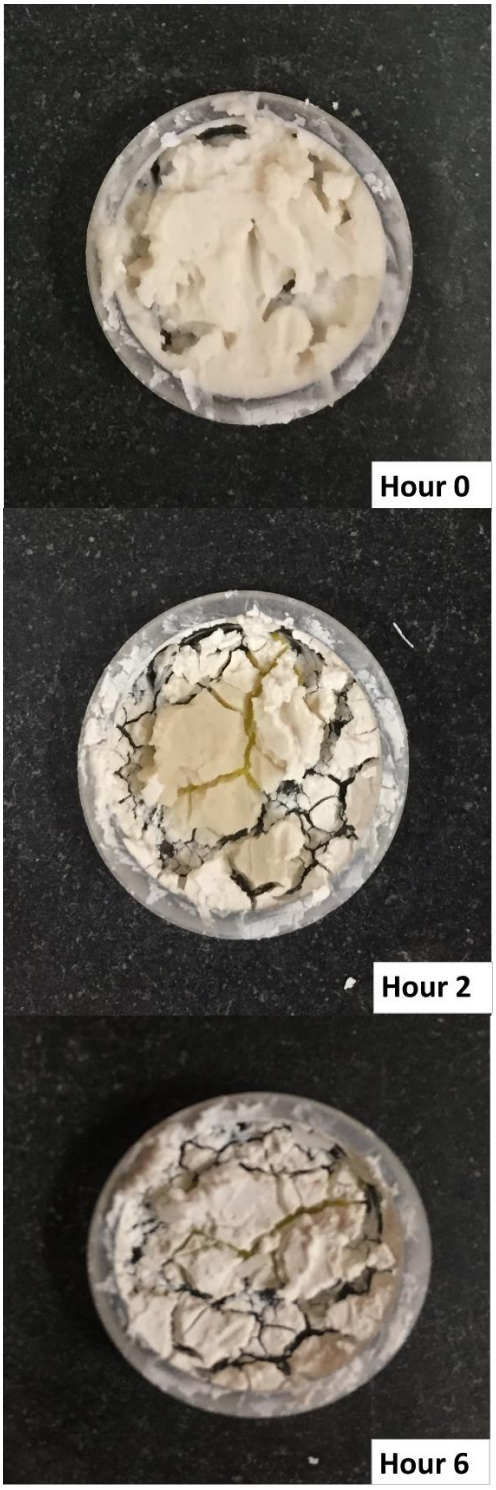

Figure 13: Montmorillonite with evaporating ultrapure water after zero, two, and six hours. The crucible measures 15 mm in diameter. As time progresses, the montmorillonite gradually forms cracks and dries.

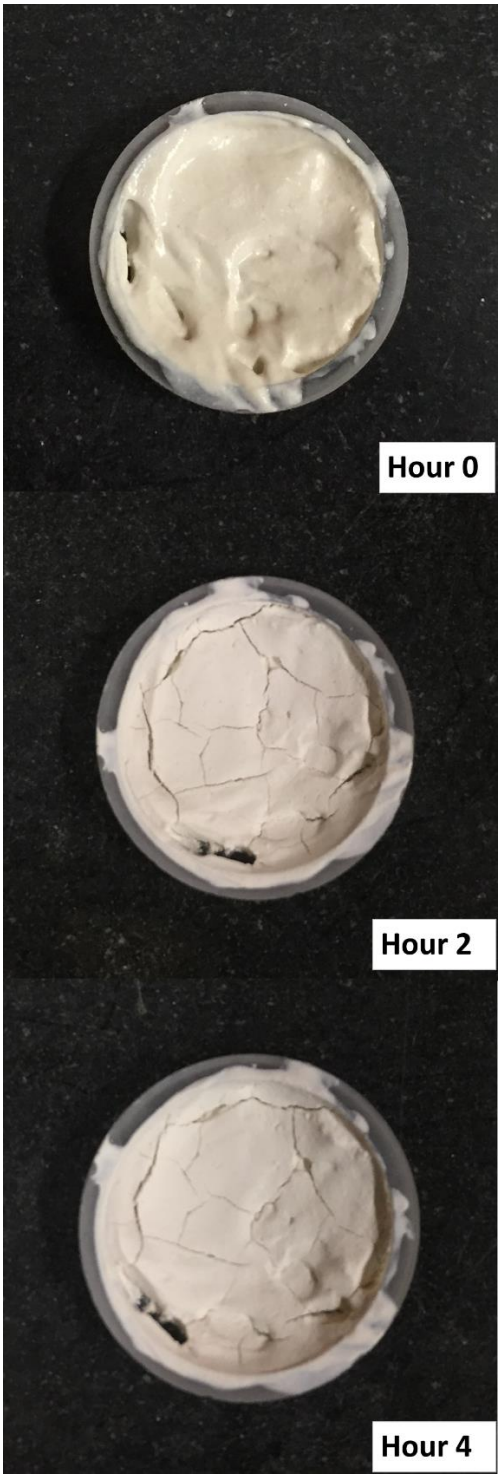

Figure 14: Kaolinite with evaporating ultrapure water after zero, two, and four hours. The crucible measures 15 mm in diameter. As time progresses, the kaolinite gradually forms cracks on its surface, though not as noticeable as those of the montmorillonite.

Discussion:

Peak Positions and Melting Points:

One of the first things notable about the Mars-analogue brines we used was the distinctiveness of many of the brines' spectra. While sulfate and perchlorate produced distinct spectra, chloride brines did not. This is largely due to the chloride anion not containing any covalent bonds.

The brine composition also influenced the melting points as expected. In addition, as the brines melt or freeze, the spectra changes significantly during the shift from solid ice to liquid brine. This solid-liquid (or vice versa) phase change would therefore imply an evolving spectrum evidenced by changes in peak location, shape, or intensity. Carried out *in situ* on Mars, these analyses would help to distinguish between liquid and frozen brines and could provide key information about past or present hydrologic processes, the capacity of an area for aqueous alteration, and/or the potential for habitability.

Two notable melting points are those of $CaCl_2$ and $MgSO_4$-NaCl, both of which had lower melting points than referenced in the literature. $CaCl_2$ had about a 4 K discrepancy between the experimentally and literature-derived melting points, with the former being the lower of the two (Table 1). This difference was slightly larger than it was for the other brines (which all melted at $\pm$2 K of the literature-derived values) and might be due to the much lower melting point of $CaCl_2$-- around 15 K lower than the melting point of the second-lowest brine tested, and almost 20 K lower than the endmember brine with the next-lowest melting point-- when compared to its higher melting temperature counterparts. $MgSO_4$-NaCl, conversely, had about a 14 K discrepancy between the experimentally derived melting point of the mixed brine

and that of NaCl, the endmember with the lower melting point. This discrepancy may be due to the formation of $MgCl_2$ (melting point of 240 K) in the mixed brine.

Ices:

Solid versus Liquid Peak Positions:

The frozen endmember brines are straightforward to interpret; many of their peaks are outlined in Table A1. The mixed brines, however, are more complicated, as their spectra typically appear as a mix of the spectra of their two endmember compositions. In the case of $MgSO_4$-NaCl, the high wavenumber peak of the mixed brine (as shown in Figure 6) maximizes at 3443 cm^{-1} when the brine is liquid, and 3406 cm^{-1} when the brine is solid. It is possible that this is due to the formation of $MgCl_2$ from the $MgSO_4$-NaCl mix, as the ~3400 cm^{-1} peak of the mixed brine is at an almost identical location and is of a very similar intensity to the ~3400 cm^{-1} peak of the $MgCl_2$ endmember brine, both when the samples are liquid and solid.

Peak position is also important to take note of when dealing with the minor peaks of sulfate and perchlorate. The ~460 cm^{-1} and ~620 cm^{-1} peaks (Figure 7) are more consistent with the average peak position of perchlorate, regardless of temperature. This could be due the perchlorate peaks being comparatively more intense than their sulfate counterparts, leading to prominent perchlorate peaks. This, in turn, may lead to sulfate peaks that, while present, have effectively become indistinguishable from background noise. This is consistent with the observation of how intense the main 938 cm^{-1} perchlorate peak is, even when compared to the otherwise very intense main 982 cm^{-1} sulfate peak.

This does not necessarily explain, however, the ~1110 cm^{-1} peak, which appears to shift from ~1100 cm^{-1} when solid to being closer to 1115 cm^{-1} as the temperature rises. While it was

unclear from the experiments we ran, both sulfate and perchlorate-- according to the literature-- can display peaks around 1100 cm^{-1} when solid. This shift might just be a case, therefore, of a sulfate peak shifting location accordingly based off the temperature. It is also possible that the perchlorate is the dominant component when the sample is solid, and that the dominant component becomes sulfate as the sample turns to liquid, similarly leading to a shift in peak position of approximately 15 cm^{-1}.

Freezing rate and hydration state of brines:

Peak position is perhaps most important when discerning the differences in the main sulfate peak position due to freezing rate. The main magnesium sulfate peak appears to shift several wavenumbers, seemingly related to the rate at which the sample was frozen (Figure 9A). At slower freezing rates, the magnesium sulfate peak generally shifts more, while at quicker freezing rates, the peak generally shifts less. These different peak positions are likely due to the different hydration states of the solid magnesium and sodium sulfate ices (Ben Mabrouk, 2013; Wang, 2006; Elif Genceli, 2009) forming minerals like meridianiite ($MgSO_4*11H_2O$, located around 984-990 cm^{-1}), epsomite ($MgSO_4*7H_2O$, located around 984cm^{-1}), or mirabilite ($Na_2SO_4*10H_2O$, located around 988-990 cm^{-1}), as the differently hydrated minerals would lead to slightly different sulfate peak positions. This shift in peak position would likely be due to changes in the crystal structure of the minerals (Wang, 2006) due to the incorporation of differing numbers of water molecules-- i.e. differing hydration states-- impacting the overall Raman spectra.

It therefore appears-- from both literature and experimentation-- that the main peak position of magnesium sulfate can be impacted by the freezing rate, which in turn can impact the hydration state. This latter category can be split into two main groups (Wang, 2006): minerals

with hydration states at or above $6H_2O$ that typically have peaks around 983 cm^{-1} to 985 cm^{-1}, and those with hydration states of $5H_2O$ or below, which typically have peaks between 1000 cm^{-1} and 1030 cm^{-1}. Even so, taking both categories into account, the inverse relationship between hydration state and wavenumber is still clear: as hydration state decreases, the wavenumber (generally) increases.

Hydration state and freezing rate therefore appear to have a positive correlation to one another when relating to peak positions. Faster rates of temperature change seem to foster higher hydration states and peaks at lower wavenumbers, and slower rates of temperature change seem to foster lower hydration states and peaks at higher wavenumbers. The differences in freezing rate appear to lead to the formation of different minerals. This mineral formation may be due to the quickly increased presence of ice as the sample is cooled. Since both ice and salt would be readily available over short time scales within the mixture, this would allow numerous nucleation sites to form, fostering largely heterogenous nucleation of the brine as it turns to ice (Zhang, 2018). Quicker cooling would also lead to the formation of smaller ice particles as the solution cools (Cook, 2010). This increase in nucleation sites would allow the remaining water molecules more places to latch onto, possibly leading to minerals with higher hydration states.

It might also be possible that different minerals are forming at different parts of the sample when frozen. While these experiments did not gather spectra of multiple locations of the same sample if the brine was still wholly frozen, spectra were gathered from different samples of the same endmember (Figure 9B). It stands to reason that if a specific part of the sample might be a certain mineral, it is possible that other minerals would be present elsewhere in the sample and would yield different peak positions. The main magnesium sulfate peak position, for

example, can shift from 985 cm^{-1} to 989 cm^{-1}, depending on which sample is analyzed, even with a consistent cooling rate.

For example, if freezing a sample at 100 K/min produces an ice that consists of 70% meridianiite and 30% epsomite, it is more than likely the meridianiite peak will be observed. However, seeing a lower wavenumber peak for epsomite would not be impossible. This may help explain why in some cases there appears to be a direct correlation between freezing rate and Mg-sulfate peak position (Figure 9A), while in other cases the correlation appears weaker (Figure 9B).

It is also possible that the same mineral-- likely meridianiite ($MgSO_4*11H_2O$), in this case-- is forming regardless of cooling rate, with the slight differences in the main sulfate peak position attributed to the slight uncertainty about the exact peak position of meridianiite. It is therefore possible that the resultant shift in peak position is a result of a combination of the freezing rate, the hydration state of the ice/the minerals observed in the sample, and/or where on the sample spectra are taken. It is further possible that different freezing rates beyond the four tested may impact the shift in sulfate peak position.

Sediment:

All the sediment brine experiments were conducted using a 0.2 g to 0.28 mL sediment-brine ratio. This converts to approximately 2 parts sediment to 3 parts brine. While this is not necessarily indicative of the only-- or even the most prevalent-- sediment-brine ratio present on Mars, it did serve to create a sample that was not fully saturated with brine, but that nonetheless retained the appearance and properties of “wet sediment” for at least one to two hours.

Even though there was proportionally more brine than clay, the spectra of the clay was much more apparent. This could be because of the absorption or adsorption of water when mixing with the clays, leading to sediment that-- despite being near-saturated with fluid-- nonetheless retained the spectral appearance of sediment. However, the presence of both sediment and brine, in many cases, is readily apparent. This is especially true for the sulfate and perchlorate brines; both brines showcase very intense peaks. These peaks are easily discernable even with the addition of clay into the mixture. Brine peaks are still discernable, though not nearly as intense, when chloride brines are detected.

Some minerals-- such as gypsum-- are also thought to have formed from the interaction of sediment and brine. It is speculated that the 1010 cm^{-1} peak observed when montmorillonite (or other calcium-rich) clays and sulfate brines interact is a result of the sulfate ion of the brine combining with the calcium in the montmorillonite and precipitating out of solution to form gypsum. This newly formed peak is in the same location as the primary peak that is observed for gypsum (Lafuente, 2015). This is likely due to the cation exchange capacity of the montmorillonite used-- 89 meq/100 g (Borden, 2001). This exchange capacity might also help explain both why new mineral formation in general is not seen in the kaolinite used-- with only 3 meq/100 g cation exchange capacity (Borden, 2001), its value is much lower than that of montmorillonite; in addition kaolinite is unlikely to contain any exchangeable calcium. Were sulfate brines to interact with clays such as montmorillonite on Mars, it is possible that minerals such as gypsum might form due to these interactions and be both present and detectable on or near the surface. Gypsum occurs, as evidenced by the *Curiosity* rover, in places such as Yellowknife Bay (Nachon, 2014).

Montmorillonite and kaolinite also appear to have different rates of evaporation. When wetted with the same amount of water, the kaolinite dries out approximately a third more quickly than the montmorillonite. This may be a result of the effectiveness with which each clay absorbs water, due in part to its chemical composition and/or crystal structure. On Mars, this difference might mean that areas on Mars with more montmorillonite might have longer lasting aqueous features associated with those clays. These features therefore might be more recognizable, but sparser, than on areas of Mars that have higher levels of kaolinite, where aqueous features might be shorter lived but more prevalent.

Implications for Mars:

Raman spectrometry:

Raman spectrometry as an analytical technique has several benefits. Unlike other analytical techniques such as x-ray diffraction or x-ray fluorescence spectrometry, Raman spectrometry does not require that a sample be prepared in any way before being analyzed (Chou, 2017). This sample can be solid rock, liquid, or something gaseous-- regardless, the sample need not be prepared for analysis. In this way, Raman spectrometry is non-destructive (Chou, 2017); samples do not need to be crushed, pressed, or mixed with anything for accurate data to be gathered. This means that, were a sample from a recurring slope lineae taken *in situ* on Mars, that Raman spectrometry could easily be used to determine the composition of the sample with virtually no preparation and without destroying the sample itself.

However, a Raman spectrometer is also only so sensitive; therefore, while it is possible that a brine might exist in some quantity at certain low temperatures in ice-brine or ice-sediment-brine matrices on Mars, it may exist in such small quantities that its signal is not detected by the

Raman, instead being overpowered by the Raman signatures of the ices and/or sediments that are also present. Therefore, in addition to cataloguing how spectra change with respect to temperature or with respect to the amount of sediment a brine contains, it is also important to establish experimentally the detection limits of the brines themselves in ice-sediment-brine matrices.

Other influences on ice-sediment-brine interactions:

There are several factors that due to timing, overall complexity, or a myriad of other issues, were not accounted for in my research. Humidity levels of the Martian atmosphere, surface pressure, and gravity should all be considered when researching recurring slope lineae and determining how they might act in a true Martian environment. Humidity levels might impact the formative conditions of each brine; surface pressure might impact the temperature range over which the brines are stable; and gravity might impact the movement of fluids either at or near the Martian surface. However, these factors were not controlled for in my experiments due to either being outside the scope of the project or being too impractical to test. They are not ultimately accounted for directly in my research.

Of these factors, two-- a differing level of gravity and surface pressure-- have little bearing on the actual data that would be gathered through Raman spectrometry, and instead pertain more to the potential for formation, the stability of, and the physical movement of these brines *in situ* on Mars. Were Raman spectra taken of surface water on Mars, that water is stable-- at least transiently-- by definition, rendering these factors non-issues.

Humidity, on the other hand, could impact the nature of these brines, even after they have formed and otherwise would be stable. While, with no other influences, it would typically only

become humid enough to form brines through deliquescence in the higher latitudes (Möhlmann, 2011), it is possible that the presence of other factors-- such as groundwater-- could lead to atmospheric conditions becoming humid enough to form brines closer to the equatorial regions (Martínez, 2013). This increase in humidity would likely also cause certain salts to become more hydrated (Wang, 2006; Chevrier, 2009), forming-- for example-- epsomite ($MgSO_4*7H_2O$) from anhydrous magnesium sulfate ($MgSO_4$). This difference in hydration state, as illustrated, can lead to varying peak positions when a sample is analyzed using Raman spectrometry.

Mars-- General:

As Mars is a dusty planet, it is not beyond reason to assume that sediment, salts, and ice might become incorporated with liquid brines as they form. This inclusion of solid material may impact our ability to detect brines and impact the peak locations and intensities of the Raman spectra that are observed. This was observed with the montmorillonite spectra when mixed with various brines. In all cases, the spectra of the clay predominated over the spectra of the brines. While the relevant peaks from the brines were by and large still visible, they were much less visible than in the saturated endmember brines alone.

It was generally much more difficult to determine the presence of brine in sediment mixtures than in mixtures with no sediment. Even though the overall amount of brine used in the sediment experiments was less, this in theory would not have posed an issue, and should have returned the same Raman spectra. It appears, therefore, that clays and sediment effectively work to “mask” the spectra of a brine to a much greater extent than would be the case if sediment-free ice were melting. This fact should especially be considered for a planet like Mars, where sediment is prevalent. Given the generally low water content of recurring slope lineae (Edwards, 2016), it is plausible that, were sample locations not scrutinized closely enough, or spectra from

potentially promising locations not analyzed carefully enough, telltale signs of aqueous activity could easily be missed.

Partial melting of brines:

The partial melting of brines can lead to the formation of liquids stable over various lengths of time at or near the Martian surface (Möhlmann, 2010). The degree of this melting depends on several independent (but interconnected) temporal, compositional, and spatial factors relevant to the provenance and chemistry of the ice in question. Once liquid, these brines have the potential to impact the surrounding environment through processes like erosion or evaporation, as may be the case with recently discovered gullies and seepages on the Martian surface (Möhlmann, 2010).

When analyzed with Raman spectroscopy, this partial melting of brines can lead to a continually varying spectral signature as the temperature rises or falls. In some cases, this melting can lead to distinct spectra within a single sample at a given temperature, while in other cases (Figure 5) there appears to be a lag between the temperature of the brine and the characteristics of the spectra that is observed versus what should be expected of the spectra given both temperature and compositional conditions.

At the temperatures at which multiple spectra were taken, these spectra have distinct differences between their solid and liquid portions. In the few degrees above the melting point, some spectra-- including those of $CaCl_2$ and $NaClO_4$-- also contain a mix of both solid and liquid spectral attributes; a spectrum looking much like the ice spectra, but at temperatures where things would not be expected to be completely solid. In the aforementioned cases, a number of the higher wavenumber peaks that are present when the brines are ices persisted past the melting

temperature, causing the resultant spectra to appear as a mix of the solid and liquid spectra (Figure 5D and 5E), sometimes with both a "hump" caused by the liquid, and a sharp spike from the residual ice. It is possible that this is due to effects of the rate at which the temperature was changed, or due to the time for which the sample remained at a given temperature before spectra were taken, possibly not having time to reach equilibrium with the surrounding environment. It is possible that some ice may still have been present, leading to a spectrum that aligned more closely with the solid samples than the liquid ones, despite the temperature. This may make it slightly more difficult-- though not impossible-- to evaluate the exact physical state of brines in the few degrees around their melting points on Mars. A similar issue appeared in the sediment experiments.

Formation of new minerals in situ on Mars:

The precipitation of gypsum in the sulfate-montmorillonite matrices (Figure 11) is of special note here. It has already been established that cation-exchange reactions can help to form gypsum in laboratory settings (Borden, 2001); it stands to reason that this same process might be forming sulfates *in situ* on Mars as well, with the help of nucleation processes (Van Driessche, 2019) occurring in the sulfate-clay mixtures.

It is possible, and perhaps likely, that the formation of ancient clays from the weathering of basalt (Milliken, 2009) has led to the subsequent formation of sulfates at various locations on Mars. At Gale Crater, for example, a depositional gradation is seen, transitioning from clays to sulfates as time progresses (Milliken, 2010). As clays generally need aqueous conditions to form-- and we know by looking at the rock record in Gale Crater that aqueous activity did take place (Bedford, 2019; Nachon, 2014)-- it is possible that these aqueous clay-forming conditions and subsequent interaction between the clays that had formed and brines on the surface led, in

part, to the formation of these sulfates through the process of nucleation (Van Driessche, 2019). While many of the sulfates and other hydrated minerals observed on Mars are Ca-poor (Nachon, 2014), and therefore would not likely be gypsum, gypsum is nevertheless found in certain locations on Mars-- including Gale and Endeavor Craters (Nachon, 2014)-- and, if conditions were favorable, could well have formed from the interaction between brine and clay. We see evidence for the precipitation out of solution of gypsum (Nachon, 2014), further lending credence to this argument. Calcium is also present in minerals such as pyroxene within basalts and in various sedimentary rocks in Gale Crater (Phillips-Lander, 2019). The formation of gypsum in a laboratory setting serves as a prime example of new material forming from this interaction of brines and clays, like what might have occurred on Mars.

Implications for RSL:

The upper limit of the water content of RSL is likely only about 3% by weight, with the RSL themselves being only a few centimeters thick (Edwards, 2016). While my research uses somewhere near a 50/50 mix of sediment and brine by weight, and is thereby nowhere close to what the actual water content of RSL would likely be, the experiments I've conducted are nevertheless beneficial, as they provide a good intermediary step to catalog the nature of partially wetted sediment. They are a balance between cataloging the spectra of completely dry sediment on one extreme and fully aqueous samples on the other. In this way, my 50/50 sediment-brine research serves as a middle ground in the gradation between collecting data on dry sediment versus liquid.

This data will help to constrain the nature of future research that is done on samples containing an unknown sediment-brine ratio and help to classify them as either predominantly granular or predominantly aqueous. By having a sediment-brine sample that contains an

approximately equal amount of both sediment and brine, there are three classifications to denote the nature of sediment-brine matrices-- purely dry sediment, purely aqueous brine, or an approximately equal mix of the two.

Additionally, while the research done may not be representative of recurring slope lineae as a whole, it could be representative of certain samples of RSL that could be taken *in situ*, if the sediment-brine ratio of a sample is closer to a 2:2 to 2:3 sediment to brine weight ratio. Therefore, my research provides an overview of what the Raman spectra of various sediment-brine mixtures may look like, as well as having the potential to showcase specific spectra of certain samples of recurring slope lineae that might be more water rich.

Future Mars missions:

While an understanding of both Martian processes and potential outside influences, how they relate to one another, and how they tie into ice-sediment-brine interactions on Mars should be considered if a holistic understanding of Martian geology is to be achieved, the results obtained here are nonetheless applicable to Martian research when determining which instrument or laser to place on a spacecraft, or when using that instrumentation to determine the make-up of *in situ* brines on Mars. The Mars 2020 mission, for example, will be launched by NASA to study Martian mineralogy (Wiens, 2017). The Raman spectrometer on board will be able to collect spectra while positioned several meters away from its target and will utilize both 1064 nm and 532 nm lasers (Wiens, 2017). The ExoMars mission, similarly, will be launched by the European Space Agency to attempt to determine the past or present habitability of Mars (Bost, 2015) as well as to determine local Martian mineralogy (Lopez-Reyes, 2013). To help facilitate this, the mission will utilize a 532 nm green laser (Moral, 2020; Rull, 2017) to conduct Raman spectroscopic analyses. This means that the laboratory data we have gathered will be directly

applicable to both the ExoMars and Mars 2020 missions, as well as any future missions that utilize either 532 nm or 785 nm lasers. This will allow for analyses to more quickly and accurately be conducted, as a directly applicable dataset will have already been produced. This will help produce higher quality and more easily accessible and interpretable data for future missions to Mars and beyond.

Implications for other extraterrestrial processes:

This research is also directly applicable to ice-sediment-brine interactions in ices near the Martian poles, or ice-sediment-brine interactions on several Jovian or Saturnian moons including Europa, Enceladus, and Titan. The data set I have produced allows scientists to differentiate more easily between brines that are subject to different conditions and will help scientists better understand how these various brines impact the sedimentology, geochemistry, and geology of the extraterrestrial locations in which they are found.

For example, the exact chemistry of the liquid the *Phoenix* lander discovered (Chevrier, 2009; McEwan, 2011) upon landing in 2008 is still debated. Had a Raman spectrometer been present on the lander, it would have been able to analyze the droplets of brine and ices that were discovered and provide definitive spectral evidence to support the presence of a certain type of brine, taking both composition and temperature into account.

Furthermore, it has already been shown that Raman spectroscopy is an effective tool to determine both the presence of brines and solubility of gasses in those brines at Europa-relevant conditions (Bonales, 2014). The research we have done would further compliment that research, allowing for a database of the spectra of various Europa-analogue brines at similar temperatures to those that might be observed in a subsurface Europan ocean.

Similarly, it is hypothesized that cryovolcanism is active on Titan (Fortes, 2007), and if present would likely consist of a mix of clathrates, ices, and sulfate brines. While the temperatures on Titan are much lower than on Mars, the Raman spectra of any brines or ices on the Saturnian moon would likely look like some of the spectra already collected. In this way, the dataset we have compiled is again beneficial, with wide-reaching applications not only to Martian geology and geochemistry, but also to planetary science and Solar System exploration.

Future Research:

There are several topics that were not addressed in full in this research. For example, how do different rates of temperature change other than the four tested impact the hydration state of and position of the main sulfate peak when the sample is ice? What is the exact interplay between the sulfate and perchlorate brines as it relates to the ~1100-1115 cm^{-1} peak? How might the partial melting of ices impact an area's geomorphology? How might all these factors coexist in an environment analogous to that of Mars or other planetary bodies-- with similar temperature, pressure, atmospheric, and humidity conditions to what those locations experiences?

While knowing the geochemistry of these brines and ices may not single-handedly help scientists determine their formation mechanisms, geochemistry can nonetheless provide information about their formative environment. For example, it is thought that chlorides and chlorates evolve into perchlorates upon interaction with high-energy radiation (Wilson, 2016). This would lead to a higher prevalence of chlorides at depth, where radiation cannot penetrate, and a greater abundance of perchlorates nearer to the Martian surface, where chlorides and chlorates have interacted with radiation and subsequently turned into perchlorates. Furthermore, having an accurate idea of these brines' chemistry can help give scientists an idea as to how

these brines and ices can impact their surrounding environment once they do form, taking variables such as composition and temperature into account.

Conclusions:

While much research has been done regarding planetary science, and specifically planetary geochemical analyses, there are still many unanswered questions when it comes to the Raman spectra of planetary-analogue brines. This work helps to provide a dataset to help answer some of those questions, as well as making note of potential applications for how the resultant dataset could be used-- from analyzing recurring slope lineae on Mars, to determining the composition of the icy moons of Jupiter and Saturn, and a litany of other purposes as of yet undiscovered. It is possible that datasets such as this will prove increasingly more beneficial in the coming years, as more human and robotic exploration is done throughout the Solar System.

Appendix:

Raman Peak Positions:

Both the solid and liquid peak positions associated with each solution tested are outlined below in Table A1.

Table A1: Raman Peak Positions

Brine	Wavenumber (cm^{-1})	Label	Notes	Reference
UPW	212; 213	Translatory mode/libration		*Berg, 2018; Narayanaswamy, 1948*
UPW	450	H_2O libration bands	Peaks around 400 cm^{-1} - 500 cm^{-1}	*Martinez-Uriartem, 2014*
UPW	1616-1665	OH-bending	Generally at 1644 cm^{-1}; varies depending on composition/hydration state of brine	*Martinez-Uriartem, 2014*
UPW	1644	H_2O vibration		*Wang, 2006*
UPW	3090; 3138; 3216	OH-stretching (ice)	The 3216 cm^{-1} peak also seems to appear when sample is liquid	*Yang, 2019; Duričković, 2011; Yang, 2019*
UPW	3150	"strong ice band"		*Berg, 2018*
UPW	3385; 3420, 3423	OH-stretching (water)		*Duričković, 2011; Duričković, 2011, Wang, 2006*
$CaCl_2$	520	H_2O libration	Specific to $CaCl_2$	*Martinez-Uriartem, 2014*
$CaCl_2$	3386, 3406, 3432	O–H stretching bands for antarcticite		*Thomas, 2017*
$MgCl_2$	3344, 3394, 3504	$MgCl_2$ hexahydrate (bischofite)	Slight shifting of peaks when thawed and then cooled again	*Thomas, 2017*
$MgSO_4$	451, 617, 1113	SO_4 (aq.) vibrational modes		*Wang, 2006*
$MgSO_4$	444; 460	SO_4 vibrational modes in meridianiite		*Elif Genceli, 2009; Wang, 2006*

$MgSO_4$	611; 619	SO_4 vibrational modes in meridianiite		*Wang, 2006; Elif Genceli, 2009*
$MgSO_4$	982	Main sulfate peak (aq.)		*Wang, 2006*
$MgSO_4$	984.3; 990	Main meridianiite peak	Hydrated $MgSO_4$: $MgSO_4*11H_2O$	*Wang, 2006; Elif Genceli, 2009*
$MgSO_4$	1095; 1116; 1133	SO_4 vibrational modes in meridianiite		*Wang, 2006; Elif Genceli, 2009; Wang, 2006*
Na_2SO_4	456	SO_4 vibrational mode in mirabilite		*Elif Genceli, 2009*
Na_2SO_4	613	SO_4 vibrational mode in mirabilite		*Elif Genceli, 2009*
Na_2SO_4	982	Main sulfate peak (aq.)		*Wang, 2006*
Na_2SO_4	990; 992	Main mirabilite peak	Hydrated Na_2SO_4: $Na_2SO_4*10H_2O$	*Elif Genceli, 2009; Ben Mabrouk, 2013*
Na_2SO_4	1112	SO_4 vibrational mode in mirabilite		*Elif Genceli, 2009*
NaCl	3403, 3420, 3434, 3535	Hydrohalite peaks	Indicative of $NaCl*2H_2O$	*Thomas, 2017*
$NaClO_4$	461	Symmetric ClO_4 bend		*Nebgen, 1965*
$NaClO_4$	626	Asymmetric ClO_4 bend		*Nebgen, 1965*
$NaClO_4$	938	Symmetric ClO_4 stretch		*Nebgen, 1965*
$NaClO_4$	1095, 1139	Asymmetric ClO_4 stretch		*Nebgen, 1965*
$NaClO_4$	3500	Chemically bound water of hydration	Peak 3540 cm^{-1} - 3550 cm^{-1} depending on brine; $MgClO_4$ in literature, but also in $NaClO_4$	*Nikolakakos, 2015*

Ices:

The following twenty-four figures detail stacked plots showcasing the effects of temperature on seven endmember and five mixed-composition Mars-analogue brines. Each brine has one figure with lines and labels denoting important peak positions (see Table A1), and a second figure of the same spectra with no lines or labels included. Lines have been color-coded as noted in figure captions on the former figures to denote the responsible brine.

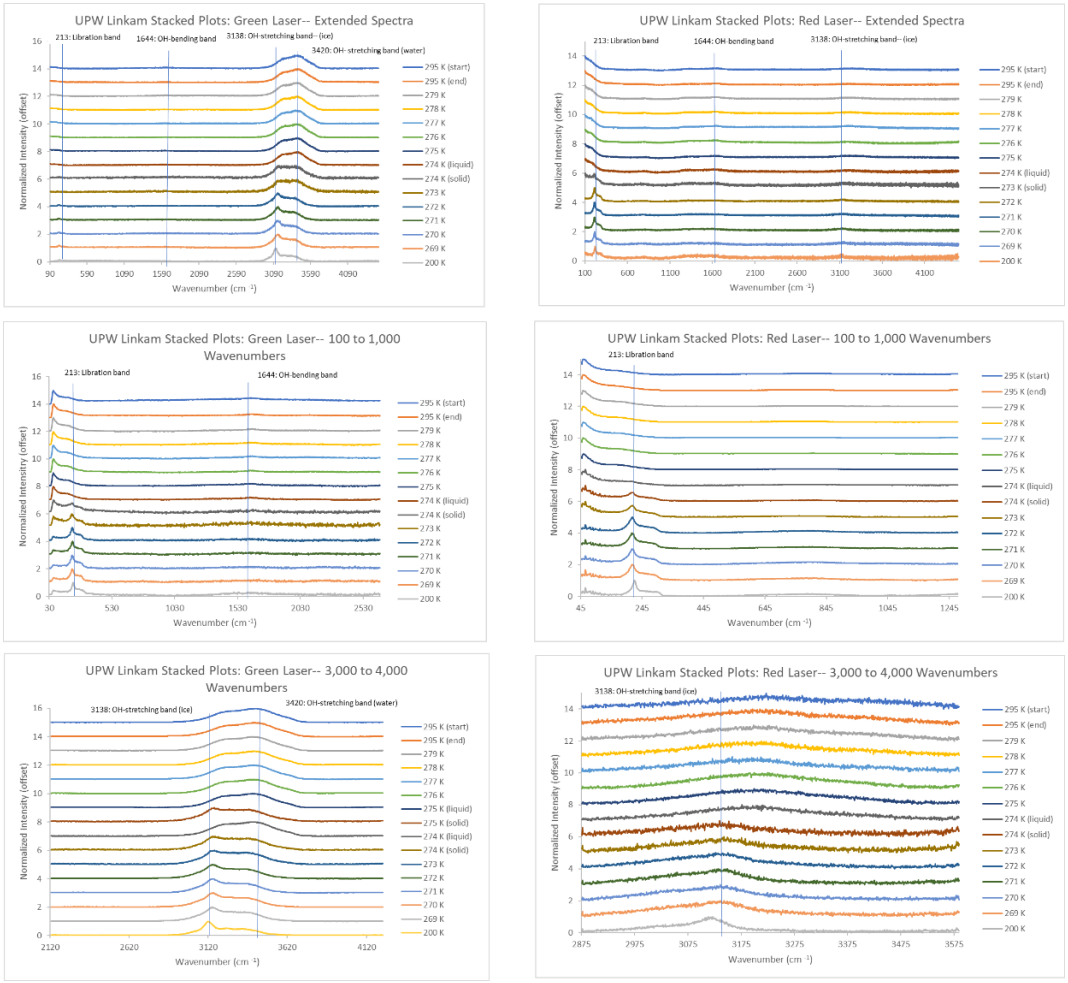

Figure A1: Ultrapure water stacked plots (green and red lasers), lines and labels included to denote important peaks of ultrapure water (light blue).

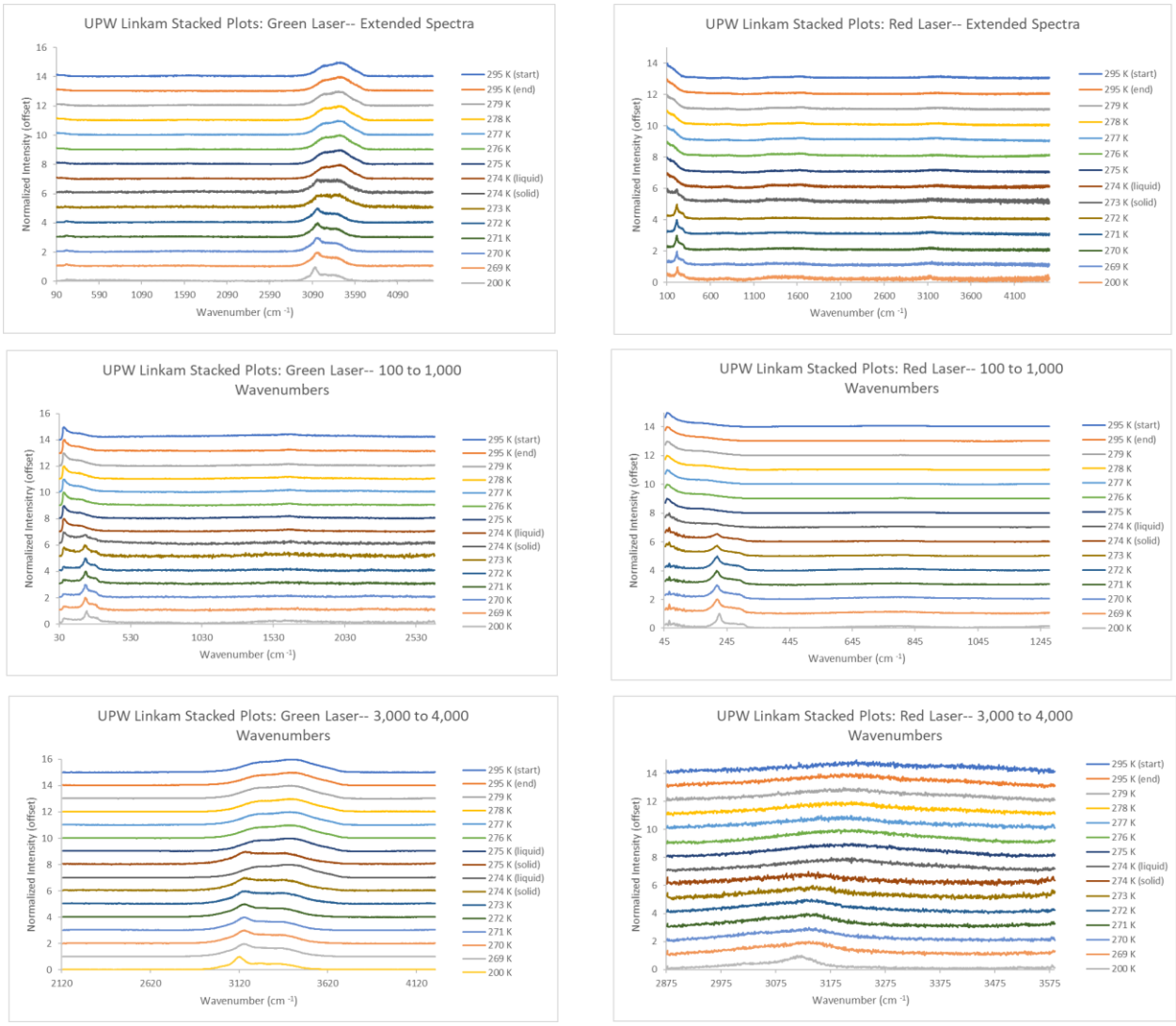

Figure A2: Ultrapure water stacked plots (green and red lasers), lines and labels not included.

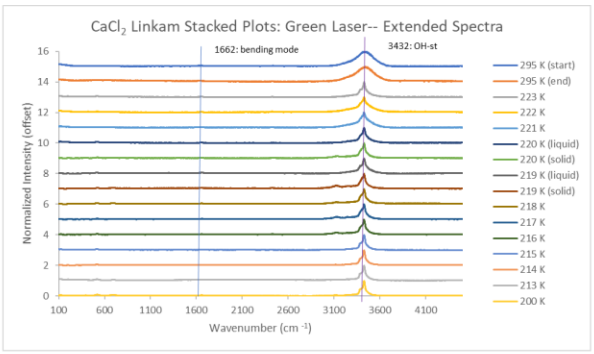

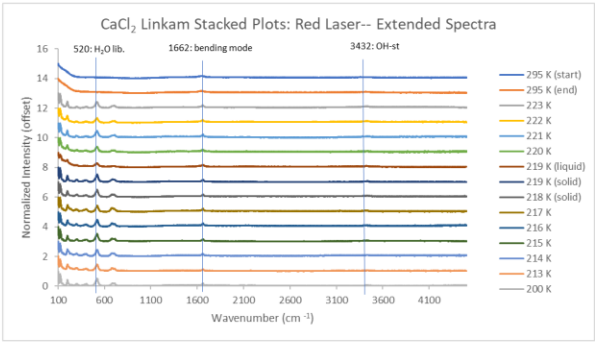

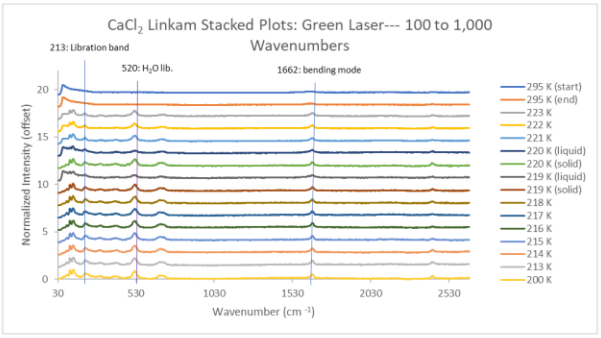

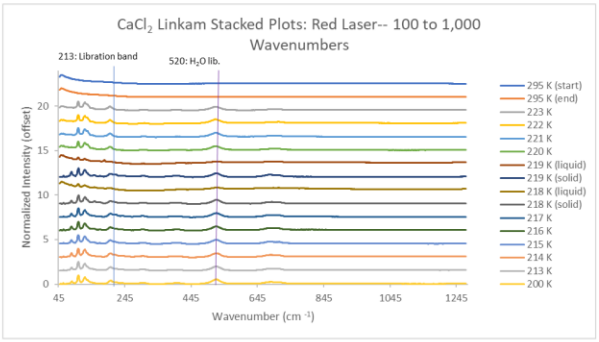

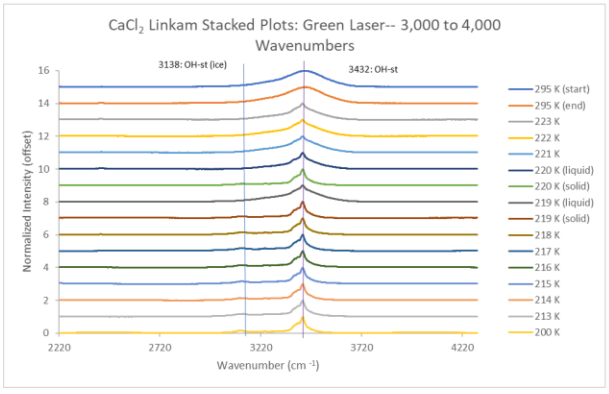

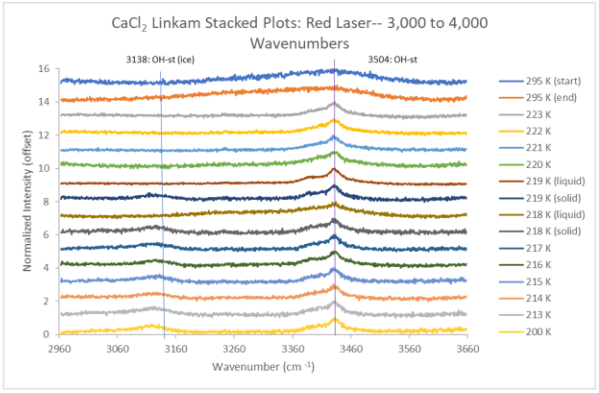

Figure A3: $CaCl_2$ stacked plots (green and red lasers), lines and labels included to denote important peaks of ultrapure water (light blue) and $CaCl_2$ (purple).

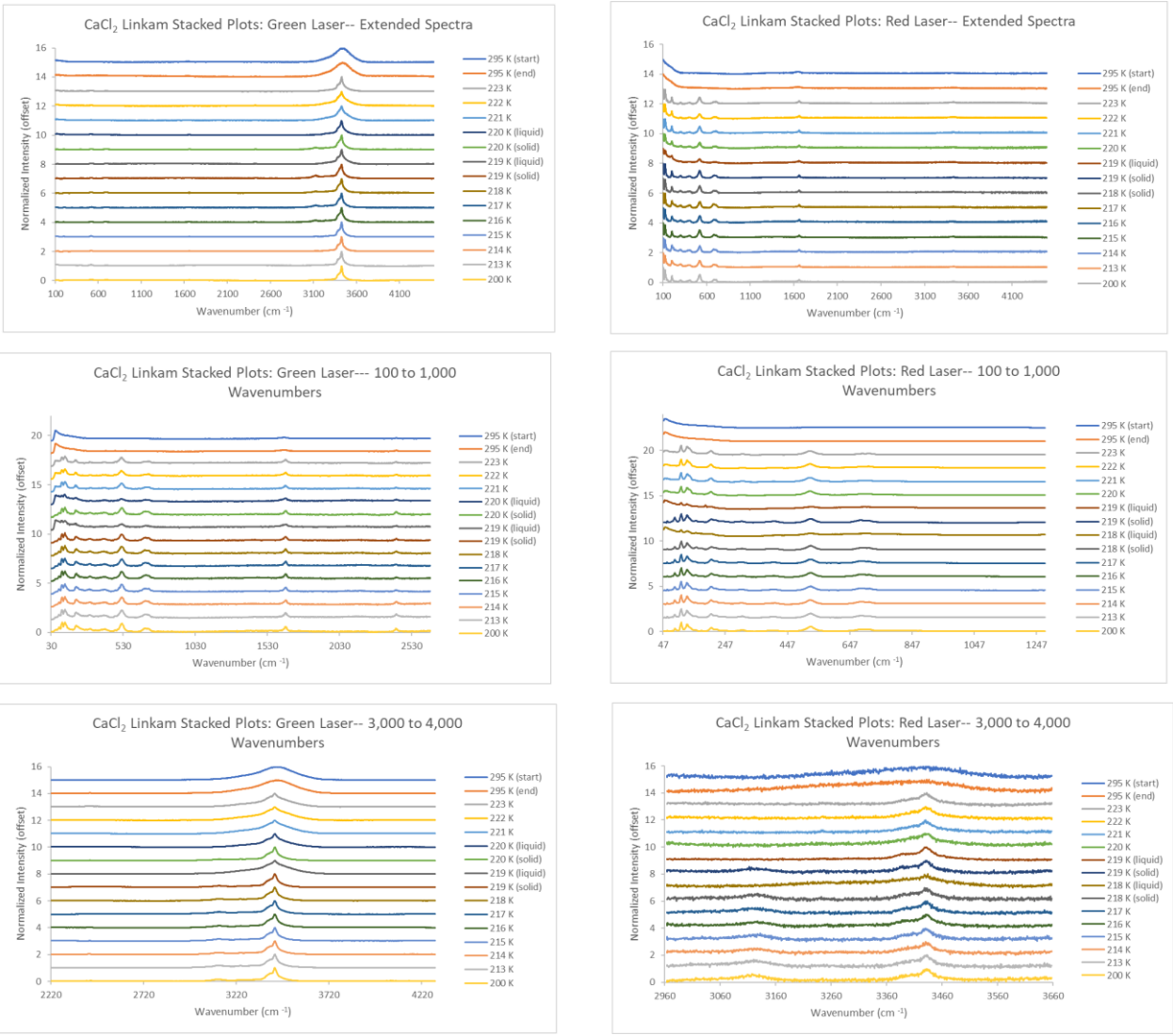

Figure A4: $CaCl_2$ stacked plots (green and red lasers), lines and labels not included.

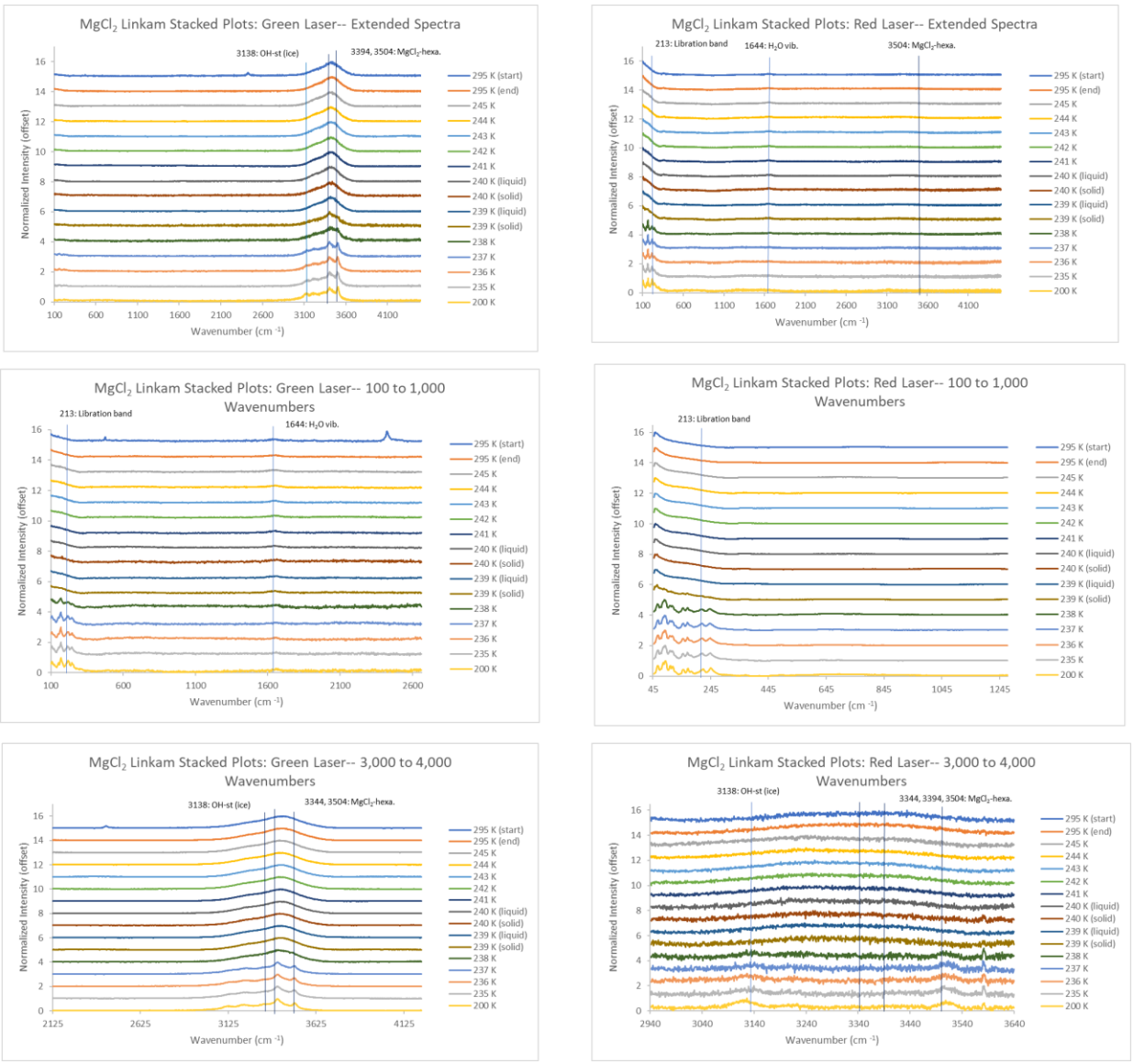

Figure A5: $MgCl_2$ stacked plots (green and red lasers), lines and labels included to denote important peaks of ultrapure water (light blue) and $MgCl_2$ (navy blue).

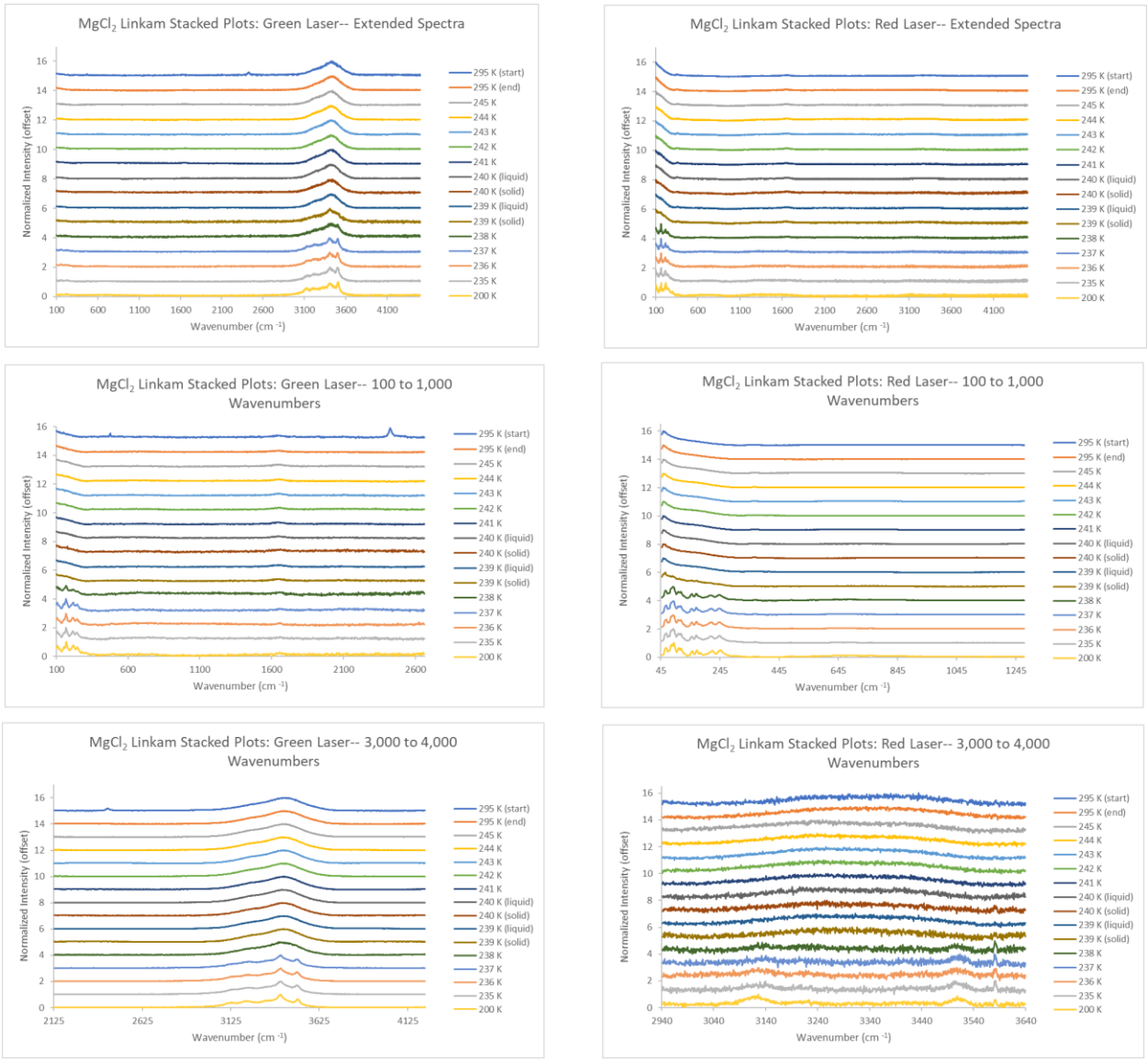

Figure A6: $MgCl_2$ stacked plots (green and red lasers), lines and labels not included.

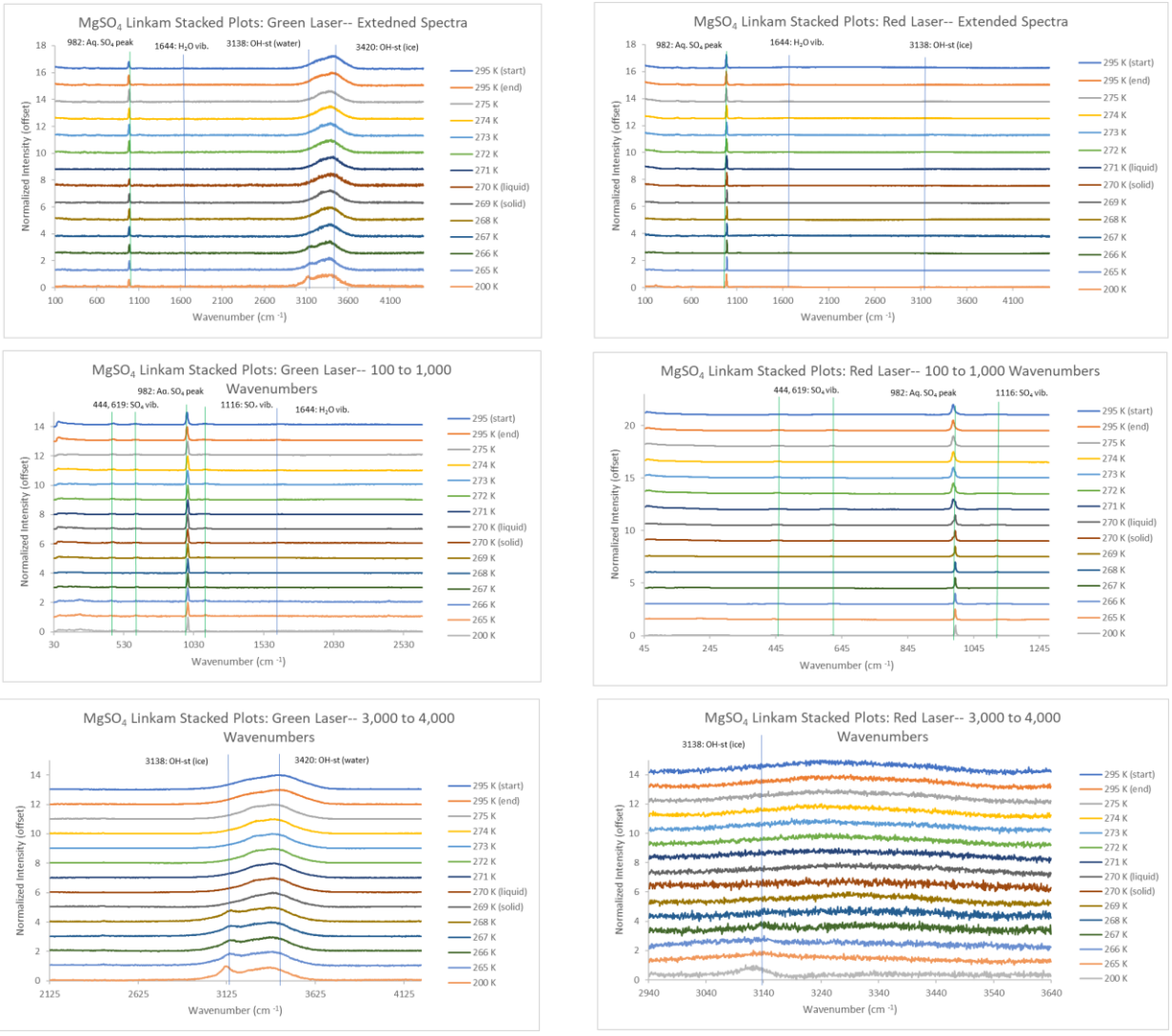

Figure A7: $MgSO_4$ stacked plots (green and red lasers), lines and labels included to denote important peaks of ultrapure water (light blue) and $MgSO_4$ (dark green).

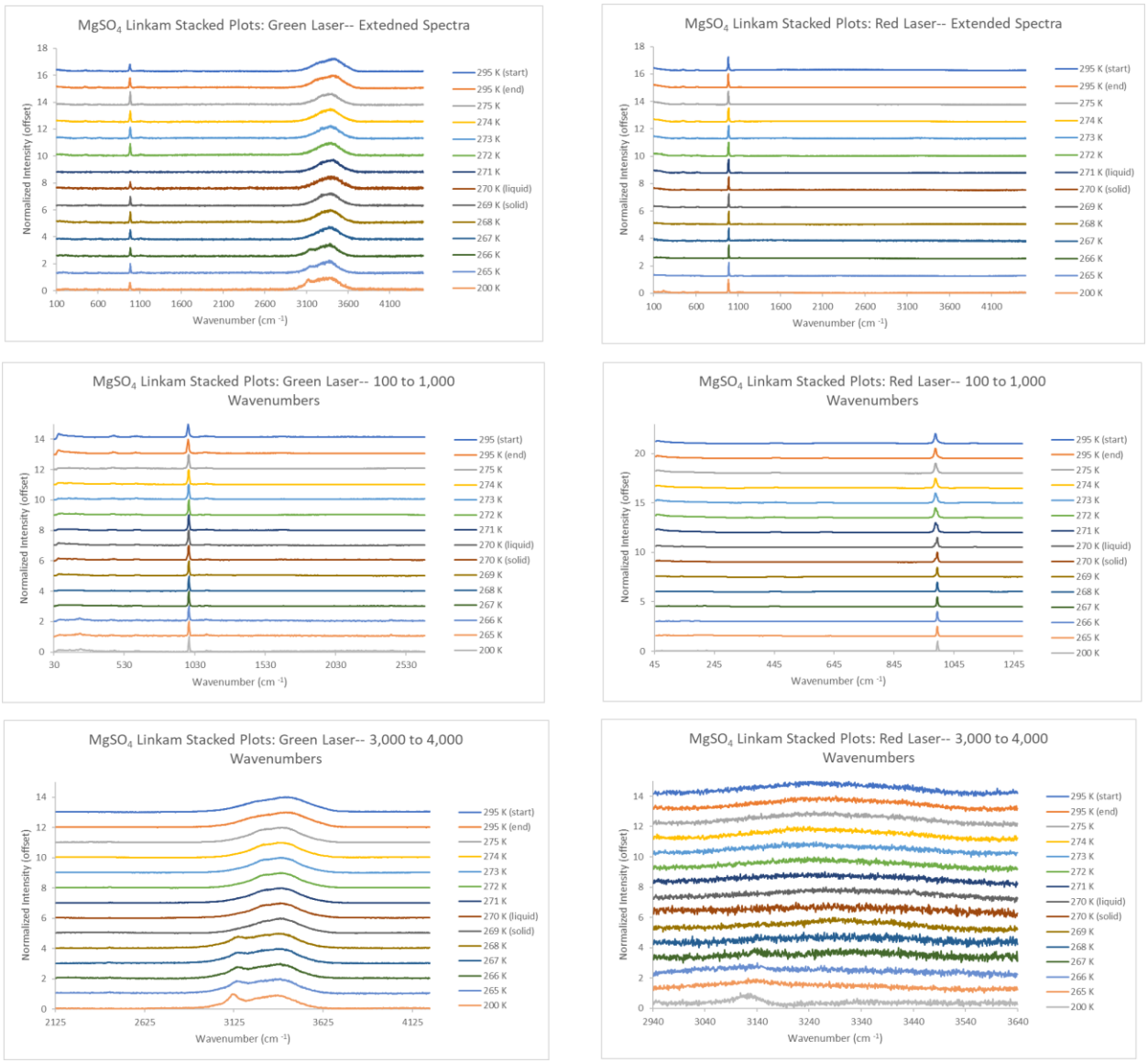

Figure A8: $MgSO_4$ stacked plots (green and red lasers), lines and labels not included.

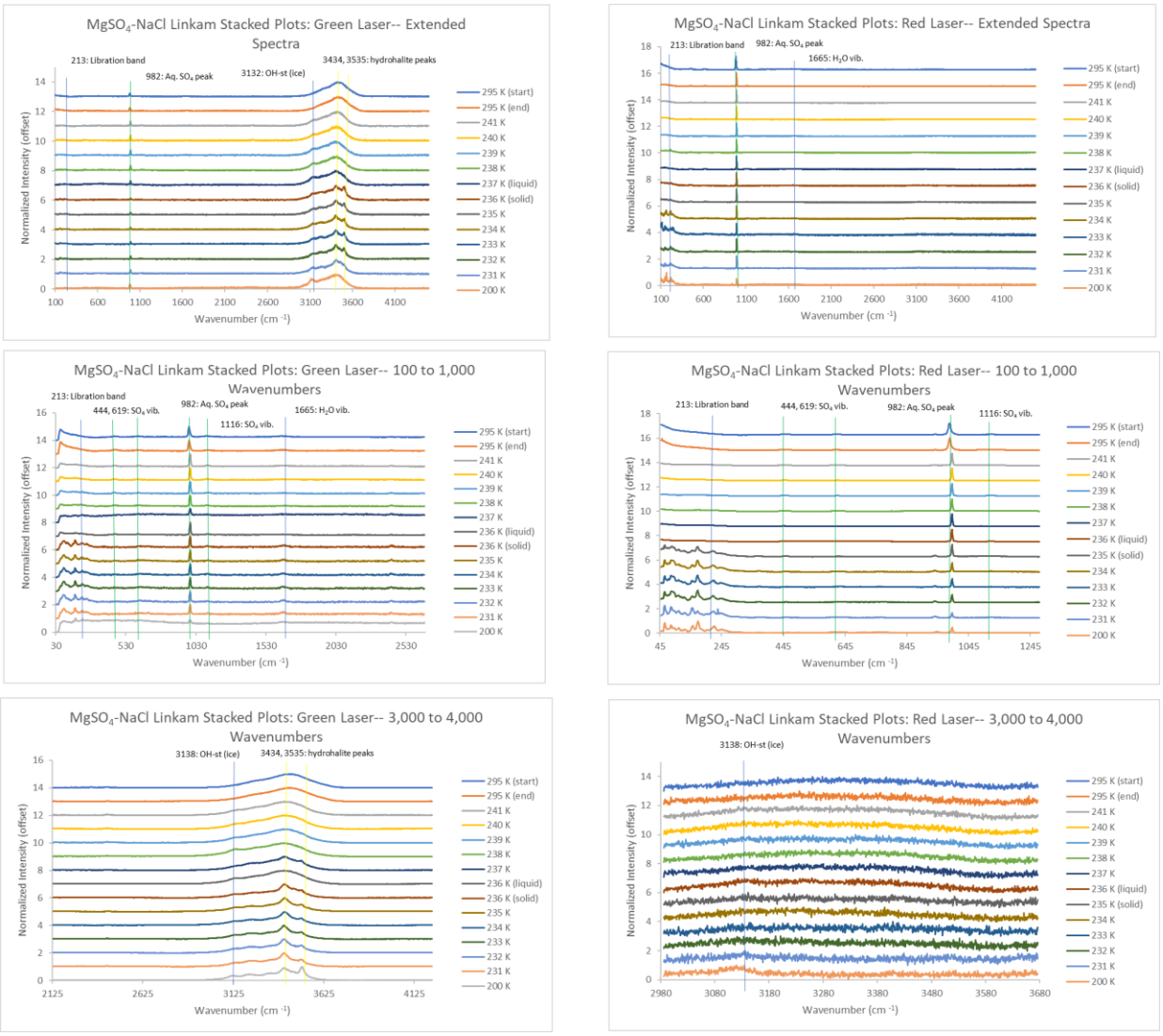

Figure A9: $MgSO_4$-NaCl stacked plots (green and red lasers), lines and labels included to denote important peaks of ultrapure water (light blue), $MgSO_4$ (dark green), and NaCl (yellow).

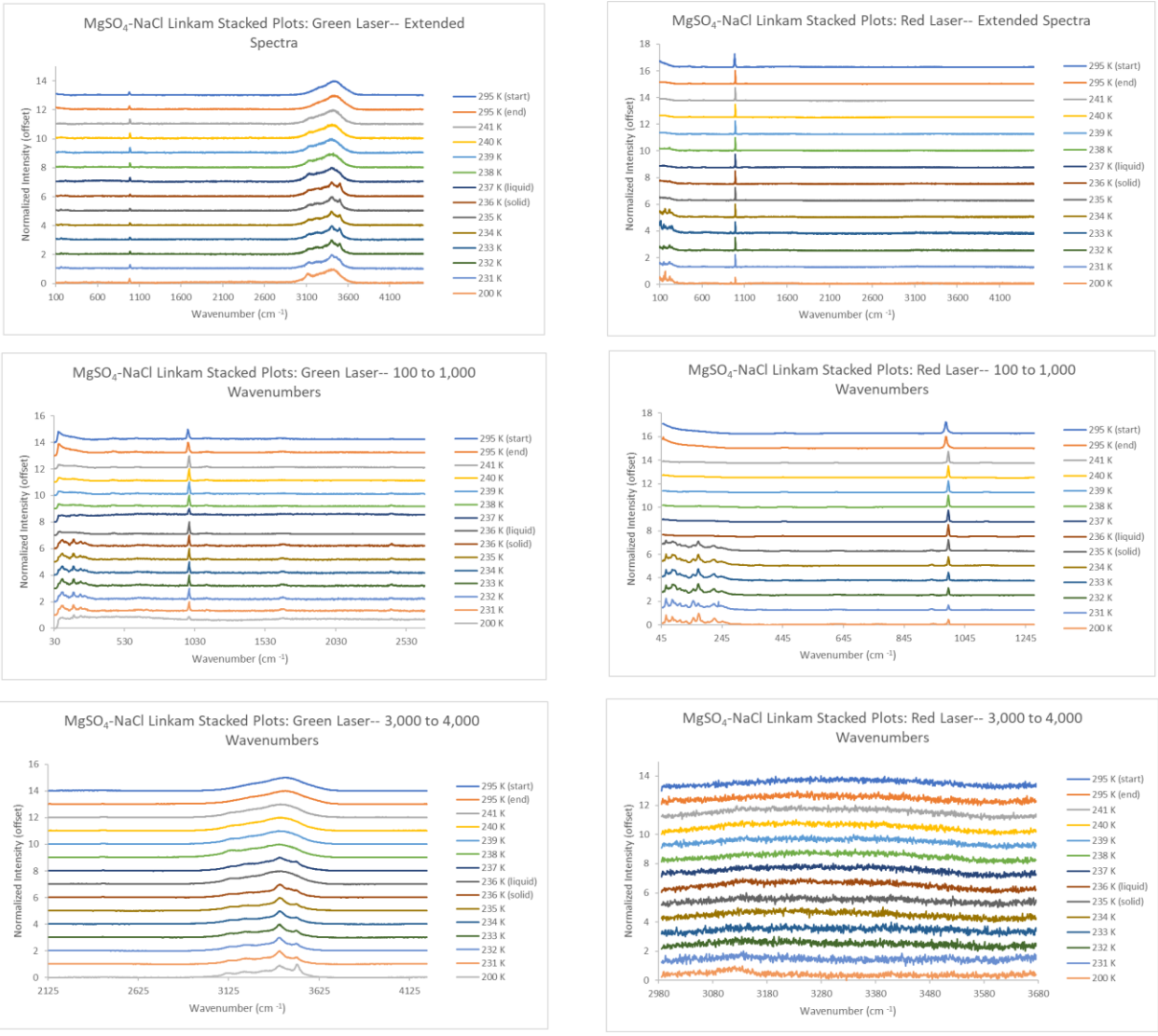

Figure A10: $MgSO_4$-NaCl stacked plots (green and red lasers), lines and labels not included.

Figure A11: $MgSO_4$-$NaClO_4$ stacked plots (green and red lasers), lines and labels included to denote important peaks of ultrapure water (light blue), $MgSO_4$ (dark green), and $NaClO_4$ (red).

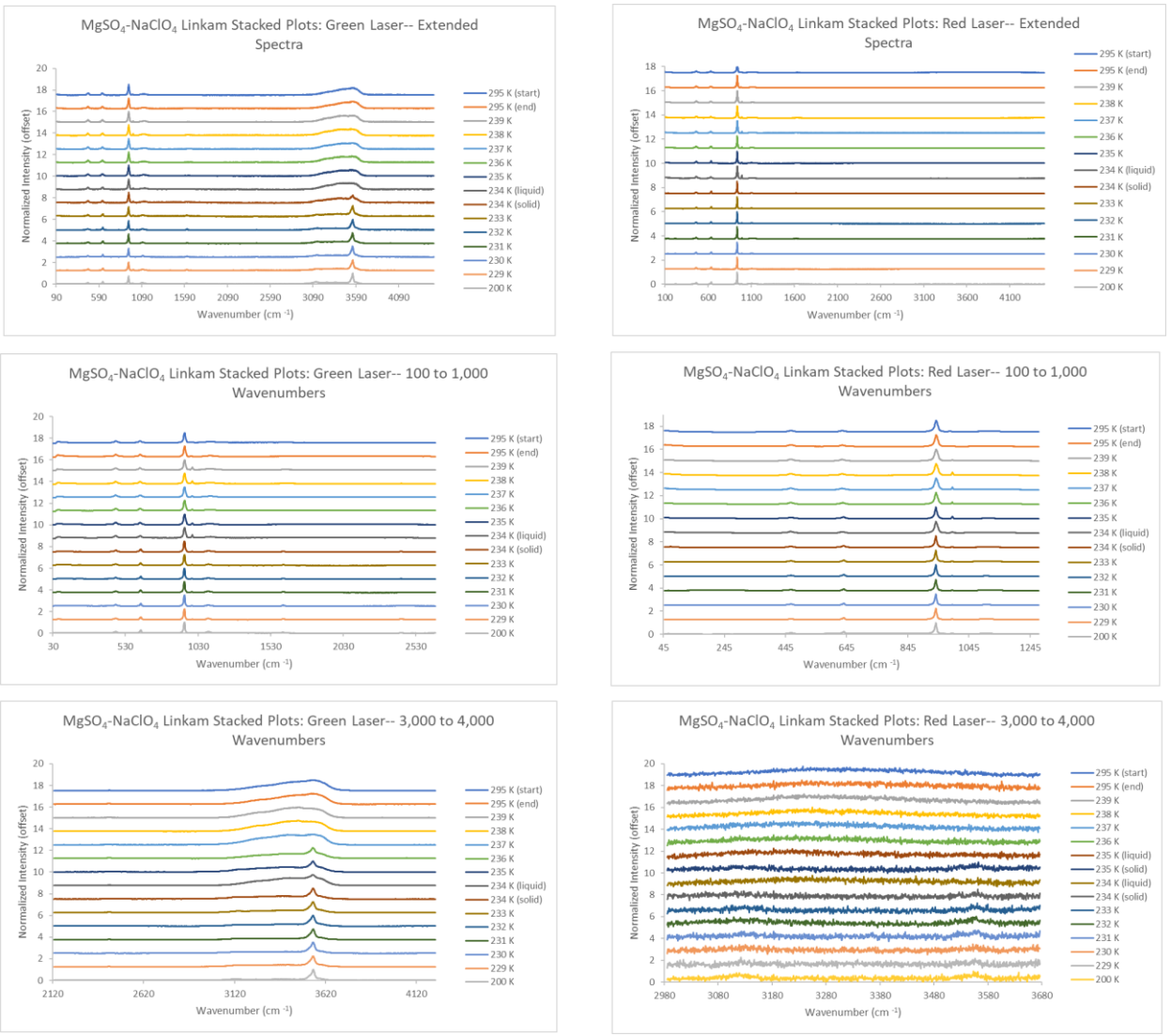

Figure A12: $MgSO_4$-$NaClO_4$ stacked plots (green and red lasers), lines and labels not included.

Figure A13: Na_2SO_4 stacked plots (green and red lasers), lines and labels included to denote important peaks of ultrapure water (light blue) and Na_2SO_4 (light green).

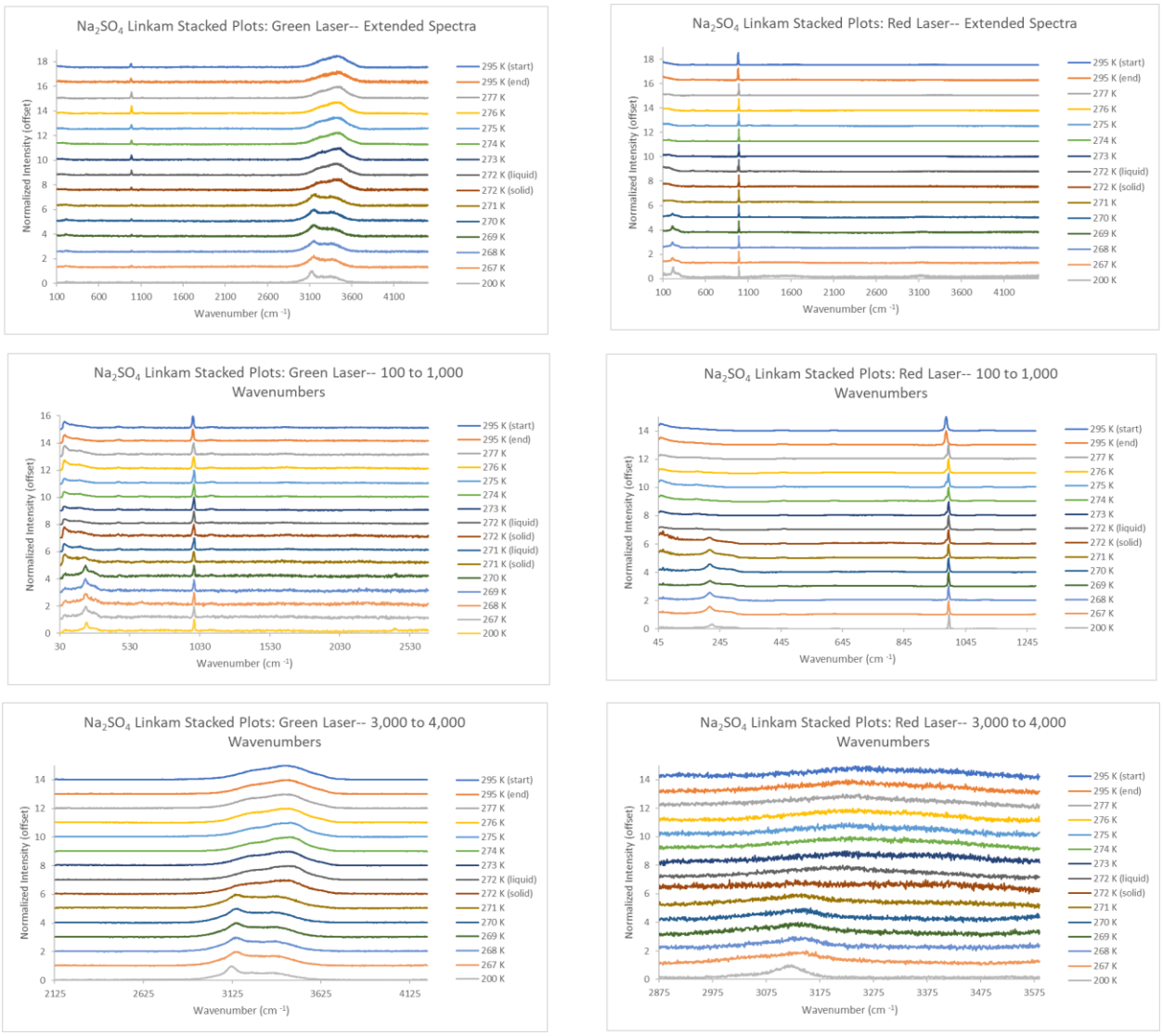

Figure A14: Na_2SO_4 stacked plots (green and red lasers), lines and labels not included.

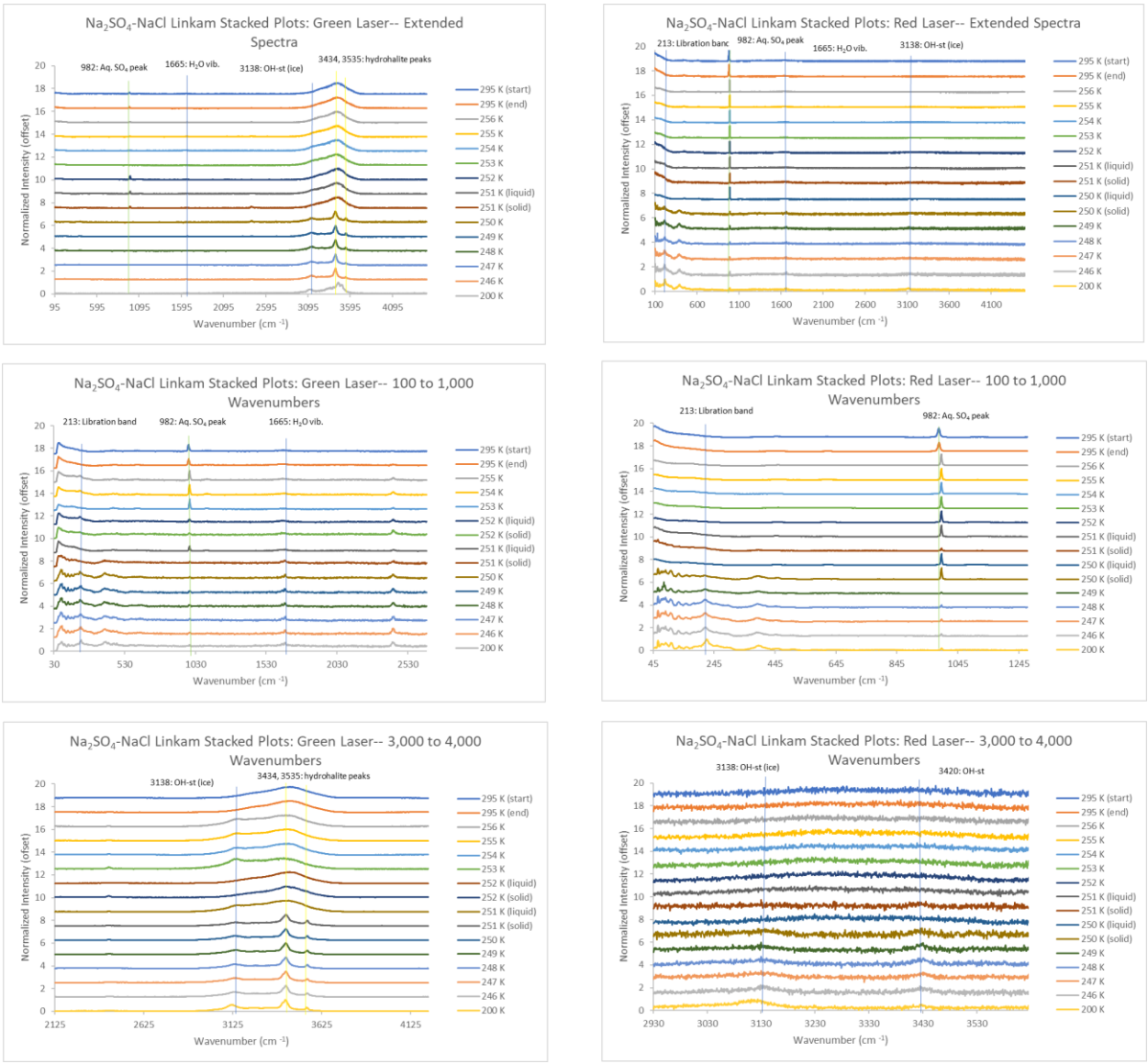

Figure A15: Na_2SO_4-NaCl stacked plots (green and red lasers), lines and labels included to denote important peaks of ultrapure water (light blue), Na_2SO_4 (light green), and NaCl (yellow).

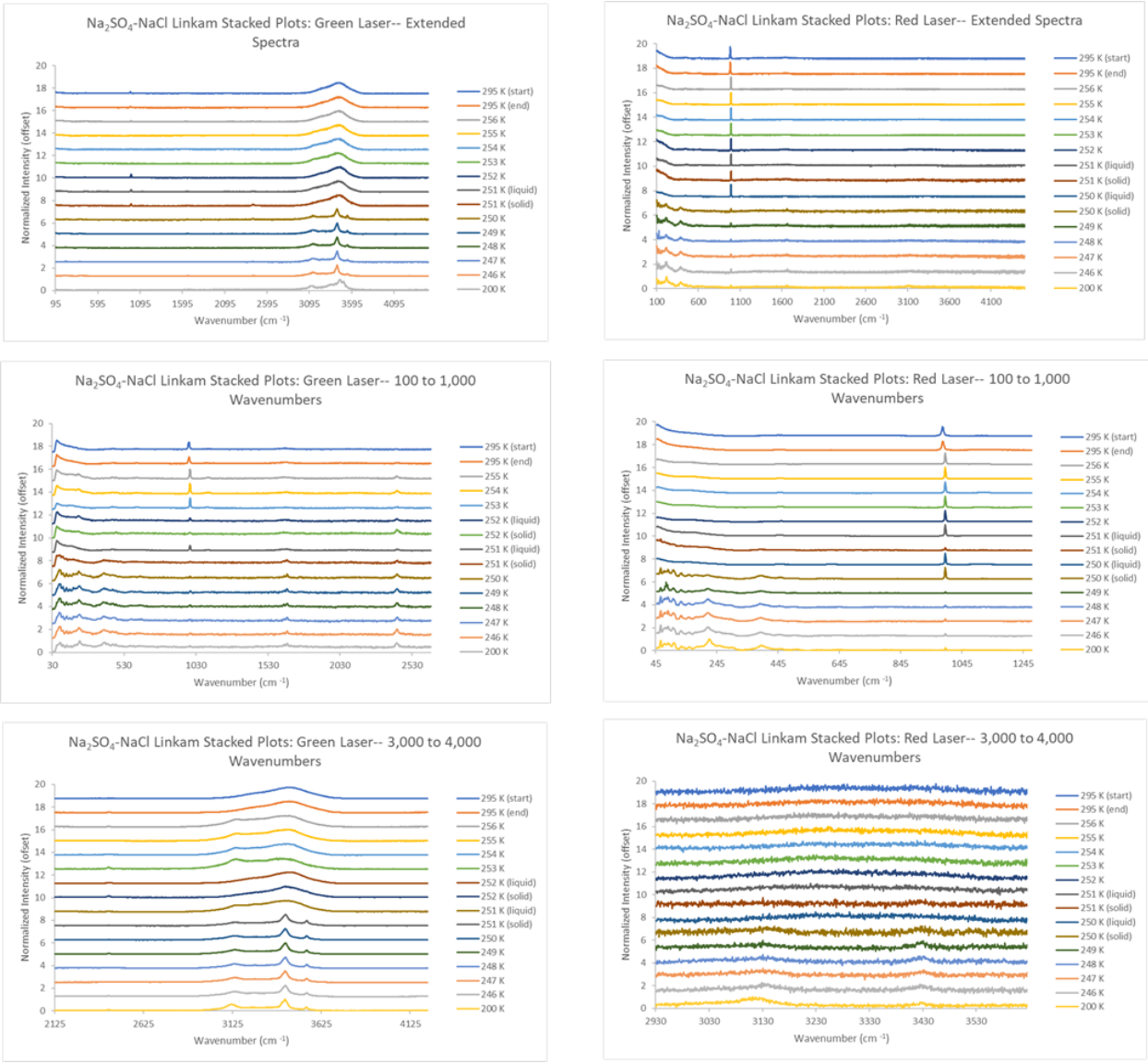

Figure A16: Na_2SO_4-NaCl stacked plots (green and red lasers), lines and labels not included.

Figure A17: Na_2SO_4-$NaClO_4$ stacked plots (green and red lasers), lines and labels included to denote important peaks of ultrapure water (light blue), Na_2SO_4 (light green) and $NaClO_4$ (red).

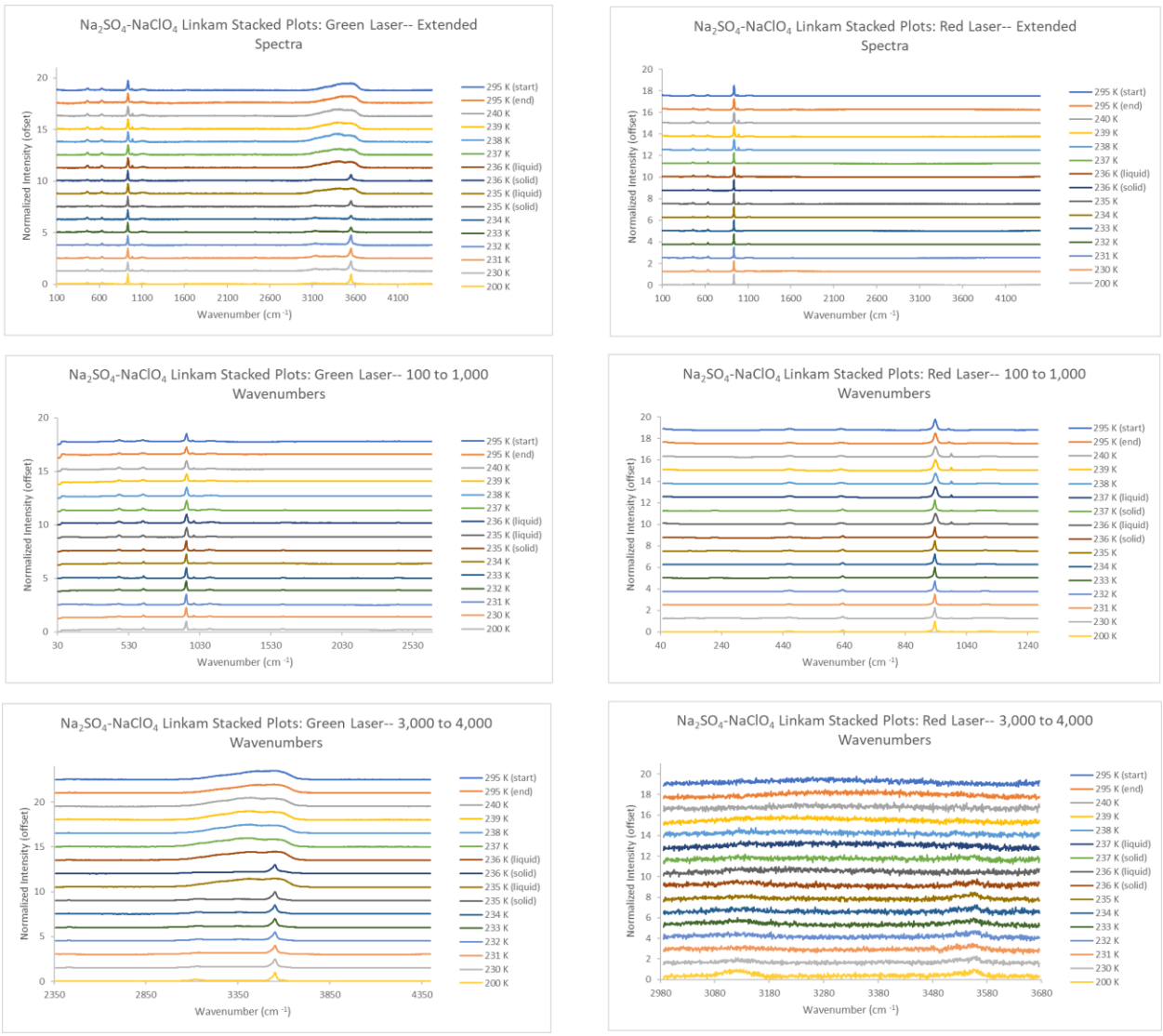

Figure A18: Na_2SO_4-$NaClO_4$ stacked plots (green and red lasers), lines and labels not included.

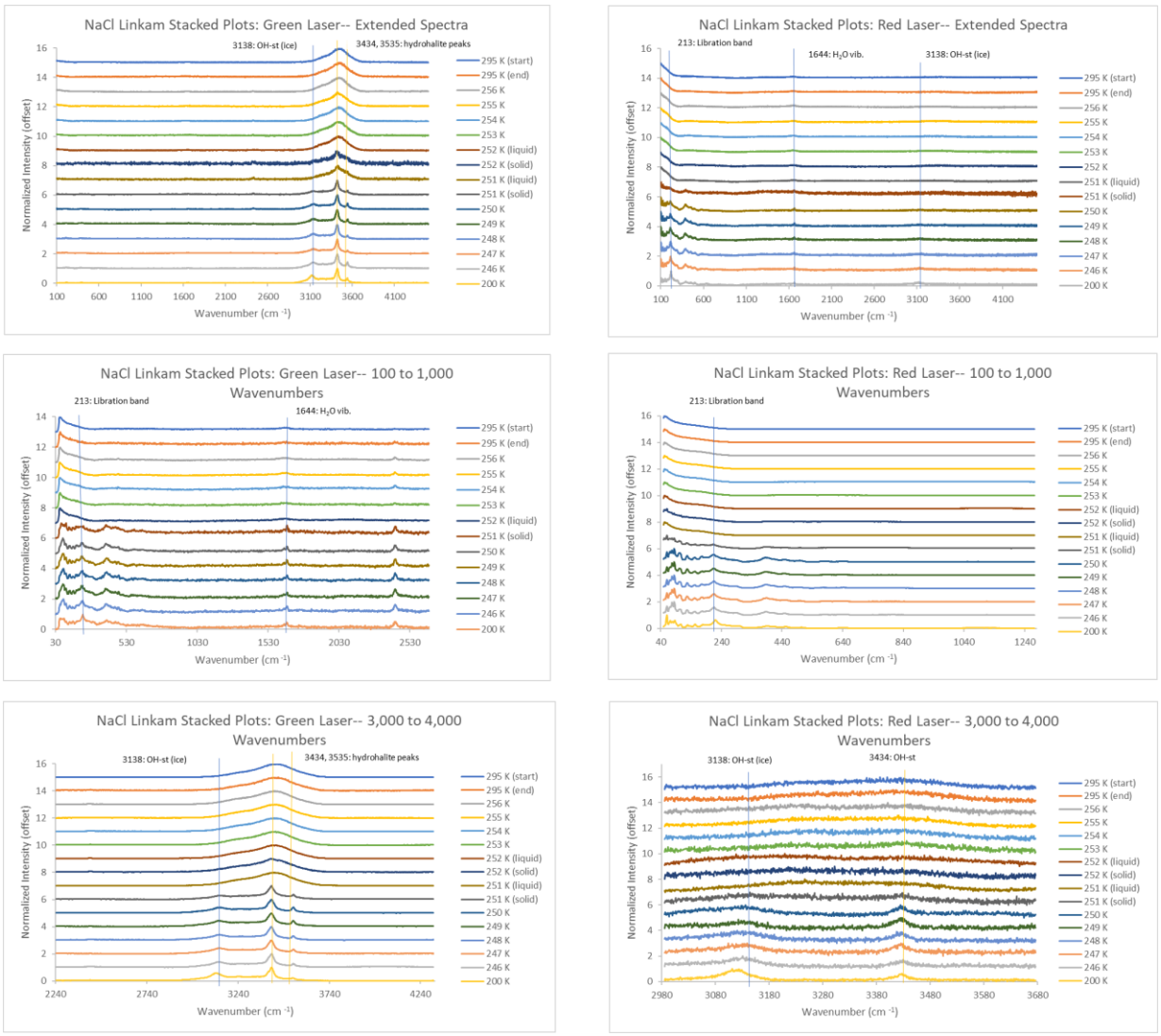

Figure A19: NaCl stacked plots (green and red lasers), lines and labels included to denote important peaks of both ultrapure water (light blue) and NaCl (yellow).

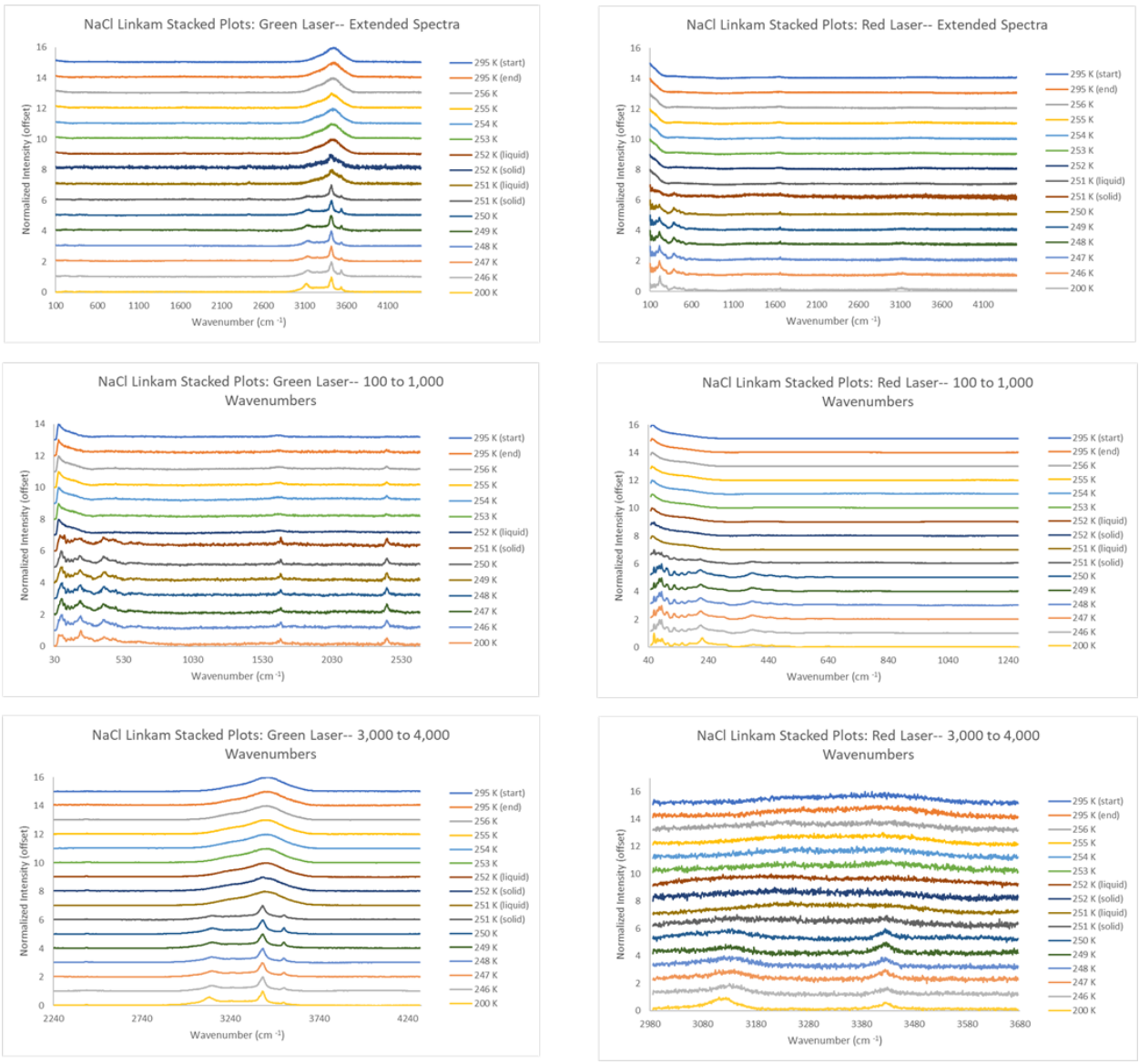

Figure A20: NaCl stacked plots (green and red lasers), lines and labels not included.

Figure A21: NaCl-NaClO4 stacked plots (green and red lasers), lines and labels included to denote important peaks of ultrapure water (light blue), NaCl (yellow), and NaClO4 (red).

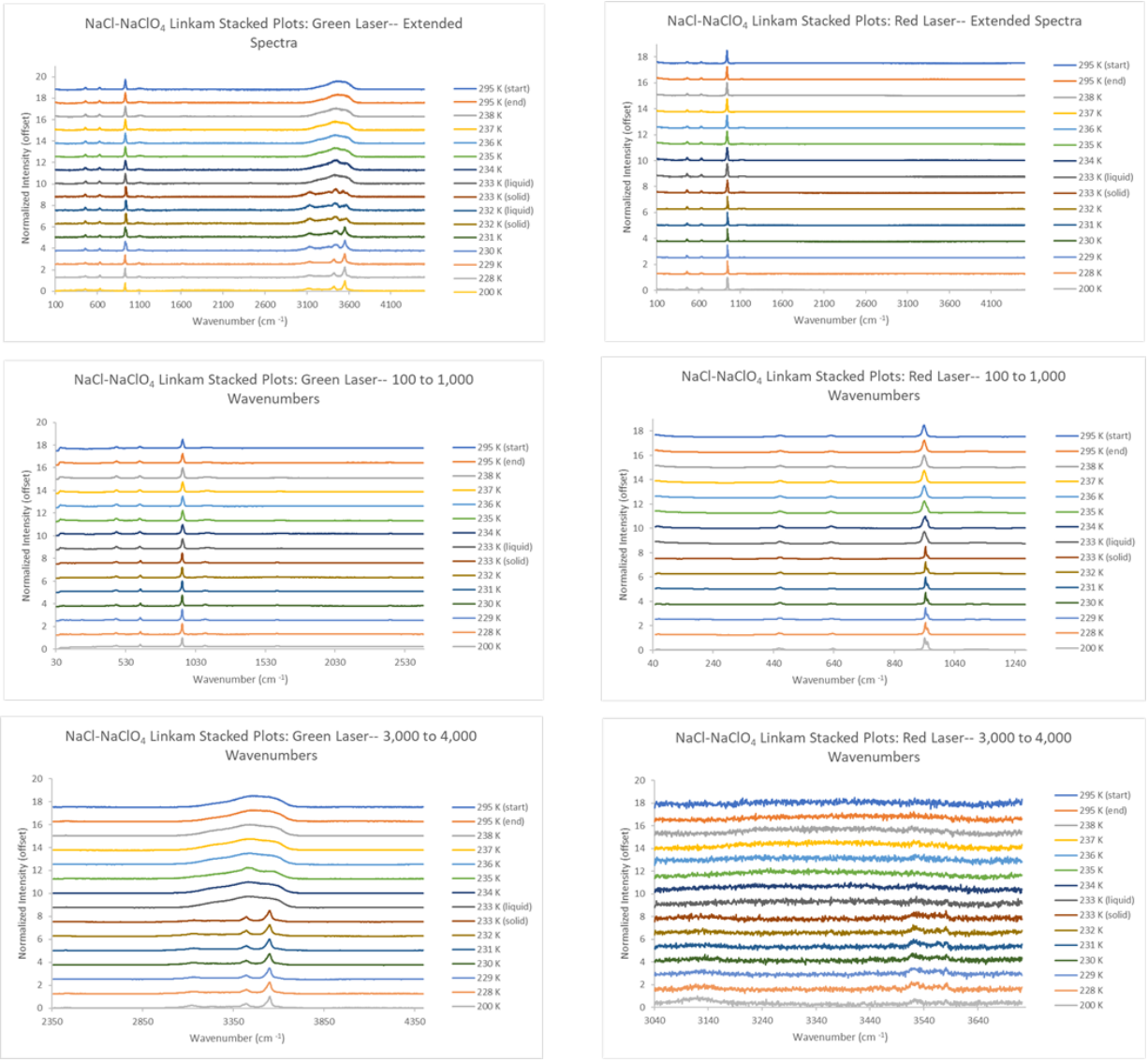

Figure A22: NaCl-NaClO₄ stacked plots (green and red lasers), lines and labels not included.

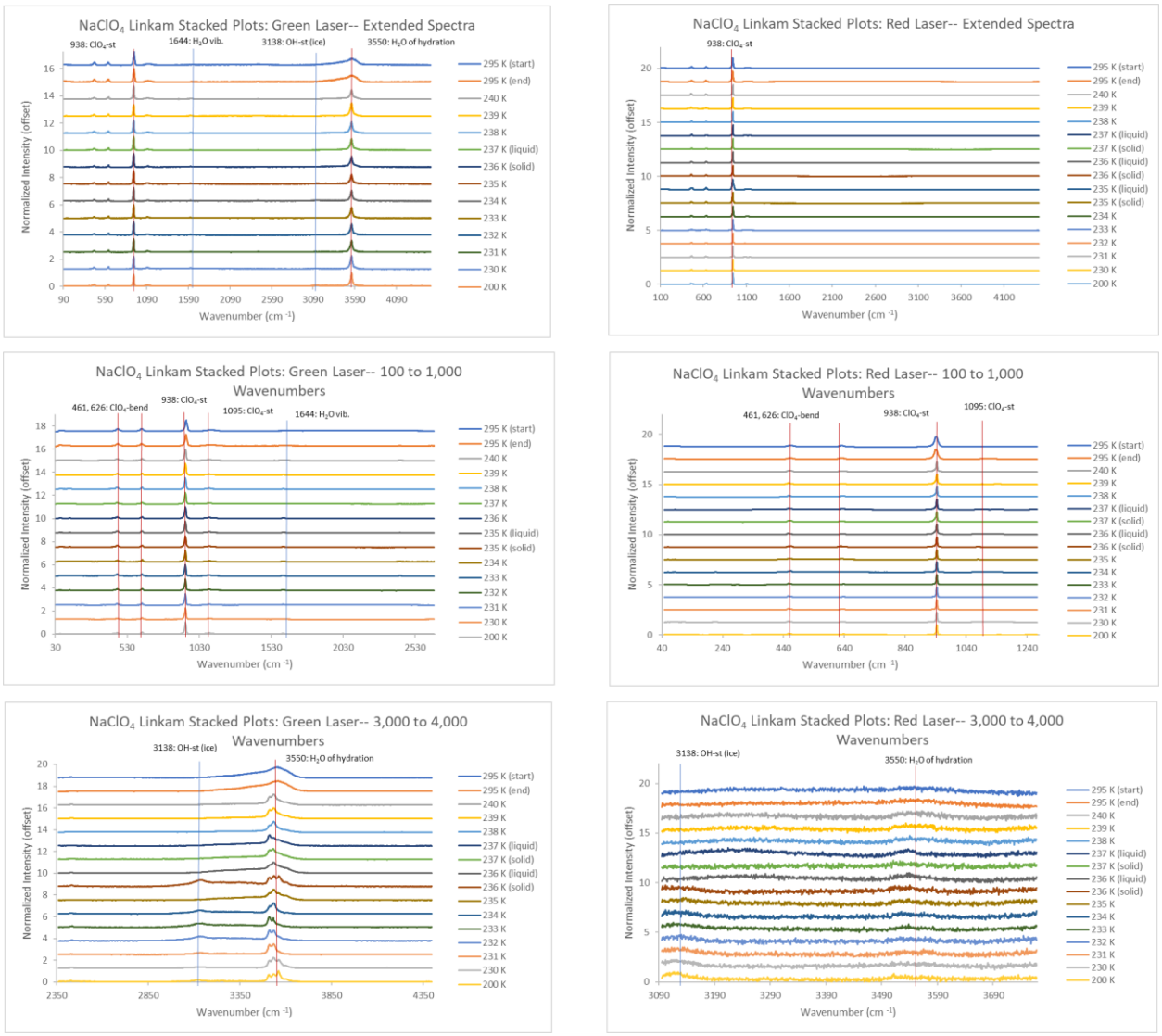

Figure A23: $NaClO_4$ stacked plots (green and red lasers), lines and labels included to denote important peaks of ultrapure water (light blue) and $NaClO_4$ (red)

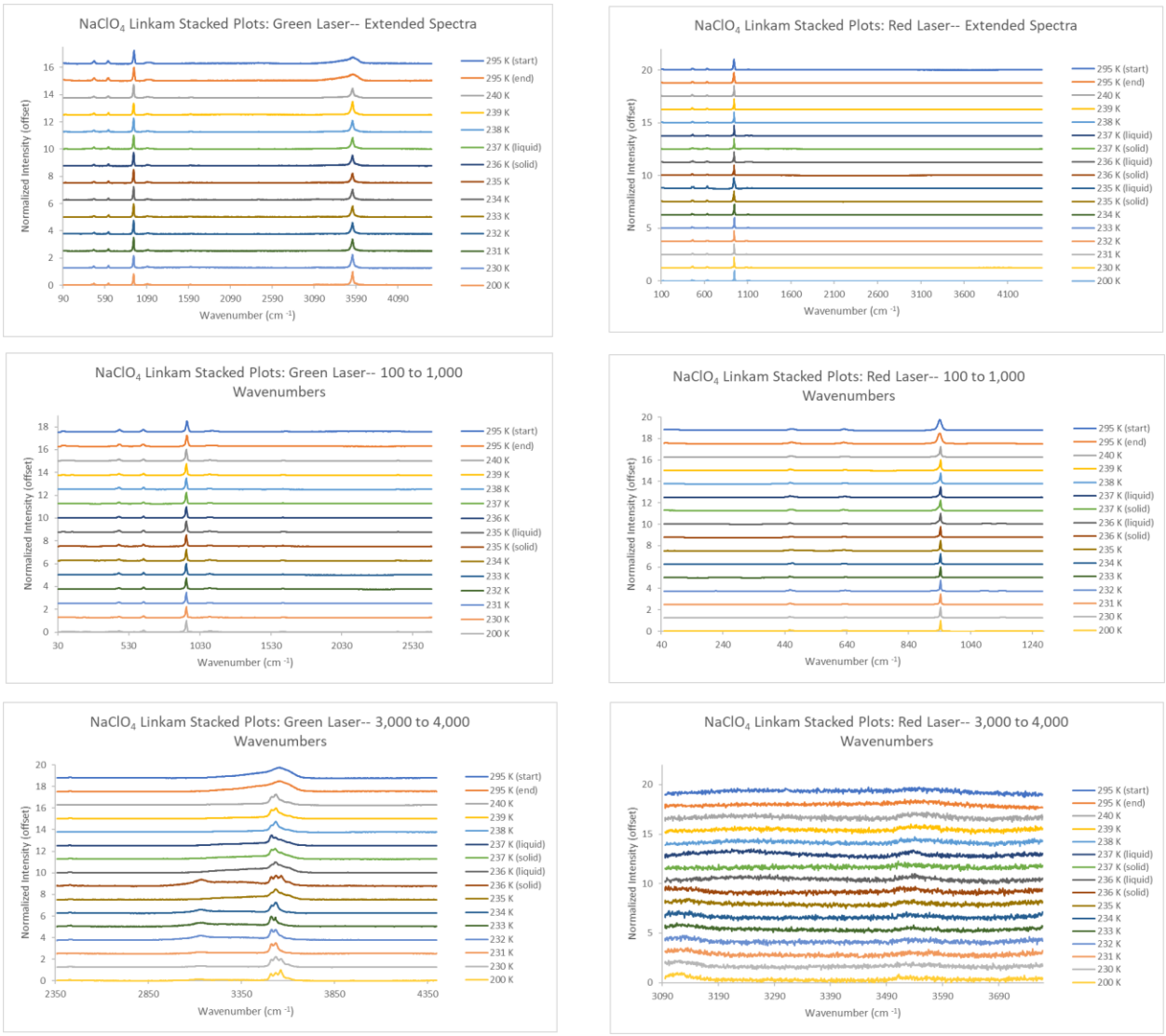

Figure A24: $NaClO_4$ stacked plots (green and red lasers), lines and labels not included.

Sediment:

The following five figures display the effects of the addition of various brines to clays like montmorillonite at Mars-analogue temperatures.

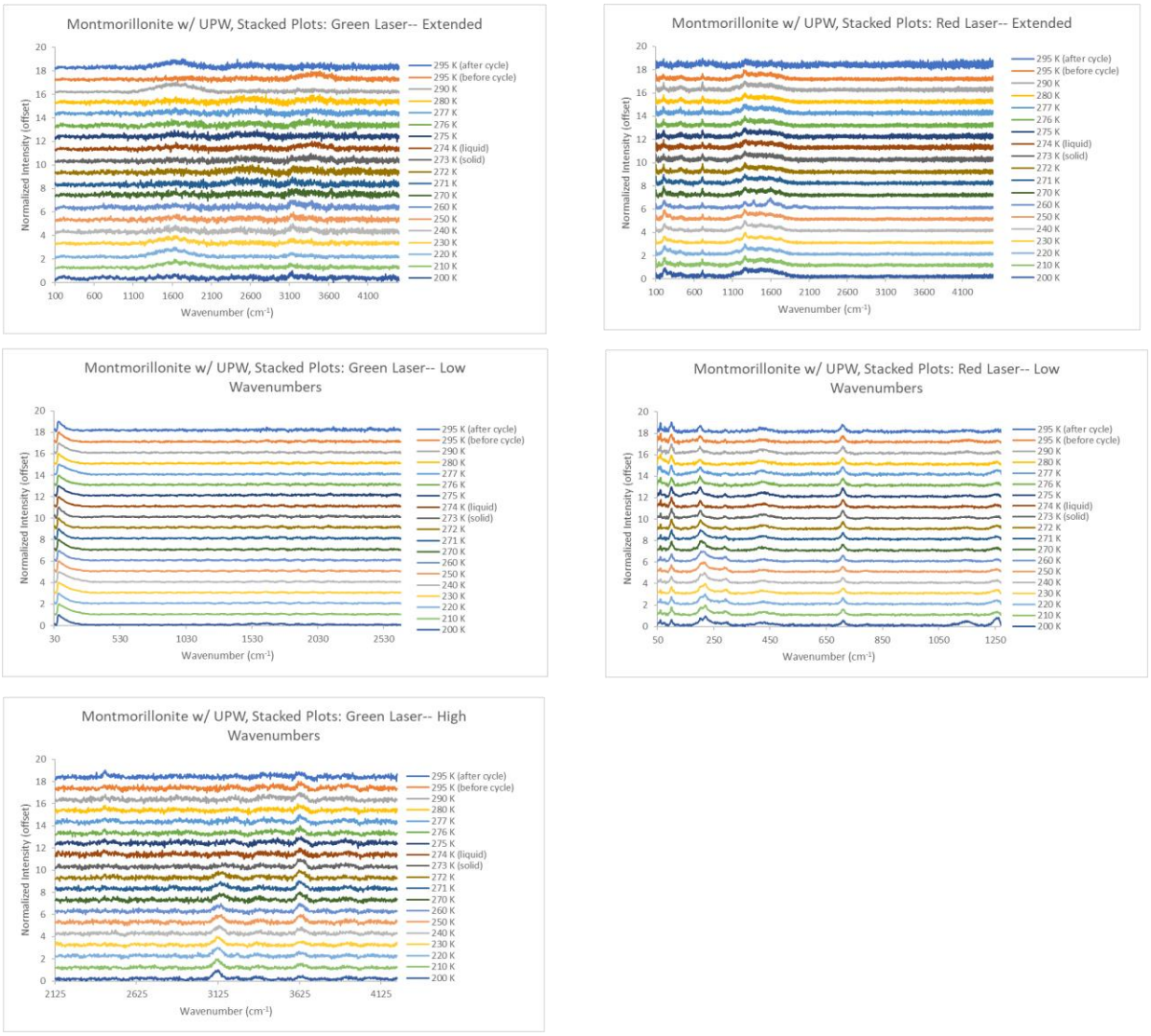

Figure A25: Montmorillonite with ultrapure water stacked plots (green and red lasers), lines and labels not included.

Figure A26: Montmorillonite with $CaCl_2$ stacked plots (green and red lasers), lines and labels not included.

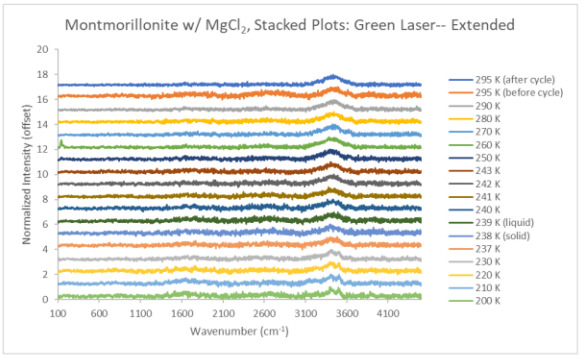

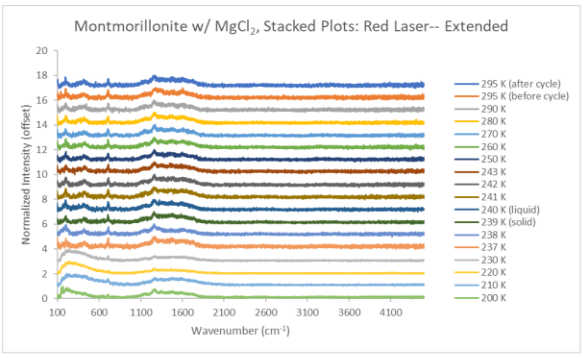

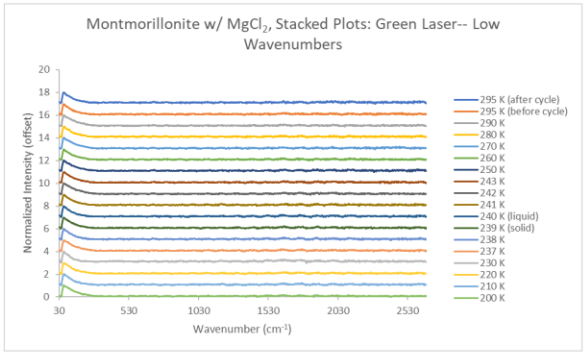

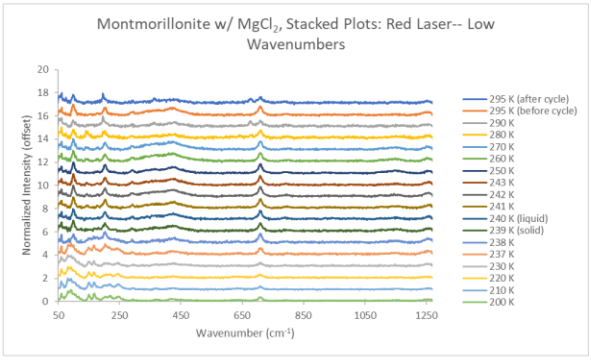

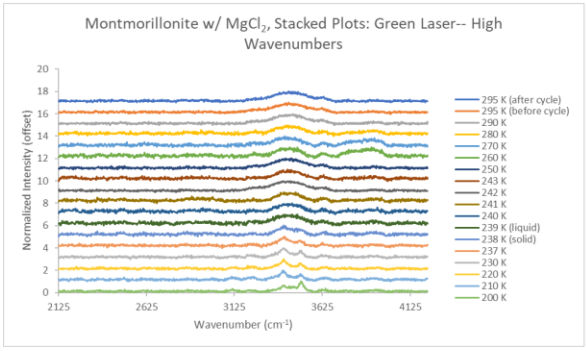

Figure A27: Montmorillonite with $MgCl_2$ stacked plots (green and red lasers), lines and labels not included.

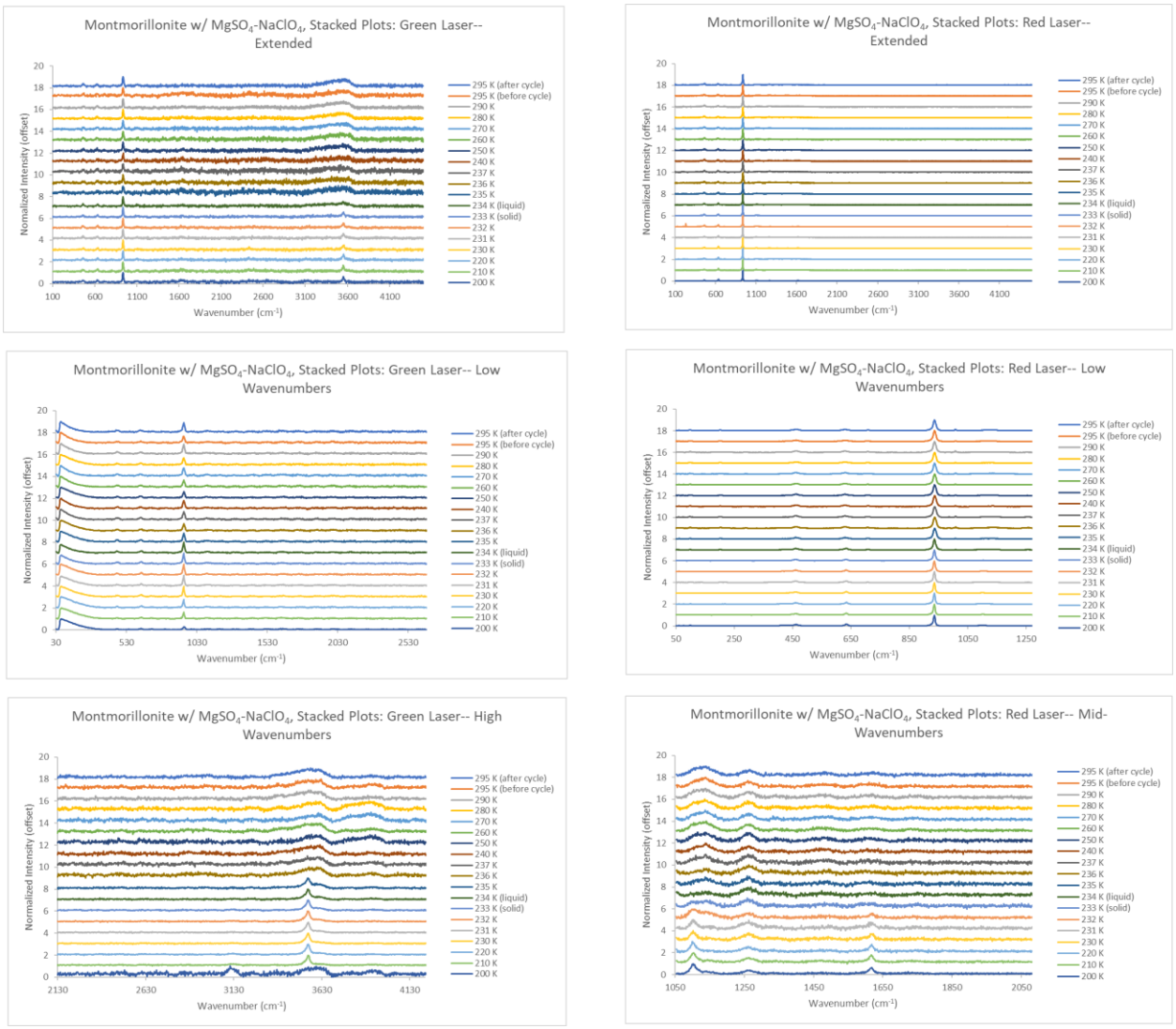

Figure A28: Montmorillonite with $MgSO_4$-$NaClO_4$ stacked plots (green and red lasers), lines and labels not included.

Figure A29: Montmorillonite with Na_2SO_4-NaCl stacked plots (green and red lasers), lines and labels not included.

Component Comparison Graphs:

The following five figures showcase a comparison between the mixed brines and their respective endmembers, at both 295 K and 200 K.

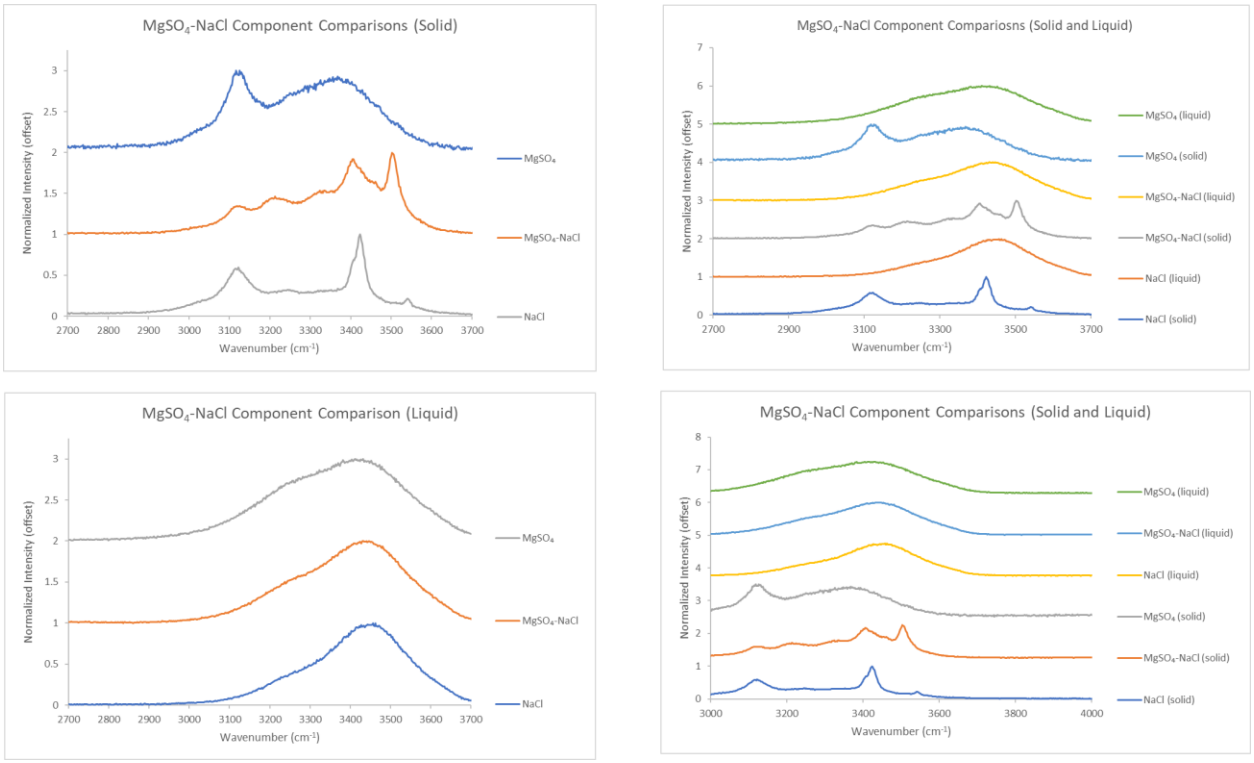

Figure A30: $MgSO_4$-NaCl comparison stacked plots between solid (200 K) and liquid (295 K) components of both endmembers and their respective mixed brine using the 532 nm green laser.

Figure A31: $MgSO_4$-$NaClO_4$ comparison stacked plots between solid (200 K) and liquid (295 K) components of both endmembers and their respective mixed brine using the 532 nm green laser.

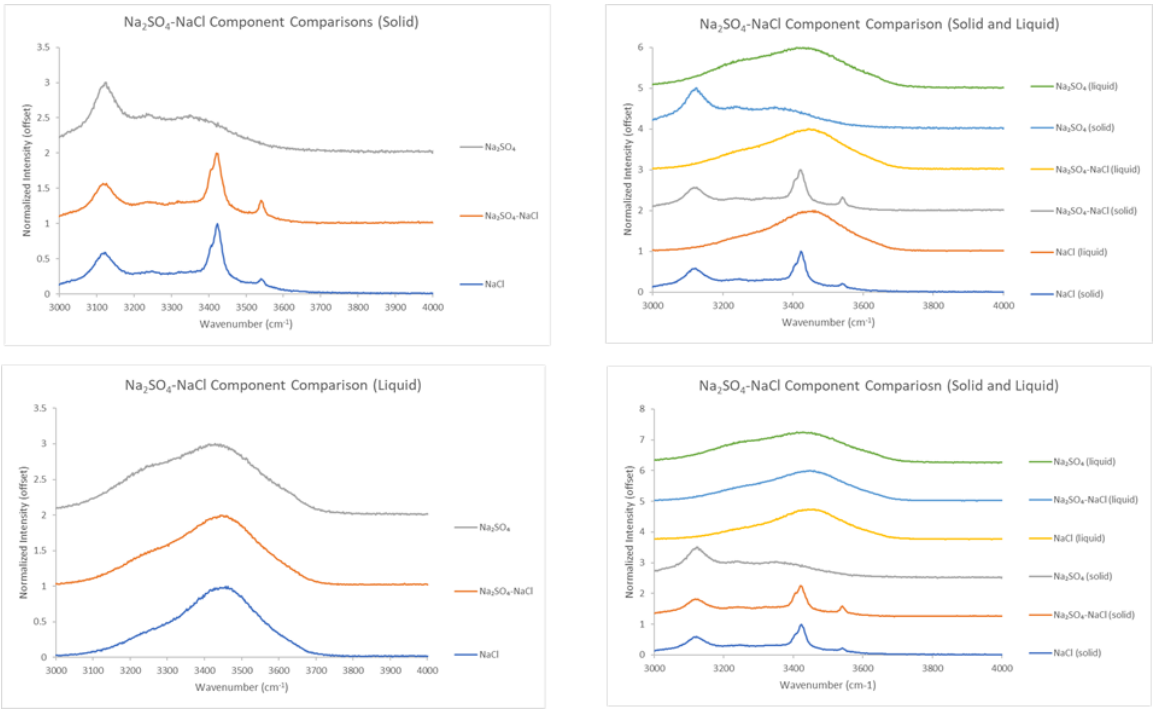

Figure A32: Na_2SO_4-NaCl comparison stacked plots between solid (200 K) and liquid (295 K) components of both endmembers and their respective mixed brine using the 532 nm green laser.

Figure A33: Na_2SO_4-$NaClO_4$ comparison stacked plots between solid (200 K) and liquid (295 K) components of both endmembers and their respective mixed brine using the 532 nm green laser.

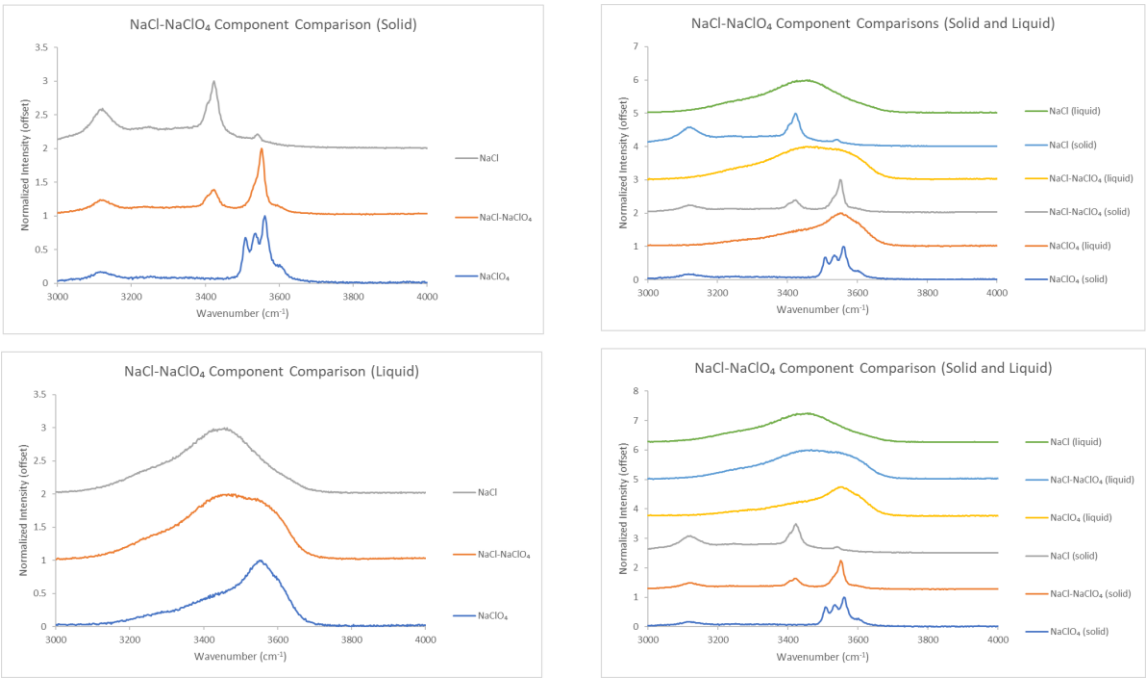

Figure A34: NaCl-$NaClO_4$ comparison stacked plots between solid (200 K) and liquid (295 K) components of both endmembers and their respective mixed brine using the 532 nm green laser.

Sulfate and Perchlorate Peak Centre Comparison:

The following nine figures denote changes in either the sulfate or perchlorate peak positions as a function of temperature.

Figure A35: The peak position of the main sulfate peak for the magnesium sulfate brine using both the 532 nm and 785 nm lasers. Note that plots denoting falling temperatures are denoted by dashed lines, while rising temperatures are denoted by solid lines.

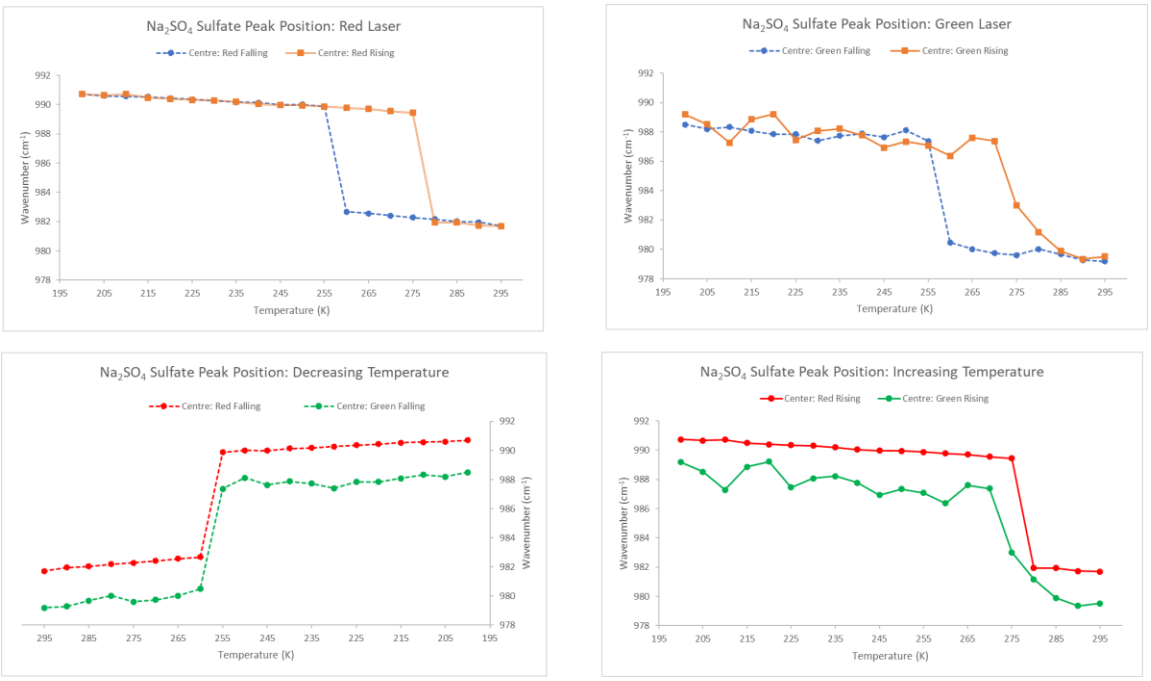

Figure A36: The peak position of the main sulfate peak for the sodium sulfate brine using both the 532 nm and 785 nm lasers. Note that plots denoting falling temperatures are denoted by dashed lines, while rising temperatures are denoted by solid lines.

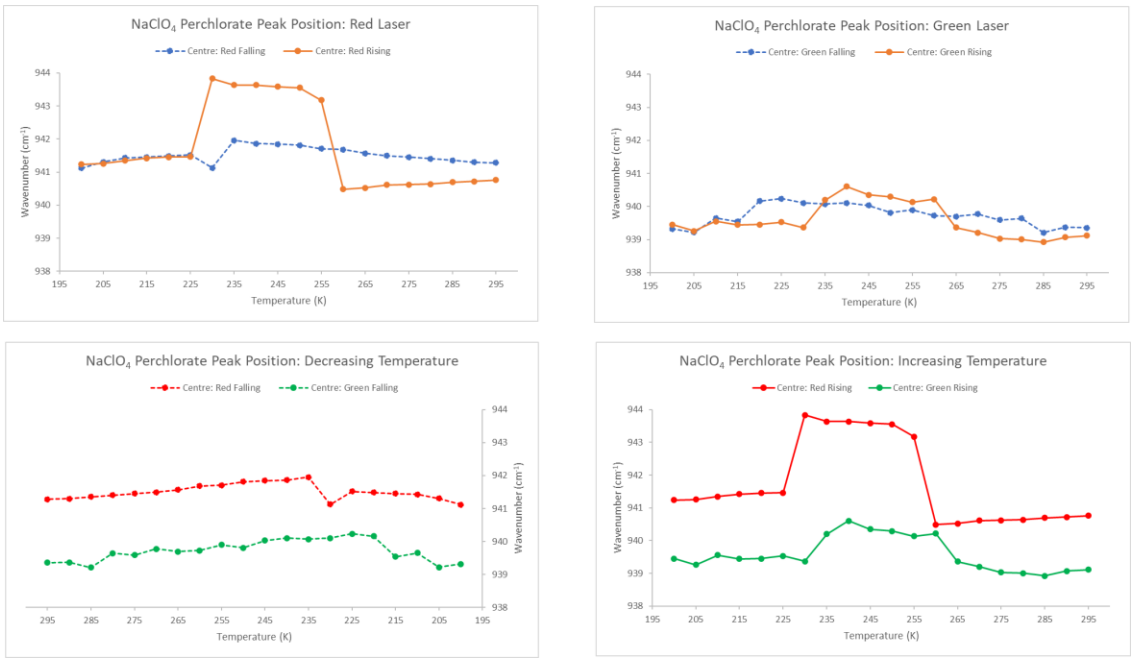

Figure A37: The peak position of the main perchlorate peak for the sodium perchlorate brine using both the 532 nm and 785 nm lasers. Note that plots denoting falling temperatures are denoted by dashed lines, while rising temperatures are denoted by solid lines.

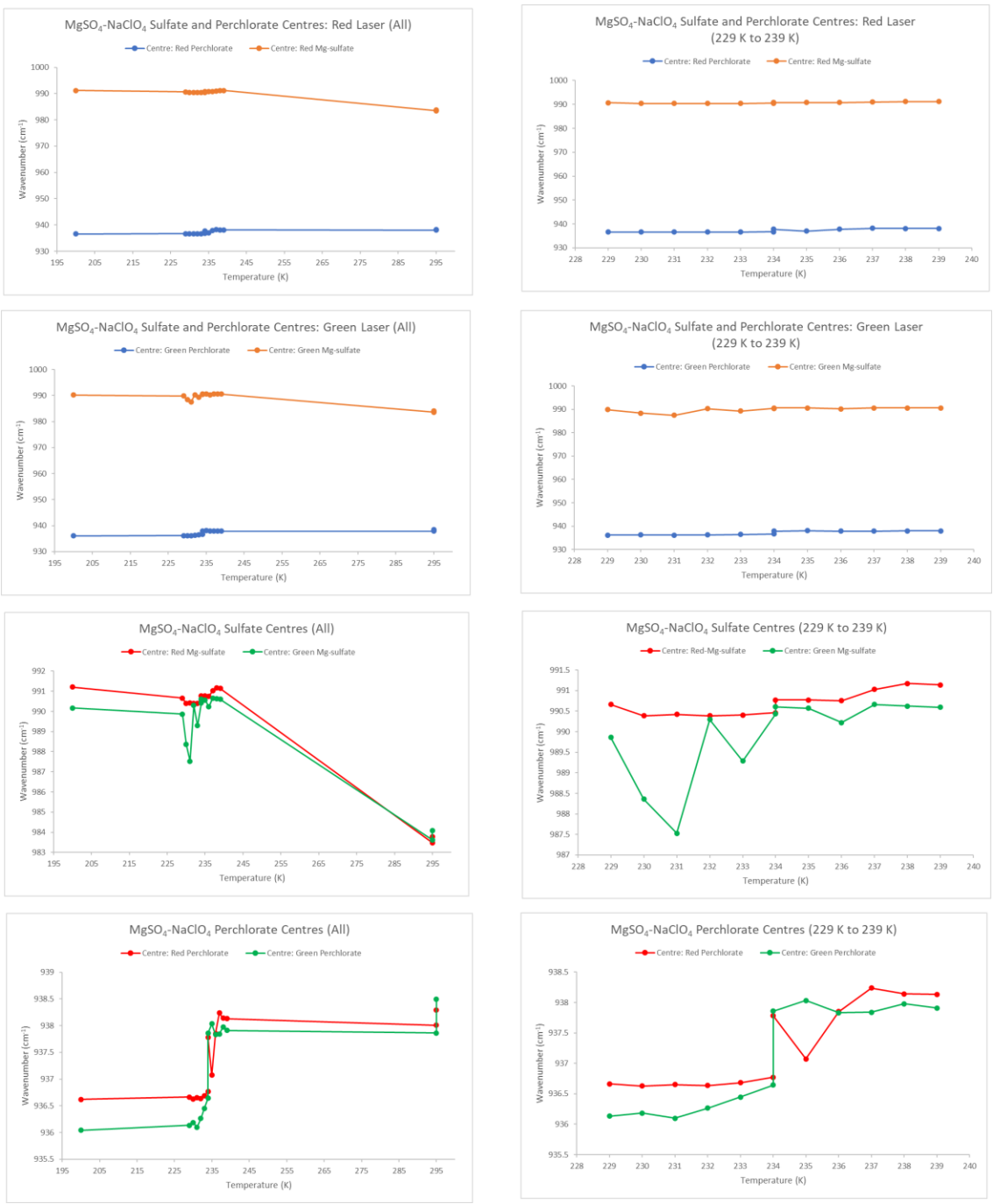

Figure A38: The peak positions of the main sulfate and perchlorate peaks for the $MgSO_4$-$NaClO_4$ brine using both the 532 nm and 785 nm lasers.

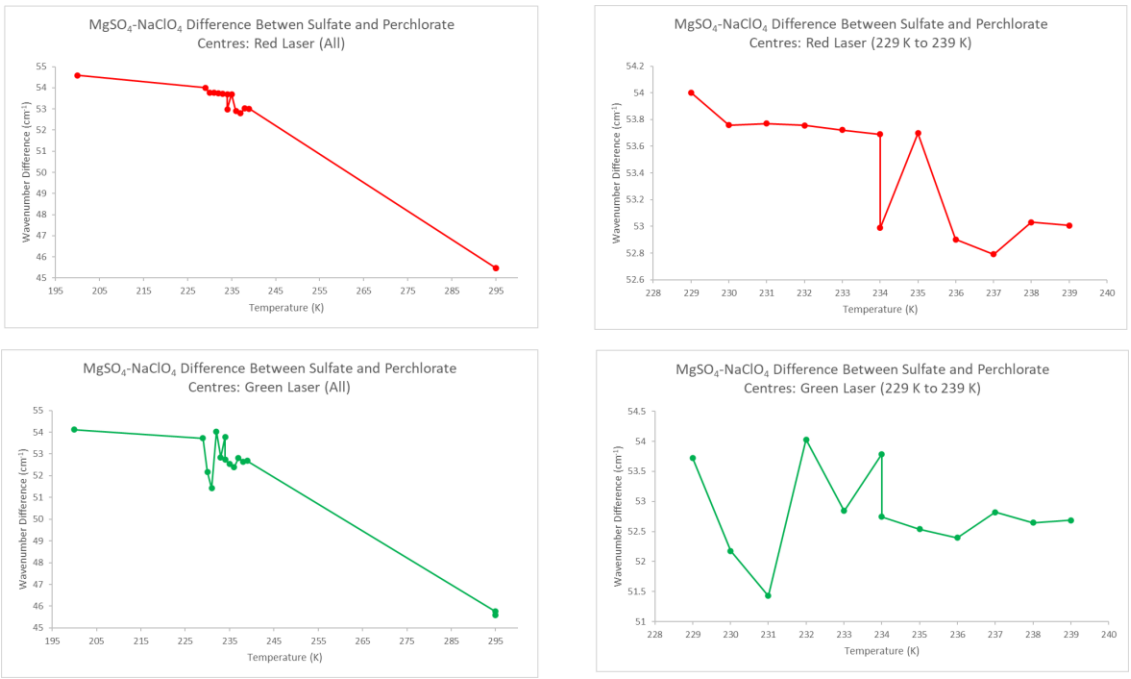

Figure A39: The difference in peak positions between the main sulfate and perchlorate peaks for the $MgSO_4$-$NaClO_4$ brine using both the 532 nm and 785 nm lasers.

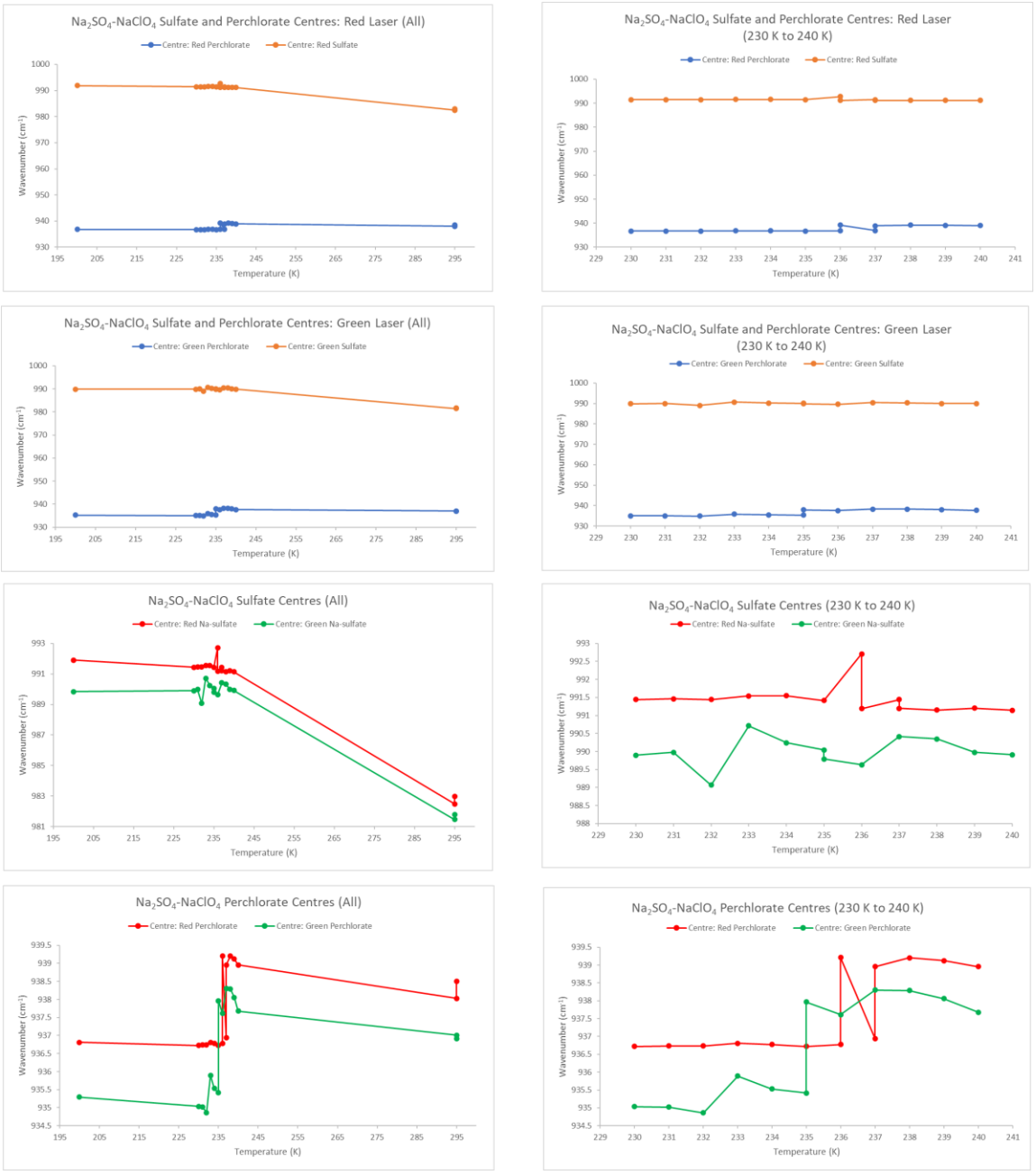

Figure A40: The peak positions of the main sulfate and perchlorate peaks for the Na_2SO_4-$NaClO_4$ brine using both the 532 nm and 785 nm lasers.

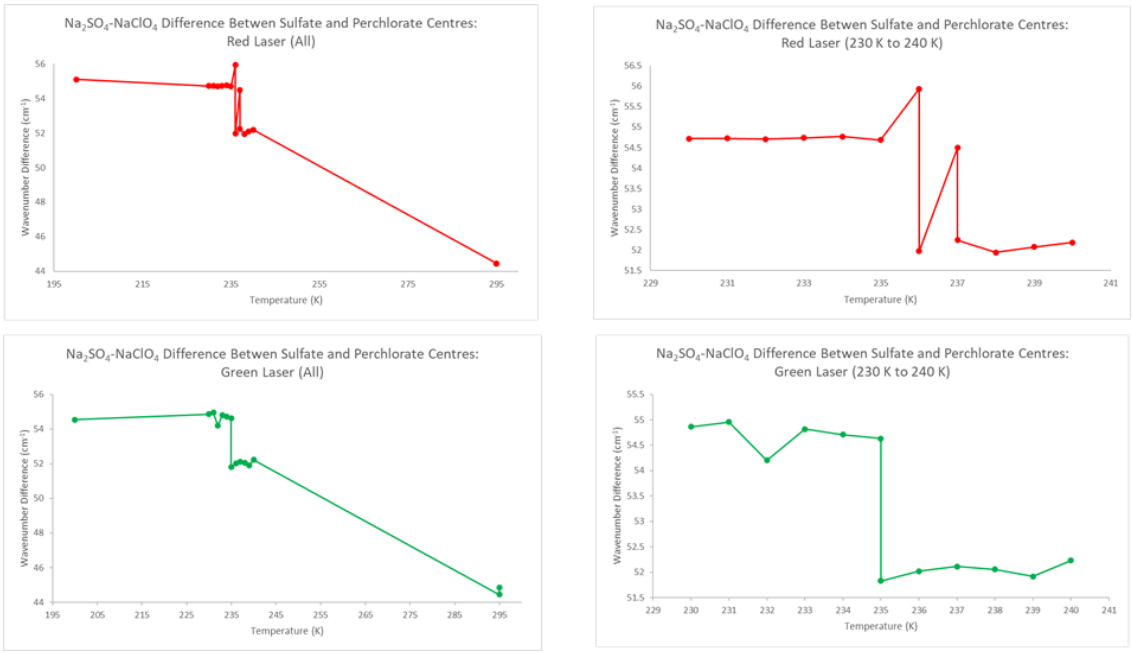

Figure A41: The difference in peak positions between the main sulfate and perchlorate peaks for the Na_2SO_4-$NaClO_4$ brine using both the 532 nm and 785 nm lasers.

Figure A42: The peak position of the main sulfate peak for four sulfate brines using both the 532 nm and 785 nm lasers. Note that plots denoting falling temperatures are denoted by dashed lines, while rising temperatures are denoted by solid lines.

Figure A43: The peak position of the main perchlorate peak for three perchlorate brines using both the 532 nm and 785 nm lasers. Note that plots denoting falling temperatures are denoted by dashed lines, while rising temperatures are denoted by solid lines.

Works Cited:

Abotalib, A. Z. and Heggy, E. (2019) 'A deep groundwater origin for recurring slope lineae on Mars', *Nature Geoscience*. Springer US, 12(4), pp. 235–241. doi: 10.1038/s41561-019-0327-5.

Bargery, A. S. *et al.* (2011) 'A background to Mars exploration and research', *Geological Society Special Publication*, 356, pp. 5–20. doi: 10.1144/SP356.2.

Bedford, C. C. *et al.* (2019) 'Alteration trends and geochemical source region characteristics preserved in the fluviolacustrine sedimentary record of Gale crater, Mars', *Geochimica et Cosmochimica Acta*. The Authors, 246, pp. 234–266. doi: 10.1016/j.gca.2018.11.031.

Ben Mabrouk, K. *et al.* (2013) 'Raman study of cation effect on sulfate vibration modes in solid state and in aqueous solutions', *Journal of Raman Spectroscopy*, 44(11), pp. 1603–1608. doi: 10.1002/jrs.4374.

Berg, R. W. (2018) 'Raman detection of hydrohalite formation: Avoiding accidents on icy roads by deicing where salt will not work', *Applied Spectroscopy Reviews*. Taylor & Francis, 53(6), pp. 503–515. doi: 10.1080/05704928.2017.1396540.

Bishop, J. L., & Murad, E. (2004). 'Characterization of minerals and biogeochemical markers on Mars: A Raman and IR spectroscopic study of montmorillonite'. Journal of Raman Spectroscopy, 35(6), 480–486. https://doi.org/10.1002/jrs.1173

Bonales, L. J., Muñoz-Iglesias, V. and Prieto-Ballesteros, O. (2014) 'Raman spectroscopy as a tool to study the solubility of CO_2 in magnesium sulphate brines: application to

the fluids of Europa's cryomagmatic reservoirs', *European Journal of Mineralogy*, 25(5), pp. 735–743. doi: 10.1127/0935-1221/2013/0025-2312.

Borden, D. and Giese, R. F. (2001) 'BASELINE STUDIES OF THE CLAY MINERALS SOCIETY SOURCE CLAYS: CATION EXCHANGE CAPACITY MEASUREMENTS BY THE AMMONIA-ELECTRODE METHOD', *Clays and Clay Minerals*, 49(5), pp. 444–445.

Bost, N. *et al.* (2015) 'Testing the ability of the ExoMars 2018 payload to document geological context and potential habitability on Mars', *Planetary and Space Science*. Elsevier, 108(2015), pp. 87–97. doi: 10.1016/j.pss.2015.01.006.

Carr, M. H. and Head, J. W. (2010) 'Geologic history of Mars', *Earth and Planetary Science Letters*. Elsevier B.V., 294(3–4), pp. 185–203. doi: 10.1016/j.epsl.2009.06.042.

Chevrier, V. F., Hanley, J. and Altheide, T. S. (2009) 'Stability of perchlorate hydrates and their liquid solutions at the Phoenix landing site, mars', *Geophysical Research Letters*, 36(10). doi: 10.1029/2009GL037497.

Chevrier, V. F. and Rivera-Valentin, E. G. (2012) 'Formation of recurring slope lineae by liquid brines on present-day Mars', *Geophysical Research Letters*, 39(21), pp. 1–5. doi: 10.1029/2012GL054119.

Chou, I. M. and Wang, A. (2017) 'Application of laser Raman micro-analyses to Earth and planetary materials', *Journal of Asian Earth Sciences*. Elsevier, 145(July), pp. 309–333. doi: 10.1016/j.jseaes.2017.06.032.

Clifford, S. M. and Parker, T. J. (2001) ‘The evolution of the Martian hydrosphere: Implications for the fate of a primordial ocean and the current state of the Northern plains’, *Icarus*, 154(1), pp. 40–79. doi: 10.1006/icar.2001.6671.

Cook, K. and Hartel, R. (2010). Crystallization in Ice Cream Production. Comprehensive Reviews in Food Science and Food Safety, 9, 213–222.

Dundas, C. M. *et al.* (2013) ‘Recurring slope lineae in equatorial regions of Mars’, *Nature Geoscience*. Nature Publishing Group, 7(1), pp. 53–58. doi: 10.1038/ngeo2014.

Duričković, I. *et al.* (2011) ‘Water-ice phase transition probed by Raman spectroscopy’, *Journal of Raman Spectroscopy*, 42(6), pp. 1408–1412. doi: 10.1002/jrs.2841.

Edwards, C. S. and Piqueux, S. (2016) ‘The water content of recurring slope lineae on Mars’, *Geophysical Research Letters*, 43(17), pp. 8912–8919. doi: 10.1002/2016GL070179.

Edwards, H. G. M. (2005) *Modern Raman spectroscopy—a practical approach. Ewen Smith and Geoffrey Dent. John Wiley and Sons Ltd, Chichester, 2005. Pp. 210. ISBN 0 471 49668 5 (cloth, hb); 0 471 49794 0 (pbk)*, *Journal of Raman Spectroscopy*. doi: 10.1002/jrs.1320.

Ehlmann, B. L. and Edwards, C. S. (2014) ‘Mineralogy of the Martian Surface’, *Annual Review of Earth and Planetary Sciences*, 42(1), pp. 291–315. doi: 10.1146/annurev-earth-060313-055024.

Ehlmann, B. L. *et al.* (2011) ‘Subsurface water and clay mineral formation during the early history of Mars’, *Nature*. Nature Publishing Group, 479(7371), pp. 53–60. doi: 10.1038/nature10582.

Elif Genceli, F. *et al.* (2009) 'Meridianiite detected in ice', *Journal of Glaciology*, 55(189), pp. 117–122. doi: 10.3189/002214309788608921.

Fairén, A. G. *et al.* (2009) 'Stability against freezing of aqueous solutions on early Mars', *Nature*, 459(7245), pp. 401–404. doi: 10.1038/nature07978.

Fortes, A. D. *et al.* (2007) 'Ammonium sulfate on Titan: Possible origin and role in cryovolcanism', *Icarus*, 188(1), pp. 139–153. doi: 10.1016/j.icarus.2006.11.002.

Hanley, J. *et al.* (2012) 'Chlorate salts and solutions on Mars', *Geophysical Research Letters*, 39(8), pp. 2–6. doi: 10.1029/2012GL051239.

Heinz, J., Schulze-Makuch, D. and Kounaves, S. P. (2016) 'Deliquescence-induced wetting and RSL-like darkening of a Mars analogue soil containing various perchlorate and chloride salts', *Geophysical Research Letters*, 43(10), pp. 4880–4884. doi: 10.1002/2016GL068919.

Horne, D. J. (2018) 'Young, small-scale surface features in Meridiani Planum, Mars: A possible signature of recent transient liquid and gas emissions', *Planetary and Space Science*. Elsevier Ltd, 157(April), pp. 10–21. doi: 10.1016/j.pss.2018.04.012.

Lafuente B, Downs R T, Yang H, Stone N (2015) The power of databases: the RRUFF project. In: Highlights in Mineralogical Crystallography, T Armbruster and R M Danisi, eds. Berlin, Germany, W. De Gruyter, pp 1-30

Lewis, A. E. *et al.* (2010) 'Design of a Eutectic Freeze Crystallization process for multicomponent waste water stream', *Chemical Engineering Research and Design*. Institution of Chemical Engineers, 88(9), pp. 1290–1296. doi: 10.1016/j.cherd.2010.01.023.

Lohumi, S., Kim, M. S., Qin, J., & Cho, B. K. (2017). Raman imaging from microscopy to macroscopy: Quality and safety control of biological materials. TrAC - Trends in Analytical Chemistry, 93, 183–198. https://doi.org/10.1016/j.trac.2017.06.002

Lopez-Reyes, G. *et al.* (2013) 'Analysis of the scientific capabilities of the ExoMars Raman Laser Spectrometer instrument', *European Journal of Mineralogy*, 25(5), pp. 721–733. doi: 10.1127/0935-1221/2013/0025-2317.

Martínez, G. M. and Renno, N. O. (2013) 'Water and brines on mars: Current evidence and implications for MSL', *Space Science Reviews*, 175(1–4), pp. 29–51. doi: 10.1007/s11214-012-9956-3.

Martinez-Uriartem, L. *et al.* (2014) 'REFERENCE RAMAN SPECTRA OF CaCl2.nH2O solids (n= 0, 2, 4, 6).', *11th International GeoRaman Conference (2014)*, pp. 5–6.

Massé, M. *et al.* (2015) 'Spectral evidence for hydrated salts in recurring slope lineae on Mars', *Nature Geoscience*, 8(11), pp. 829–832. doi: 10.1038/ngeo2546.

McEwen, A. *et al.* (2015) 'Recurring Slope Lineae on Mars : Atmospheric Origin ?', *European Planetary Science Congress*, 10, pp. 10–11.

McEwen, A. S. *et al.* (2011) 'Seasonal flows on warm Martian slopes', *Science*, 333(6043), pp. 740–743. doi: 10.1126/science.1204816.

McGraw, L. E., McCollom, N. D. S., Phillips-Lander, C. M., & Elwood Madden, M. E. (2018). Measuring Perchlorate and Sulfate in Planetary Brines Using Raman Spectroscopy [Research-article]. ACS Earth and Space Chemistry, 2(10), 1068–1074. https://doi.org/10.1021/acsearthspacechem.8b00082

Milliken, R. E., Fischer, W. W. and Hurowitz, J. A. (2009) 'Missing salts on early Mars', *Geophysical Research Letters*, 36(11), pp. 1–5. doi: 10.1029/2009GL038558.

Milliken, R. E., Grotzinger, J. P. and Thomson, B. J. (2010) 'Paleoclimate of mars as captured by the stratigraphic record in gale crater', *Geophysical Research Letters*, 37(4), pp. 1–6. doi: 10.1029/2009GL041870.

Möhlmann, D. and Thomsen, K. (2011) 'Properties of cryobrines on Mars', *Icarus*, 212(1), pp. 123–130. doi: 10.1016/j.icarus.2010.11.025.

Möhlmann, D. T. F. (2010) 'Temporary liquid water in upper snow/ice sub-surfaces on Mars?', *Icarus*. Elsevier Inc., 207(1), pp. 140–148. doi: 10.1016/j.icarus.2009.11.013.

Moral, A. G. *et al.* (2020) '49th Lunar and Planetary Science Conference 2018 (LPI Contrib. No. 2083) 2449.pdf RAMAN LASER SPECTROMETER FOR 2020 EXOMARS MISSION. ENGINEERING AND QUALIFICATION MODEL CAPABILITIES AND FUTURE ACTIVITIES', 2018(2083), pp. 4–5.

Nachon, M. et al (2014) 'Calcium sulfate veins characterized by ChemCam/Curiosity at Gale crater, Mars', *Journal of Geophysical Research: Planets*, 119. doi: 10.1002/2013JE004588.

Narayanaswamy, P. K. (1948) 'THE RAMAN SPECTRA OF WATER, HEAVY WATER AND ICE'.

Nebgen, J. W., Mcelroy, A. D. and Klodowski, H. F. (1965) 'Raman and Infrared Spectra of Nitronium Perchlorate', *Inorganic Chemistry*, 4(12), pp. 1796–1799. doi: 10.1021/ic50034a030.

Nikolakakos, G. and Whiteway, J. A. (2015) 'Laboratory investigation of perchlorate deliquescence at the surface of Mars with a Raman scattering lidar', *Geophysical Research Letters*, 42(19), pp. 7899–7906. doi: 10.1002/2015GL065434.

Phillips-Lander, C. M., Elwood Madden, A. S., Hausrath, E. M., & Elwood Madden, M. E. (2019). Aqueous alteration of pyroxene in sulfate, chloride, and perchlorate brines: Implications for post-Noachian aqueous alteration on Mars. Geochimica et Cosmochimica Acta, 257, 336–353. https://doi.org/10.1016/j.gca.2019.05.006

Root, M. J. and Elwood Madden, M. E. (2012) 'Potential effects of obliquity change on gas hydrate stability zones on Mars', *Icarus*. Elsevier Inc., 218(1), pp. 534–544. doi: 10.1016/j.icarus.2011.12.024.

Rull, F. *et al.* (2017) 'The Raman Laser Spectrometer for the ExoMars Rover Mission to Mars', *Astrobiology*, 17(6–7), pp. 627–654. doi: 10.1089/ast.2016.1567.

Schmidt, F. *et al.* (2017) 'Formation of recurring slope lineae on Mars by rarefied gas-triggered granular flows', *Nature Geoscience*, 10(4), pp. 270–273. doi: 10.1038/ngeo2917.

Solomon, S. C. *et al.* (2005) 'New perspectives on ancient Mars', *Science*, 307(5713), pp. 1214–1220. doi: 10.1126/science.1101812.

Squyres, S. (1984) 'The History of Water on Mars', *Annual Review of Earth and Planetary Sciences*, 12(1), pp. 83–106. doi: 10.1146/annurev.earth.12.1.83.

Stillman, D. E. and Grimm, R. E. (2018) 'Two pulses of seasonal activity in martian southern mid-latitude recurring slope lineae (RSL)', *Icarus*. Elsevier Inc., 302, pp. 126–133. doi: 10.1016/j.icarus.2017.10.026.

Stillman, D. E. *et al.* (2016) 'Observations and modeling of northern mid-latitude recurring slope lineae (RSL) suggest recharge by a present-day martian briny aquifer', *Icarus*. Elsevier Inc., 265, pp. 125–138. doi: 10.1016/j.icarus.2015.10.007.

Thomas, E. C. *et al.* (2017) 'Composition and Evolution of Frozen Chloride Brines under the Surface Conditions of Europa', *ACS Earth and Space Chemistry*, 1(1), pp. 14–23. doi: 10.1021/acsearthspacechem.6b00003.

Toner, J. D., Catling, D. C. and Light, B. (2014) 'The formation of supercooled brines, viscous liquids, and low-temperature perchlorate glasses in aqueous solutions relevant to Mars', *Icarus*. Elsevier Inc., 233, pp. 36–47. doi: 10.1016/j.icarus.2014.01.018.

Van Driessche, A. E. S., Stawski, T. M. and Kellermeier, M. (2019) 'Calcium sulfate precipitation pathways in natural and engineered environments', *Chemical Geology*. Elsevier, 530(August), p. 119274. doi: 10.1016/j.chemgeo.2019.119274.

Wang, A. *et al.* (2006) 'Sulfates on Mars: A systematic Raman spectroscopic study of hydration states of magnesium sulfates', *Geochimica et Cosmochimica Acta*, 70(24), pp. 6118–6135. doi: 10.1016/j.gca.2006.05.022.

Wang, Z. *et al.* (2004) 'Vibrational substructure in the OH stretching transition of water and HOD', *Journal of Physical Chemistry A*, 108(42), pp. 9054–9063. doi: 10.1021/jp048545t.

Wiens, R. C., Maurice, S., & Perez, F. R. (2017). The SuperCam remote sensing instrument suite for the mars 2020 rover: A preview. Spectroscopy (Santa Monica), 32(5), 50–55.

Wilson, E. H., Atreya, S. K., Kaiser, R. I., & Mahaffy, P. R. (2016). Perchlorate formation on Mars through surface radiolysis-initiated atmospheric chemistry: A potential mechanism. Journal of Geophysical Research: Planets, 1472–1487. https://doi.org/10.1002/2016JE005078

Yang, D., Xiong, X. and Chen, W. (2019) 'Cryogenic raman spectroscopic studies on common Ore-forming Fluid Systems', *Minerals*, 9(6), pp. 1–14. doi: 10.3390/min9060363.

Zhang, Z. and Liu, X. Y. (2018) 'Control of ice nucleation: Freezing and antifreeze strategies', *Chemical Society Reviews*. Royal Society of Chemistry, 47(18), pp. 7116–7139. doi: 10.1039/c8cs00626a.